DISSERTATION

REGULATION OF DYNEIN ACTIVITY DURING SPINDLE POSITIONING IN BUDDING YEAST

Submitted by

Lindsay Lammers

Department of Biochemistry and Molecular Biology

In partial fulfillment of the requirements

For the Degree of Doctor of Philosophy

Colorado State University

Fort Collins, Colorado

Spring 2020

Doctoral Committee:

Advisor: Steven Markus

Jennifer DeLuca
Tingting Yao
Anireddy Reddy

ABSTRACT

REGULATION OF DYNEIN ACTIVITY DURING SPINDLE POSITIONING IN BUDDING YEAST

Cytoplasmic dynein is a minus-end directed, microtubule motor that is highly regulated to ensure it is targeted to the correct location at a specific time for its function in cells. This is particularly important for the process of spindle positioning during mitosis. Dynein is targeted to the cell cortex and activated to pull on astral microtubules attached to spindle poles to move the spindle into position at the site of cytokinesis. The position of the spindle dictates the plane of division and influences whether a cell divides asymmetrically or symmetrically- an important distinction during embryonic development and homeostasis. Using the model organism budding yeast, we confirmed that dynein is held in an inactive state before reaching its destination at the cell cortex by identifying a key factor in dynein activation- the cortical receptor Num1. We determined that the mechanism of activation involves enhancing dynein-dynactin interaction and releasing the recruitment factor, Pac1/Lis1. Additionally, I determined the role of another regulator in the dynein pathway, Ndl1/NudE. Ndl1/NudE aids the recruitment factor, Pac1/Lis1 in targeting dynein to astral microtubule plus ends that then deliver the motor to the cortex. Interestingly, it appears Ndl1/NudE may have another function that competes Pac1/Lis1 off dynein in a specific context. Next, I explored the two possible mechanisms of Num1-mediated dynein activation. First, I established an in vitro motility assay to observe how the regulators dynactin, Num1 and Pac1/Lis1 may coordinate to affect dynein activity. I determined the purification conditions for complete dynactin complexes as well as Num1 constructs to test whether Num1 acts as an adapter to activate the dynein-dynactin complex. Finally, I examined the second mechanism of Num1-mediated activation by initiating the release of Pac1/Lis1 from dynein complexes. I predicted that Num1 may influence the conformational changes of dynein during its mechanochemical cycle in conjunction with dynein engaging the microtubule that could induce

Pac1/Lis1 release. To test this, I mutated dynein in a way that restricted conformation changes and observed how this affected Pac1/Lis1 interaction. The results show that Pac1/Lis1 binding is profoundly affected by dynein structure. Further, Num1 can still initiate Pac1/Lis1 release despite restriction in conformational changes, which suggests Num1 may initiate Pac1/Lis1 disassociation in another way. Together these data reveal important details of how regulatory proteins coordinate to spatially and temporally regulate dynein during spindle positioning.

ACKNOWLEDGEMENTS

I would like to thank and acknowledge the following people for making this work possible.

Steven Markus. Your passion for dynein and enthusiasm for research was what led me to your lab. Thank you for taking a risk on me as your first student as I did you as a new professor. I learned how to be a thorough and critical scientist through your mentorship. You were encouraging and understanding when things failed and failed again. I am grateful that you let me explore different areas of science that I was interested in and excelled. I look forward to seeing what great things the Markus lab accomplishes in the future.

My committee. Thank you for your insights and encouragement over the last 6 years. Dr. DeLuca, thank you for your support as I pursued science policy activities. Your interest and support were encouraging and helped me explore my place in the scientific community.

The lab. To Kari, Marzo, Tyler, Dilsaver, Rachel, and Kristina. I was incredibly fortunate to have you as my lab family. I needed each of you to get to the end and will cherish every laugh, cry, frustration and conversation that we shared. Hazheen, Amanda, Rob, Jeanne, and Keith. Thank you for your scientific insight, and sympathetic ears. Thank you all for supporting me. Lydia Heasley. Your time in our lab was critical to my success. I loved discussing science with you, but even more so your constant belief that I earned this degree was paramount to my achievement.

My family. My mom who has truly understood every part of this journey and has endlessly listened and empathized. And my dad who in not so many words has never doubted my ability to succeed. Rod. You also have never doubted my ability, never let me quit, and encouraged me every single day. You kept me fed and my clothes clean. I wouldn't want anyone else to be on my team. And Teddy. You sweet, sweet babe- we love you.

DEDICATION

To anyone who has ever thought about quitting

and

To Rod, my number one draft pick

TABLE OF CONTENTS

CHAPTER 1

INTRODUCTION

Arguably the most complex molecular motor, dynein was first discovered as the force generating protein responsible for ciliary movement (Gibbons and Rowe, 1965). Cytoplasmic dynein (herein called dynein) was later found to be the major minus-end directed microtubule motor in the cell (Paschal et al., 1987). However due to its complexity, the details of how the motor coordinates its stepping and communicates ATP hydrolysis to microtubule binding were only recently worked out (reviewed in Schmidt and Carter, 2016; Bhabha et al., 2015). Allosteric communication from the AAA+ ATPase ring must be transmitted through the buttress and stalk domain to the microtubule binding domain (Figure 1.1A). Its linker domain is also coordinated with ATP hydrolysis and is responsible for the powerstroke that drives forward motion toward the minus end of microtubules. The linker connects the motor to the large tail domain that associates with the light and intermediate chains (Figure 1.1A).

Not only is its intramolecular communication complex, but dynein is highly regulated by a variety of proteins for its myriad roles. This is in contrast with the kinesin motor family, which comprises many different kinesins for various functions rather than a single, versatile motor that completes a variety of tasks. For example, during mitosis dynein is recruited to the nuclear envelope for breakdown, the centrosome for pole separation, the kinetochore for checkpoint silencing, and the cell cortex for spindle positioning, while more than ten different kinesins are involved in mitosis (Raaijmakers and Medema, 2014; Vicente and Wordeman, 2015). Exactly how dynein is spatially and temporally regulated to function at all these sites is not well understood. I addressed this gap by exploring dynein regulation during its spindle positioning function in mitosis. Specifically, I examine how dynein is recruited to and activated at the cell cortex to generate forces on the spindle to place it in the correct location by its many regulatory proteins.

Figure 1.1

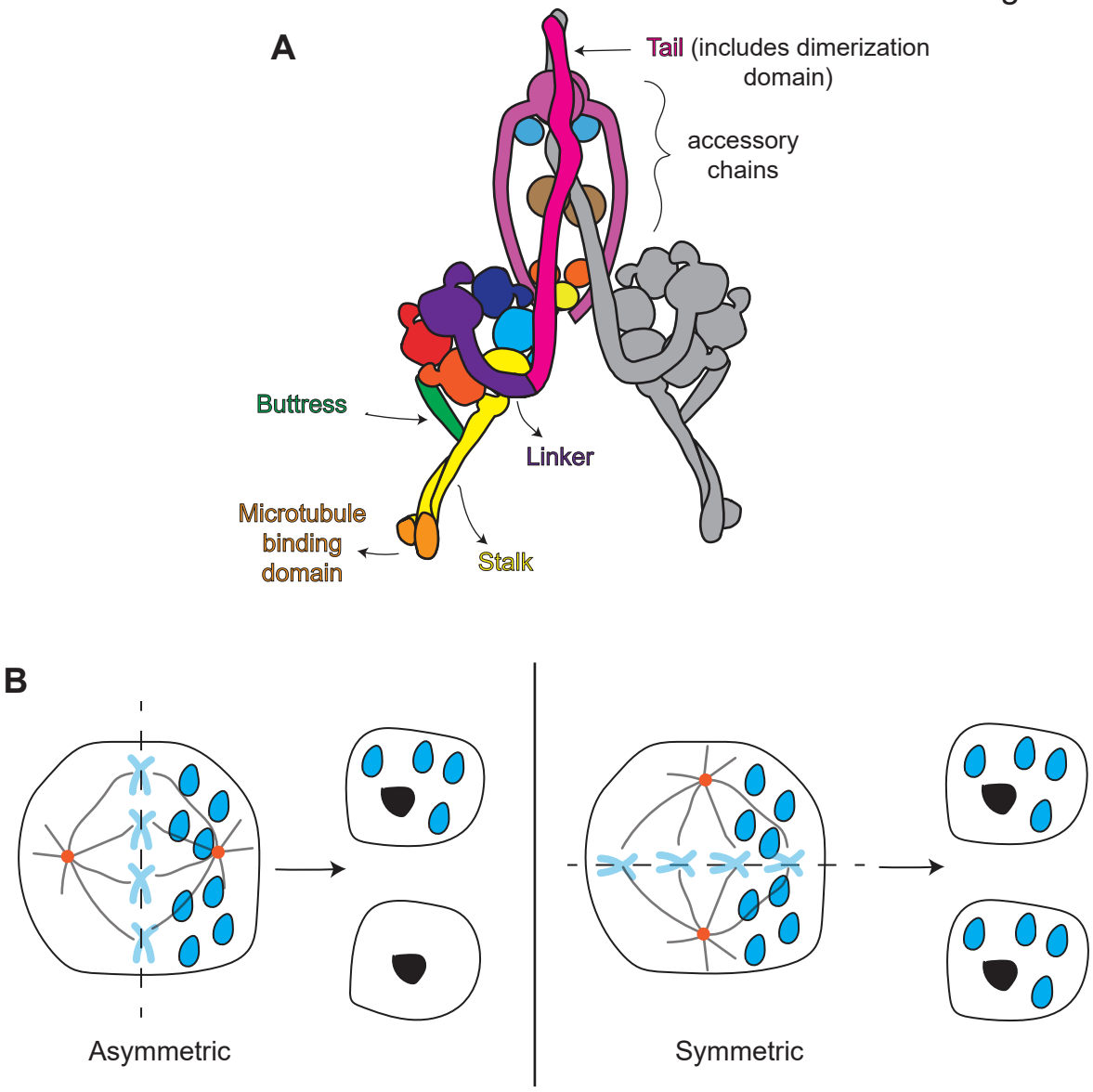

Figure 1.1 Cartoon of dynein strucutral features and asymmetric cell division. (A) The single polypeptide, dynein heavy chain comprises the tail, AAA+ ring, stalk, microtubule binding domain, and buttress. The tail domain includes the dimerization domain and interacts with several accessory chains. (B) Asymmetric vs. symmetric divisions: The plane of division (dotted line) is dictated by the spindle orientation. The spindle is made up of grey microtubules growing from spindle poles (orange) with astrals emanating toward the cell edge. Light blue X's within the spindle show chromosomes aligned on the metaphase plate. The blue circles indicate polarity markers that will be separated depending on the plane of division to create identical or asymmetric cells. Black spots show the reformed nuclei in new cells.

Mitosis is the intricate, mechanical process of one cell physically dividing all its components in two. Cell divisions can be self-renewing or differentiating - forming two identical or unidentical cells (Figure 1.1B). Asymmetric division is critical for the development of cell diversity and is balanced with symmetric divisions to maintain homeostasis (Noatynska et al., 2012; Williams et al., 2011). For example, breast cancer stem cells lose their ability to divide asymmetrically, which leads to more self-renewing divisions and tumor growth (Cicalese et al., 2009). Asymmetry is dictated by the location of the spindle, which defines the plane of division where cytokinesis occurs. To position the spindle, dynein motors are recruited to specific sites at the cell cortex and are activated to pull on astral microtubules emanating from spindle poles. If dynein is depleted from cortical sites in mouse neuronal stem cells by loss of the regulatory protein, Lis1 (Pac1 in yeast), severe brain abnormalities occur because the stem cell pool is prematurely depleted by asymmetric divisions (Yingling et al., 2008; Wynshaw-Boris et al., 2010). It is important to understand how these regulatory proteins coordinate to recruit and activate dynein appropriately during this mitotic process. I use budding yeast as a model system to examine how these regulators affect dynein for its spindle positioning function.

Using model organisms to better understand human processes is a great strength of biology and has led to important discoveries in cell function. *Saccharomyces cerevisiae,* or budding yeast, are single-celled eukaryotic organisms that experience asymmetric cell division each cell cycle. Mitosis is closed, meaning that the nucleus remains intact and is positioned along with the mitotic spindle at the neck, between the mother and daughter cells. To position the spindle correctly, two pathways exist: the KAR9 pathway and the dynein pathway. The KAR9 pathway first orients the spindle via actin/myosin, while dynein takes over to pull the now oriented spindle through the neck during anaphase. Because this is the only known role for dynein in yeast, it is easier to study how dynein is regulated for this specific function than in more complex systems, such as humans or mice, where dynein has many roles.

In the past 15 years, the pathway in which yeast dynein is delivered to the cortex has been well characterized. Dynein first associates with Pac1 (Lis1 in humans) and its partner Ndl1 (NudE/NudEL in humans) in the cytoplasm, which targets the motor to the plus end of an astral microtubule (Figure 1.2; Lee et al., 2003; Sheeman et al., 2003; Li et al., 2005). Pac1/Lis1 interacts with a +TIP protein, Bik1 (Clip170 in humans), to mediate dynein tip-tracking on the astral microtubule (Roberts et al., 2014a; Sheeman et al., 2003). Next, the activating factor, dynactin, associates with the plus end in a dynein-dependent manner (Sheeman et al., 2003; Lee et al., 2003b). The microtubule, loaded with dynein complexes, probes the cytoplasm until encountering a patch of Num1 cortical receptors distributed along the cell cortex. Dynein-dynactin offload to a Num1 patch and are active to exert force on the microtubule and pull the spindle (Lee et al., 2005; Markus and Lee, 2011; Markus et al., 2009). At each of these steps, dynein is associated with one or more regulatory proteins: Pac1/Lis1, Ndl1/NudE, dynactin, or Num1. Although the identity of these regulators has been known for some time, it is unclear how they coordinate to regulate dynein activity. In the first steps before reaching the cortex, dynein appears to be inactive because it does not leave the plus end- if it were active, it would decorate the microtubule or accumulate at the minus end (spindle poles). Once offloaded to the cortex, dynein-dynactin must be active, indicated by spindle movements. How dynein switches from being inactive at the plus end, to active at the cortex is the overarching question that I address in this dissertation.

To begin, I reasoned that the cortical receptor, Num1, may play a role in dynein activation because it is the site of dynein activity. I investigated this hypothesis in Chapter 2 and concluded that Num1 is sufficient to activate dynein motility and likely does this by either enhancing dynein-dynactin interaction or releasing Pac1/Lis1 binding from the motor complex. These two mechanisms are not mutually exclusive, and I explore them in Chapters 4 and 5.

Figure 1.2

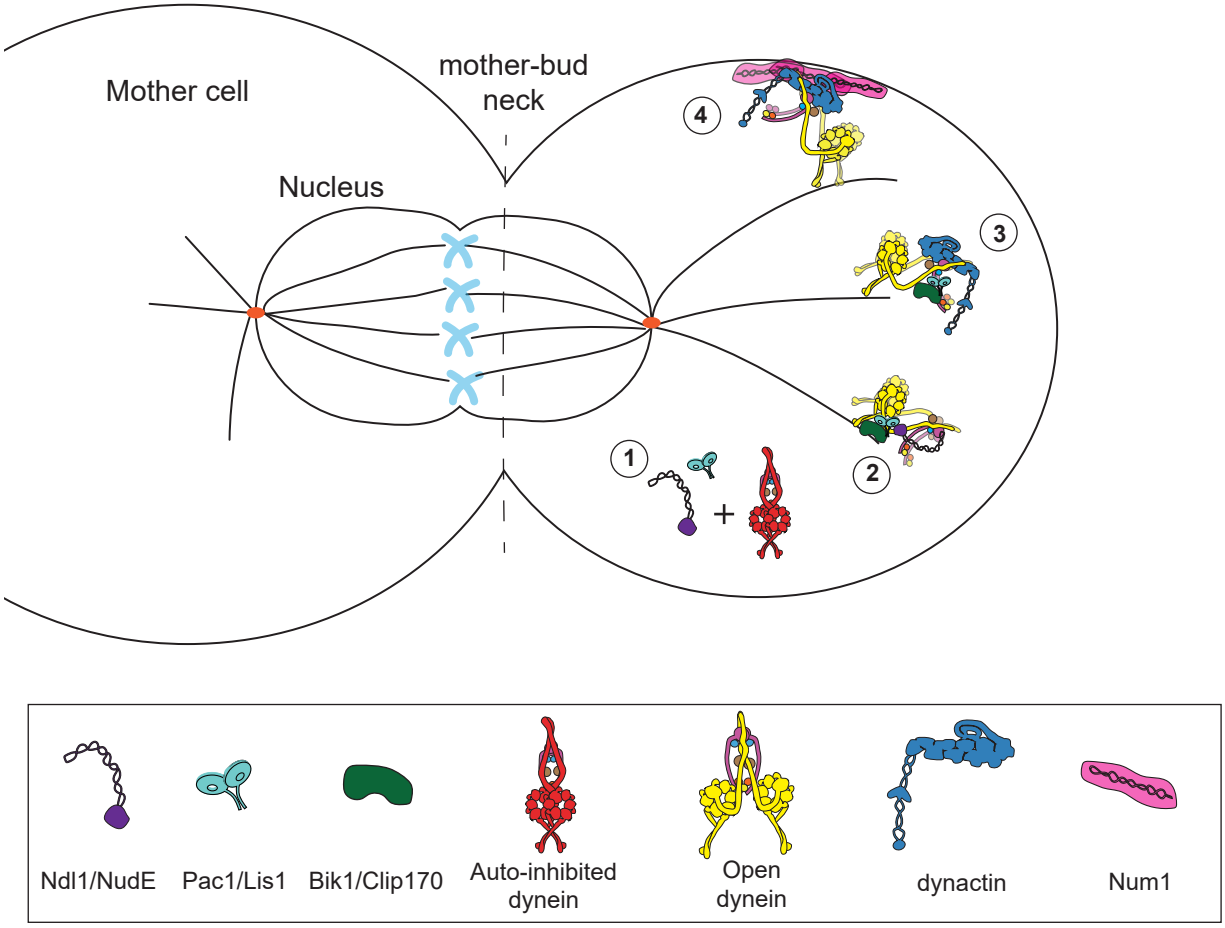

Figure 1.2. Dynein pathway for spindle positioning in budding yeast. Cartoon representation of the steps in dynein regulation to be recruited to the its site of activity-the cortex- to pull on astral microtubules and position the mitotic spindle between the mother and daughter cells. The drawing shows for 4 points of regulation. 1. Dynein associates with Pac1/Lis1 and Ndl1/NudE to open up its autoinhibition. 2. Open dynein is targeted to astral microtubule plus ends and tip tracks through association with Pac1/Lis1 and Bik1/Clip170. 3. Dynein associates with dynactin. 4. Dynein-dynactin is offloaded to Num1 cortical sites and becomes active upon Pac1/Lis1 release to pull the spindle into position at the mother-bud neck.

Next, I explored how the regulatory protein, Ndl1/NudE, may have a role in dynein activation in Chapter 3. Although Ndl1/NudE has been identified as a partner to Pac1/Lis1, its role in spindle positioning is not clear (Li et al., 2005). In humans, Ndl1/NudE works with Pac1/Lis1, but also maintains independent functions (Sasaki et al., 2005). I determined that depending on the context, Ndl1/NudE can improve Pac1/Lis1-mediated targeting of dynein or it can compete for Pac1/Lis1 binding to dynein, potentially as a mechanism for Pac1/Lis1 release.

In Chapter 4, I reconstituted dynein motility in vitro to examine how dynactin and Num1 may enhance dynein movement along microtubules. Dynactin is required for most dynein functions in humans and has been shown to reorient the motor domains for processive movement with the aid of an adapter protein (McKenney et al., 2014; Schlager et al., 2014; Urnavicius et al., 2015). However, the function of dynactin and a possible adapter have not been defined in yeast. Here, I determined the best conditions to visualize complete dynactin complexes and purified Num1 constructs to test whether Num1 can act as an adapter protein to enhance dynein-dynactin motility.

The second mechanism of Num1-mediated dynein activation suggests that Pac1 release is required. Pac1 targets dynein to microtubule plus ends but does not localize to the cortex (Lee et al., 2003b; Markus and Lee, 2011). Further, work in Chapter 2 shows that loss of Pac1/Lis1 association with dynein coincides with Num1 activation. I wondered if the mechanism of Pac1/Lis1 release involved structural changes in the dynein motor domain triggered during offloading to Num1. In Chapter 5, I generated dynein mutations that restrict allosteric communication in the motor to test how this may affect Pac1 dissociation from the complex.

CHAPTER 2

THE DYNEIN CORTICAL ANCHOR NUM1 ACTIVATES DYNEIN MOTILITY BY RELIEVING PAC1/LIS1-MEDIATED INHIBITION [1]

2.1 INTRODUCTION

The means by which dynein is delivered to the cell cortex and subsequently activated to pull on astral microtubules emanating from spindle poles in order to move the spindle are unclear. Recent studies in budding and fission yeast have revealed two distinct mechanisms by which dynein can be targeted to the cell cortex, its site of action in both organisms. During meiotic prophase in fission yeast, studies suggest that dynein first binds along astral microtubules that are in close proximity to the cell cortex (Ananthanarayanan et al., 2013). Rather than walking toward the minus end of these microtubules, dynein undergoes one dimensional diffusion until it encounters Mcp5, its cortical anchor. Once bound to Mcp5, dynein motors switch from diffusive to directed motion, and consequently move the spindle appropriately. Thus, in addition to anchoring dynein at the cortex, Mcp5 appears to activate dynein motility by an unknown mechanism.

A similar but somewhat distinct scenario takes place in budding yeast, in which dynein is first targeted to the plus ends of astral microtubules before being offloaded to cortical Num1 (Mcp5 homolog) receptor sites where it functions to move the mitotic spindle toward the daughter cell (Adames and Cooper, 2000; Lee et al., 2005; Markus and Lee, 2011). It is unknown if dynein

[1] The work in this chapter was published in October 2015 under same title. The introduction has been re-written for this dissertation.

S.M. conceived the content; S.M. wrote the original manuscript with input from me. I contributed in data collection, analysis, and interpretation.

Lammers, L.G., and S.M. Markus. 2015. The dynein cortical anchor Num1 activates dynein motility by relieving Pac1/LIS1-mediated inhibition. *J. Cell Biol.* 1–14. doi:10.1083/jcb.201506119.

motility is activated subsequent to offloading; however, several lines of evidence suggest its activity is switched from being off at plus ends, to being on at the cell cortex. For instance, in spite of its minus end-directed motility, dynein is transported to, and remains associated with the plus ends of dynamic microtubules (Carvalho et al., 2004; Lee et al., 2003b). Plus end-targeting requires the dynein motor domain, the +TIP Bik1 (CLIP-170 homolog), and the dynein associated factor Pac1 (Lis1 homolog) (Lee et al., 2003b; Markus et al., 2009; Sheeman et al., 2003). Recent studies suggest that Pac1 plays two distinct and important roles in targeting dynein to plus ends. First, Pac1 mediates the interaction between dynein and plus end-bound Bik1 (Roberts et al., 2014a; Sheeman et al., 2003). Second, by inhibiting dynein motility (Huang et al., 2012; Markus and Lee, 2011), and/or by prolonging its microtubule attachment (Huang et al., 2012; McKenney et al., 2010; Yamada et al., 2008), Pac1 holds dynein at plus ends by keeping dynein in a non-motile, or "off" state. Thus, plus end-associated dynein may be poised to walk toward the minus ends of microtubules, but is prevented from doing so by Pac1. However, upon offloading to cortical Num1 receptor sites, dynein is active, as apparent by its capacity to pull on astral microtubules, and consequently move the spindle. Thus, in budding yeast, as in fission yeast, dynein may undergo a switch in its activity upon attachment to its cortical receptor. However, evidence for such a switch is lacking.

Although factors have been identified that can inhibit dynein motility (*e.g.*, MAP4, She1, Pac1) (Huang et al., 2012; Markus et al., 2012; Markus and Lee, 2011; Samora et al., 2011), it remains unclear whether or not dynein from organisms other than fission yeast need to be switched on to perform their cellular functions, or whether they are constitutively active. Recent studies have indicated that purified metazoan dynein is functional for motility in ensemble assays (*e.g.*, microtubule gliding), but requires a stable interaction with the dynactin complex for single molecule processivity (McKenney et al., 2014; Schlager et al., 2014). Stabilization of the dynein-dynactin interaction by various coiled-coil-containing adaptor proteins (*e.g.*, BicD2, Spindly, Hook3, Rab11-Fip3) is sufficient to significantly enhance dynein processivity, and thereby

"activate" dynein motility. This is in contrast to budding yeast dynein, which is processive in the absence of dynactin or other adaptors or regulators (Reck-Peterson et al., 2006). It is unclear if such a mechanism generally governs dynein regulation within a cell given that certain functions of dynein in animal cells, such as centrosome anchoring, pole focusing, and spindle length regulation have been shown to occur independently of several such adaptors (Raaijmakers et al., 2013). It is also unclear if dynactin-mediated processivity enhancement is the means by which cortical dynein activity is promoted. Interestingly, plus end association of dynein in higher eukaryotes – which occurs in a dynactin-dependent manner – does not require such adaptor proteins (Duellberg et al., 2014; Splinter et al., 2012). Given the lack of minus end-directed motility of these plus end associated dynein motors, an interaction between dynein and dynactin is not necessarily sufficient to active dynein motility.

Using budding yeast, we set out to test the hypothesis that binding of dynein-dynactin to its cortical receptor provides the switch that activates cortical dynein activity. Dynein pathway function is best understood in this genetically tractable organism, in which many of the regulatory components and accessory chains, which are each encoded by only one gene, are highly conserved. We found that overexpression of the dynein-dynactin-interacting coiled-coil domain of Num1 ($Num1_{CC}$) is sufficient to activate dynein motility, causing a depletion of dynein-dynactin from microtubule plus ends, their accumulation at minus ends, and their apparent minus end-directed motility along astral microtubules. Our data reveal that the mechanism for this activation is likely a $Num1_{CC}$-mediated release of Pac1 – a potent dynein inhibitor – from the dynein motor domain.

2.2 RESULTS

Overexpression of $Num1_{CC}$ depletes dynein-dynactin from microtubule plus ends

A recent study revealed that the N-terminal coiled-coil domain of Num1 – the dynein cortical receptor – directly interacts with dynein-dynactin complexes (Tang et al., 2012). If this region of Num1 ($Num1_{CC}$; Figure 2.1A) is sufficient to activate dynein motility, we reasoned that

its overexpression would result in: (1) the depletion of dynein and dynactin from microtubule plus ends; and, (2) an accumulation of dynein-dynactin at spindle pole bodies (SPBs), where microtubule minus ends are anchored (Figure 2.1B). We found this latter phenomenon to be an inherent property of dynein motility, as single molecule motility experiments demonstrated that upon reaching the end of a microtubule, dynein pauses for several seconds before detaching, much longer than the ~0.1 second per step dwell time (Figure S1.1 and Video S1.1[2]). To test our hypothesis, we engineered yeast cells such that the galactose-inducible *GAL1* promoter (*GAL1p*) was immediately upstream of a truncated *num1$_{CC}$* allele (Figure 2.1C). Since Num1$_{CC}$ is expressed from the native *NUM1* locus, these cells do not possess a full-length Num1. Consequently, dynein and dynactin are excluded from the cell cortex, and are unable to properly orient the spindle in these cells.

In the absence of Num1$_{CC}$ induction (by growth in glucose-containing media), we observed fluorescent foci of functional Dyn1- (dynein heavy chain) and Jnm1-3mCherry (p50 subunit of dynactin) fusions (Markus et al., 2011) at microtubule plus ends in 77.2% and 41.4% of cells, respectively (Figure 2.1D and E). In contrast, upon induction of Num1$_{CC}$ overexpression (by growth in galactose-containing media) the number of cells exhibiting Dyn1- and Jnm1-3mCherry plus end foci was reduced by approximately 5-fold, to 14.8% and 8.1%, respectively. Fluorescence intensity measurements revealed that those plus ends with Dyn1- and Jnm1-3mCherry foci had significantly fewer molecules of each upon Num1$_{CC}$ overexpression (Figure 2.1F). Coincident with the reduction in plus end dynein and dynactin, we also observed a 4 to 5-fold increase in the number of cells with Dyn1- and Jnm1-3mCherry foci at SPBs upon Num1$_{CC}$ induction (also see Figure 2.4A, bottom). We observed similar results for Pac11-3mCherry (dynein intermediate chain) and Dyn3-3mCherry (dynein light-intermediate chain; Figure S1.2A - E). In contrast, overexpression of Num1$_{CC}$ had no effect on the extent of plus end localization of

[2] Supplementary figures refer to Appendix 1. Videos can viewed in the published paper online at DOI: 10.1083/jcb.201506119 supplementary data.

Figure 2.1

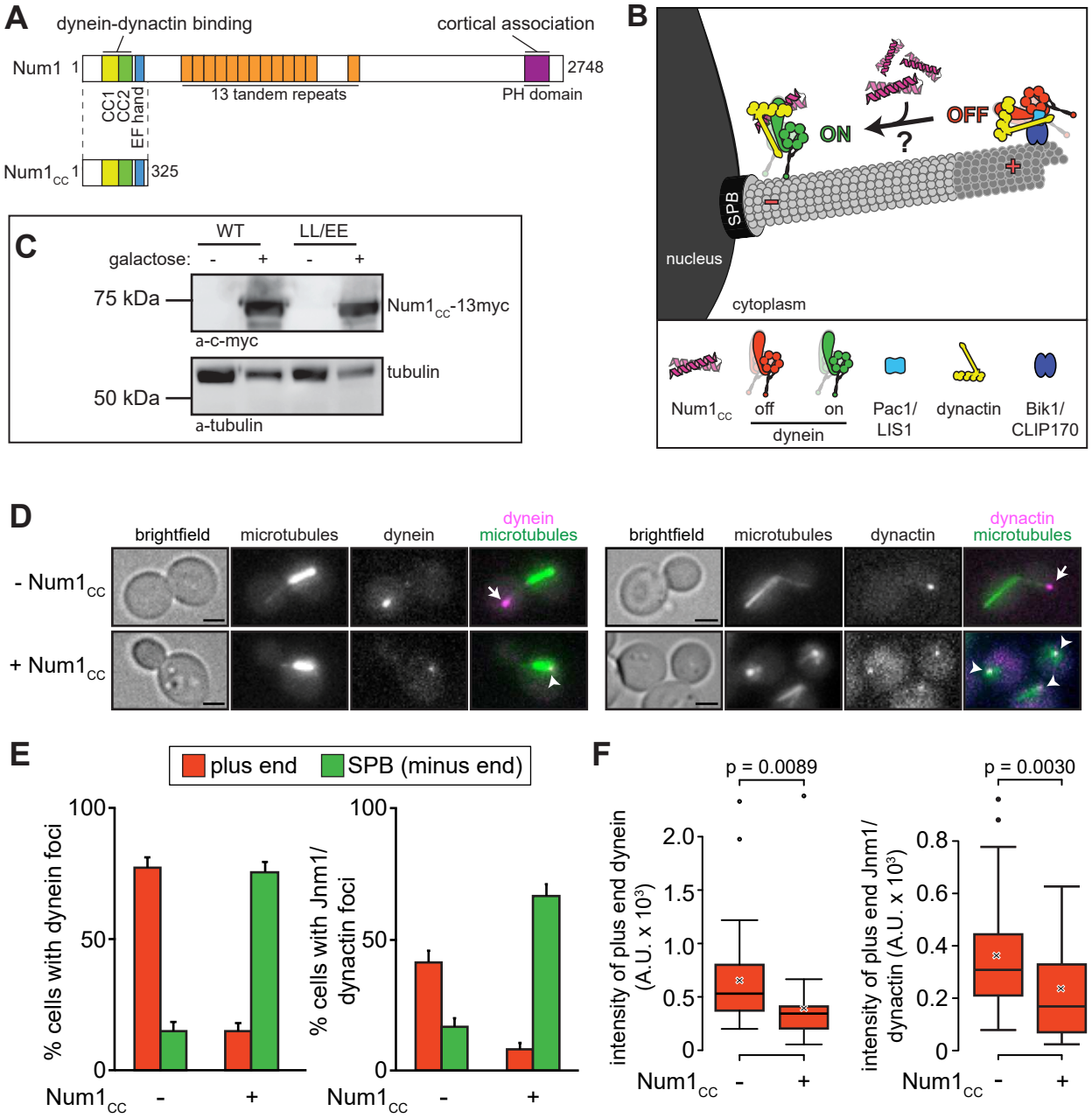
A
dynein-dynactin binding
cortical association
Num1
1
2748
CC1
CC2
EF hand
13 tandem repeats
PH domain
Num1cc
1
325
B
ON
OFF
?
SPB
nucleus
cytoplasm
Num1cc
off
on
dynein
Pac1/
LIS1
dynactin
Bik1/
CLIP170
C
WT
LL/EE
galactose:
- + - +
75 kDa
Num1cc-13myc
a-c-myc
50 kDa
tubulin
a-tubulin
D
brightfield
microtubules
dynein
dynein
microtubules
brightfield
microtubules
dynactin
dynactin
microtubules
- Num1cc
+ Num1cc
E
plus end
SPB (minus end)
% cells with dynein foci
% cells with Jnm1/
dynactin foci
100
50
0
Num1cc
-
+
F
p = 0.0089
p = 0.0030
intensity of plus end dynein
(A.U. x 10³)
intensity of plus end Jnm1/
dynactin (A.U. x 10³)
2.0
1.5
1.0
0.5
0
0.8
0.6
0.4
0.2
0
Num1cc
-
+

Figure 2.1. Overexpression of Num1$_{CC}$ depletes dynein and dynactin from microtubule plus ends. (A) Schematic representation of Num1 and Num1$_{CC}$ with domain structure indicated (CC1 and CC2, predicted coiled-coil domains; PH, pleckstrin homology domain). (B) Diagram depicting experimental design (see text). (C) Western blot of *GAL1p:num1$_{CC}$-13myc* (wild-type or LL/EE mutant) cells grown in the absence or presence of galactose, as indicated, with loading control (anti-alpha-tubulin). (D) Representative images of *GAL1p:num1$_{CC}$* cells expressing mTurquoise2-Tub1 (alpha-tubulin) and either Dyn1-3mCherry (left) or Jnm1-3mCherry (right) used for quantitation in panels E and F. Cells were grown to mid-log phase in SD media supplemented with glucose (uninduced; - Num1$_{CC}$) or galactose plus raffinose (induced; + Num1$_{CC}$). Each image is a maximum intensity projection of a 2-µm Z-stack of wide-field images. Arrows indicate plus end foci, and arrowheads indicate SPB foci. Scale bars correspond to 2 µm. (E) The percentage of cells that exhibit plus end (red) or SPB (green) fluorescent foci is plotted for the strains shown in panel D. Plus end or SPB foci were identified in two-color movies and scored accordingly (see Materials and Methods). Error bars represent standard error of proportion (n ≥ 114 cells). (F) Box plot of fluorescence intensity values of plus end associated Dyn1- or Jnm1-3mCherry foci (n ≥ 30 foci). Whiskers define the range of data, boxes encompass the 25th to 75th quartiles, the line depicts the median value, and the "x" depicts the mean value. See also Video S2.1 and Figures S2.1, S2.2, S2.3.

Bik1-3mCherry (CLIP170 homolog), a protein that is required for the plus end targeting of dynein (Figure S1.2F - G) (Sheeman et al., 2003). To determine if there is a cell cycle regulated component to Num1$_{CC}$-mediated dynein relocalization, we categorized plus end and SPB localization frequencies into: G1, preanaphase and anaphase (as determined by cell and spindle morphology; see Figure S1.2H). Although both G1 and preanaphase cells exhibited an equivalent extent of Num1$_{CC}$-mediated dynein relocalization, we found that anaphase cells were less susceptible to dynein plus end depletion, in spite of a significant enhancement in the prevalence of SPB localized dynein in these cells (Figure S1.2H). This is consistent with the higher frequency of dynein plus end-localization noted in wild-type anaphase cells (Markus et al., 2009; Sheeman et al., 2003), and further suggests that the plus end targeting mechanism is more robust at this point of the cell cycle. Taken together, our data indicate that overexpression of Num1$_{CC}$ specifically depletes dynein-dynactin from microtubule plus ends.

We next wanted to determine whether a Num1-dynein interaction was required for the plus end depletion phenotype. First, we introduced two point mutations within Num1$_{CC}$ (L167E L170E; Num1$_{CC}$ $^{LL/EE}$; Figure 2.2A) that disrupt its interaction with dynein-dynactin, but have no effect on Num1 localization, or its mitochondria cortical attachment function (Tang et al., 2012).

We found that overexpression of $Num1_{CC}^{LL/EE}$ (Figure 2.1C) had no effect on dynein plus end or SPB localization (Figure 2.2B and C), indicating that an intact dynein-dynactin binding surface within $Num1_{CC}$ is required for plus end depletion. Second, we used two dynein motor domain variants ($Dyn1_{MOTOR}$ and GST-$Dyn1_{MOTOR}$) that are sufficient for association with microtubule plus ends, but lack the N-terminal tail domain that is required for association with Num1 (Figure 2.2D) (Markus et al., 2009). We found that $Num1_{CC}$ overexpression had little effect on the frequency by which monomeric (non-motile) $Dyn1_{MOTOR}$-3YFP, or the dimeric (motile (Reck-Peterson et al., 2006)) GST-$Dyn1_{MOTOR}$-3mCherry fragment was observed at plus ends or SPBs (Figure 2.2E and F). Taken together, these data indicate that $Num1_{CC}$-mediated plus end depletion of dynein requires an interaction between dynein and $Num1_{CC}$. Several lines of evidence indicate that an intact dynein-dynactin complex is required for interaction with Num1. Yeast dynactin deletion mutants exhibit a complete loss of cortical dynein, and a higher than normal accumulation of dynein at microtubule plus ends (Lee et al., 2005, 2003b). This latter observation is also noted in *num1*Δ mutants (Lee et al., 2003b), and is presumed to be due to an inability to offload dynein-dynactin to cortical Num1 receptor sites. Finally, a bead-immobilized recombinant $Num1_{CC}$ fragment was sufficient to isolate dynein from cell extracts, but was unable to do so from extracts prepared from *nip100*Δ cells (homolog of human dynactin component $p150^{Glued}$) (Tang et al., 2012). To determine if $Num1_{CC}$ can deplete plus end dynein in the absence of dynactin, we overexpressed $Num1_{CC}$ in *nip100*Δ cells. We found that $Num1_{CC}$ overexpression reduced the frequency of dynein plus end localization in *nip100Δ* cells to a lesser extent than in *NIP100* cells (Figure S1.3A and B; 38% reduction in *nip100*Δ, versus 81% reduction in *NIP100* cells; compare to Figure 2.1E); however, fluorescence intensity measurements of plus end dynein revealed no significant difference (Figure S1.3C). These data suggest that the ability of dynein to interact with $Num1_{CC}$ is compromised, but not abolished in the absence of dynactin.

We next asked if plus end targeting of dynein is a requisite for $Num1_{CC}$-mediated accumulation of dynein at SPBs. To test this, we deleted either Pac1 or Bik1, both of which are

Figure 2.2

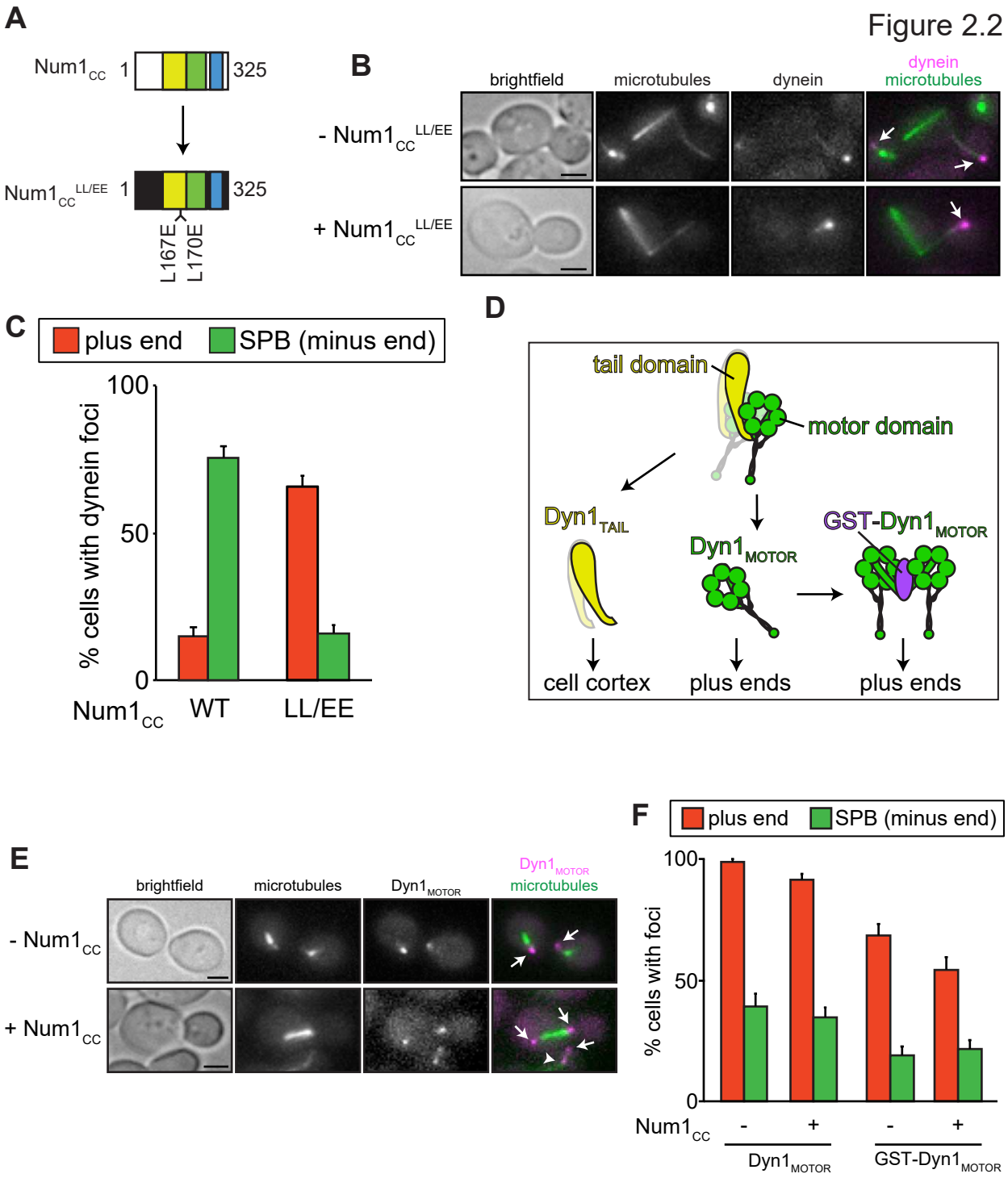
A
Num1CC 1 325
Num1CC LL/EE 1 325
L167E
L170E
B
brightfield
microtubules
dynein
dynein microtubules
- Num1CC LL/EE
+ Num1CC LL/EE
C
plus end
SPB (minus end)
% cells with dynein foci
100
50
0
Num1CC
WT
LL/EE
D
tail domain
motor domain
Dyn1TAIL
Dyn1MOTOR
GST-Dyn1MOTOR
cell cortex
plus ends
plus ends
E
brightfield
microtubules
Dyn1MOTOR
Dyn1MOTOR microtubules
- Num1CC
+ Num1CC
F
plus end
SPB (minus end)
% cells with foci
100
50
0
Num1CC
-
+
-
+
Dyn1MOTOR
GST-Dyn1MOTOR

Figure 2.2. Interaction between dynein and Num1$_{CC}$ is required for plus end depletion. (A) Schematic representation of the Num1$_{CCLL/EE}$ mutant. (B) Representative images of *GAL1p:num1$_{CCLL/EE}$* and *GAL1p:num1$_{CC}$* cells expressing mTurquoise2-Tub1 and Dyn1-3mCherry used for quantitation in panel C. (C) The percentage of cells that exhibit plus end (red) or SPB (green) fluorescent foci is plotted for the strains overexpressing wild-type (WT) or mutant (LL/EE) Num1$_{CC}$. Error bars represent standard error of proportion (n ≥ 170 cells). (D) Diagram depicting dynein N- (tail) and C- (motor) terminal domains, and artificially dimerized GST-Dyn1$_{MOTOR}$ construct (see text). (E) Representative images of *GAL1p:num1$_{CC}$* cells expressing mTurquoise2-Tub1 and Dyn1$_{MOTOR}$-3YFP used for quantitation in panel F. (F) The percentage of cells that exhibit plus end (red) or SPB (green) fluorescent Dyn1$_{MOTOR}$-3YFP or GST Dyn1$_{MOTOR}$-3mCherry foci is plotted. Error bars represent standard error of proportion (n ≥ 87 cells). All images are maximum intensity projections of a 2-µm Z-stack of wide- field images. Arrows indicate plus end foci, and arrowhead indicates SPB focus. Scale bars correspond to 2 µm.

required for dynein plus end-targeting (Lee et al., 2003b; Sheeman et al., 2003). As expected, neither *pac1*Δ nor *bik1*Δ cells overexpressing Num1$_{CC}$ exhibited plus end dynein foci; additionally, SPB localization of dynein was apparent in only a small number of cells in both mutants, suggesting that the accumulation of dynein at SPBs requires a pool of dynein-dynactin at plus ends from which to draw (Figure S1.3D – G).

Microtubule binding by dynein is required for plus end depletion

If Num1$_{CC}$-mediated redistribution of dynein from plus ends to SPBs is a consequence of activated dynein motility, then we reasoned that a motility incompetent dynein mutant would remain associated with plus ends in the presence of overexpressed Num1$_{CC}$. To test this, we generated a dynein mutant lacking its microtubule-binding domain (Figure 2.3A; Dyn1$_{\Delta MTBD}$). Surprisingly, we found that in the absence of Num1$_{CC}$ induction, Dyn1$_{\Delta MTBD}$ was capable of plus end-binding (Figure 2.3B, top, and Figure 2.3C), indicating that dynein associates with plus ends independently of its MTBD, and thus likely through its interaction with Pac1 and Bik1. Furthermore, we found that the extent of plus end localization of Dyn1$^{\Delta MTBD}$ was greater than wild-type Dyn1 (26% increase in frequency; 148% increase in intensity; $p < 0.0001$), while its SPB localization was lower (Figure 2.3C and D; compare to Figure 2.1E and F). These data suggest that SPB localization of dynein in wild-type cells may be due to minus end-directed motility of

active dynein motors. Consistent with our hypothesis, upon induction of Num1$_{CC}$ overexpression, Dyn1$^{\Delta MTBD}$ localization to plus ends and SPBs remained unchanged (Figure 2.3C and D), suggesting that Num1$_{CC}$-mediated depletion of dynein from plus ends, and accumulation at SPBs both require dynein motility.

Num1$_{CC}$ has only a modest effect on dynein-dynactin interaction at plus ends

In contrast to yeast dynein, metazoan dynein exhibits mostly non-processive, diffusive motility in single molecule assays (McKenney et al., 2014; Miura et al., 2010; Schlager et al., 2014). A family of coiled-coil containing adaptor proteins that recruit dynein and dynactin to various cellular sites were recently shown to be sufficient to activate processive single molecule motility by stably linking dynein to dynactin (McKenney et al., 2014; Schlager et al., 2014). Like these adaptor proteins, Num1 interacts only with intact dynein-dynactin complexes through its coiled-coil domain (Splinter et al., 2012; Tang et al., 2012). Although dynein recruits dynactin to plus ends in a Num1-independent manner, dynactin is present at substoichiometric amounts relative to dynein (~3 dynein to 1 dynactin) (Markus et al., 2011). Thus, we reasoned that Num1$_{CC}$ may activate dynein motility by enhancing the dynein-dynactin interaction at plus ends. To test this, we assessed the extent by which Num1$_{CC}$ affects dynein-mediated recruitment of dynactin to plus ends. For these experiments, we used *dyn1$_{\Delta MTBD}$* mutant cells, in which dynein remains associated at plus ends in spite of Num1$_{CC}$ overexpression (see Figure 2.3B – D). We found that Num1$_{CC}$ overexpression had no effect on the frequency of observing plus end localized dynactin (*i.e.*, Jnm1- or Nip100-3mCherry; Figure 2.3E – G); however, the fluorescence intensities of both Jnm1 and Nip100 at plus ends were modestly, but significantly increased (Figure 2.3H; 58.9% and 30.9%, respectively; $p \leq 0.0012$), suggesting that Num1$_{CC}$ may in fact enhance or stabilize the dynein-dynactin interaction. However, given the small apparent change in dynein-dynactin interaction at plus ends, and the observation that yeast dynein processivity enhancement by dynactin does not require additional factors *in vitro* (*i.e.*, Num1) (Kardon et al., 2009), it is unclear

Figure 2.3

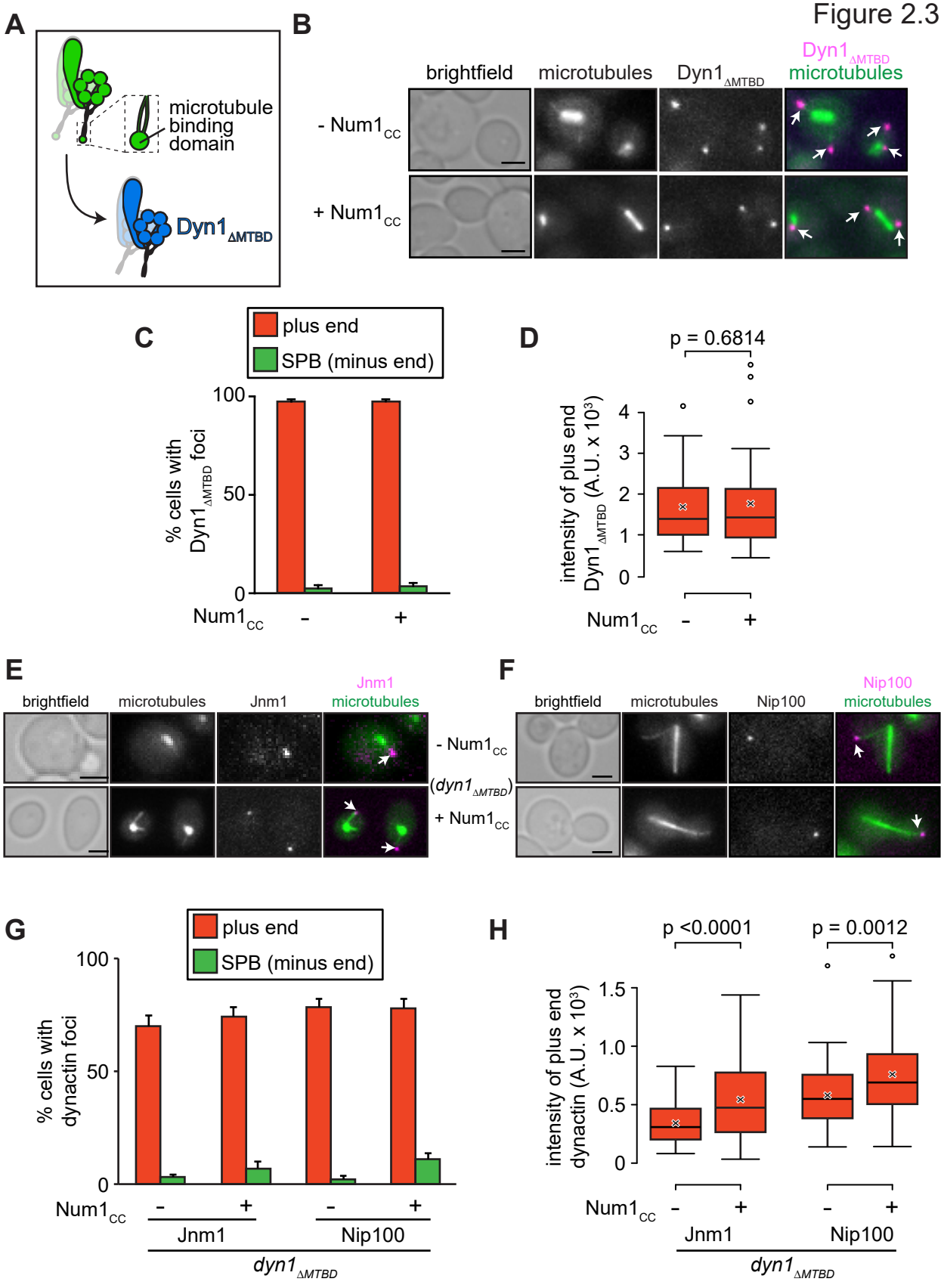
A
microtubule binding domain
Dyn1 ΔMTBD
B
brightfield
microtubules
Dyn1 ΔMTBD
Dyn1 ΔMTBD microtubules
- Num1CC
+ Num1CC
C
plus end
SPB (minus end)
% cells with Dyn1 ΔMTBD foci
100
50
0
Num1CC - +
D
p = 0.6814
intensity of plus end Dyn1 ΔMTBD (A.U. x 10³)
4
3
2
1
0
Num1CC - +
E
brightfield
microtubules
Jnm1
Jnm1 microtubules
- Num1CC
(dyn1 ΔMTBD)
+ Num1CC
F
brightfield
microtubules
Nip100
Nip100 microtubules
G
plus end
SPB (minus end)
% cells with dynactin foci
100
50
0
Num1CC - + - +
Jnm1
Nip100
dyn1 ΔMTBD
H
p <0.0001
p = 0.0012
intensity of plus end dynactin (A.U. x 10³)
1.5
1.0
0.5
0
Num1CC - + - +
Jnm1
Nip100
dyn1 ΔMTBD

Figure 2.3. The dynein microtubule binding-domain is dispensable for plus end-targeting, but required for Num1$_{CC}$-mediated plus end depletion. (A) Schematic representation of the Dyn1$_{\Delta MTBD}$ mutant. (B) Representative images of *GAL1p:num1$_{CC}$* cells expressing mTurquoise2-Tub1 and Dyn1$_{\Delta MTBD}$-3mCherry used for quantitation in panels C and D. (C) The percentage of cells that exhibit plus end (red) or SPB (green) Dyn1$_{\Delta MTBD}$-3mCherry foci is plotted for cells shown in panel B. Error bars represent standard error of proportion (n ≥ 126 cells). (D) Box plot of fluorescence intensity values of plus end associated Dyn1$_{\Delta MTBD}$-3mCherry (n ≥ 40 foci). (E and F) Representative images of *GAL1p:num1$_{CC}$ dyn1$_{\Delta MTBD}$* cells expressing mTurquoise2-Tub1 and either (E) Jnm1-, or (F) Nip100-3mCherry used for quantitation in panels G and H. (G) The percentage of *dyn1$_{\Delta MTBD}$* cells that exhibit plus end or SPB Jnm1- or Nip100-3mCherry foci is plotted for *GAL1p:num1$_{CC}$* cells grown in glucose (-Num1$_{CC}$) or galactose (+Num1$_{CC}$; n ≥ 100 cells). (H) Box plot of fluorescence intensity values of plus end associated Jnm1- or Nip100-3mCherry (n ≥ 56 foci). For all box plots, whiskers define the range of data, boxes encompass the 25th to 75th quartiles, the line depicts the median value, and the "x" depicts the mean value. All images are maximum intensity projections of a 2-µm Z-stack of wide-field images. Arrows indicate plus end foci. Scale bars correspond to 2 µm. See also Figure S1.5.

if stabilization of the dynein-dynactin interaction is the mechanism by which Num1 functions to activate dynein motility. For these reasons, we explored an alternative hypothesis.

Overexpression of Num1$_{CC}$ reduces colocalization of dynein and Pac1

Cells in which Pac1 is deleted exhibit a complete loss of plus end dynein (Lee et al., 2003b; Markus et al., 2009), similar to our observations of cells overexpressing Num1$_{CC}$. We hypothesized that Num1$_{CC}$ may deplete dynein from plus ends by interfering with dynein-Pac1 binding. To test this, we assessed localization of a functional Pac1-3mCherry fusion (Markus et al., 2011) in cells overexpressing Num1$_{CC}$. As we observed for dynein and dynactin, Pac1-3mCherry foci were depleted from microtubule plus ends upon Num1$_{CC}$ overexpression (Figure 2.4A and B), consistent with their codependence for plus end-targeting (Markus et al., 2011). However, in contrast to dynein and dynactin, the fraction of cells exhibiting Pac1-3mCherry foci at SPBs was reduced with respect to cells not expressing Num1$_{CC}$, suggesting that dynein localizes at SPBs without Pac1 upon Num1$_{CC}$ overexpression. This reduction in localization was not due to a decrease in Pac1 protein expression or stability, as evidenced by immuoblotting (Figure 2.4D). Consistent with a Num1$_{CC}$-mediated reduction in the dynein-Pac1 interaction, we found that the fraction of Dyn1-3YFP and Pac1-3mCherry foci that colocalized (either SPB or plus

end) was reduced upon induction of Num1$_{CC}$ (from 59.6% to 26.2%; Figure 2.4E), while the fraction of Dyn1-3YFP foci alone (*i.e.*, not colocalized with Pac1) increased (from 28.3% to 62.3%). These data suggest that overexpression of Num1$_{CC}$ may disrupt plus end binding of dynein-dynactin by interfering with the dynein-Pac1 interaction.

We next wanted to determine whether the reduction in Pac1-dynein colocalization was a direct consequence of Num1$_{CC}$-mediated Pac1-dynein dissociation, or whether it was a secondary consequence of dynein plus end depletion. To distinguish between these two possibilities, we ectopically targeted dynein to the plasma membrane using an exogenous PH (pleckstrin homology) domain, and assessed the degree of colocalization of Pac1 with cortical PH-Dyn1 in the presence of either Num1$_{CC}^{LL/EE}$, or Num1$_{CC}$. We found that the PH domain was sufficient to target dynein (Figure 2.4F and S2.4A) and dynactin (*i.e.*, Jnm1; Figure S1.4B) to the cell cortex in cells lacking cortical Num1. Interestingly, we found a greater frequency of cortical PH-Dyn1-3mCherry foci in Num1$_{CC}$-overexpressing cells than in either Num1$_{CC}^{LL/EE}$ overexpressing cells (45.5% versus 13.9%, respectively), or *NUM1* cells (21.3%; not shown). In addition, we noted that Num1CC-overexpressing cells exhibited larger cortical patches than either wild-type *NUM1*, or Num1$_{CC}$ $^{LL/EE}$-overexpressing cells (Figure S1.4A, and data not shown). These data suggest that PH-Dyn1-Num1$_{CC}$ complexes may be oligomerizing at the cell cortex, which is consistent with the previously described role for the Num1$_{CC}$ domain in assembly of higher order cortical patches (Tang et al., 2012). In cells overexpressing Num1$_{CC}^{LL/EE}$, Pac1-3YFP colocalized with 65.3% of cortical PH-Dyn1-3mCherry foci; however, upon overexpression of Num1$_{CC}$, only 29.1% of PH-Dyn1-3mCherry foci contained Pac1-3YFP fluorescence (Figure 2.4G). Fluorescence intensity measurements also revealed a significant reduction in the number of Pac1 molecules associated with cortical PH-dynein patches (Figure 2.4H). In contrast, we noted no significant change in either the frequency or intensity of colocalized dynactin (*i.e.*, Jnm1; Figure 2.4I and J, and S2.4B). These data support the notion that Num1$_{CC}$ disrupts the dynein-Pac1 interaction, thereby leading to the plus end depletion phenotype.

Figure 2.4

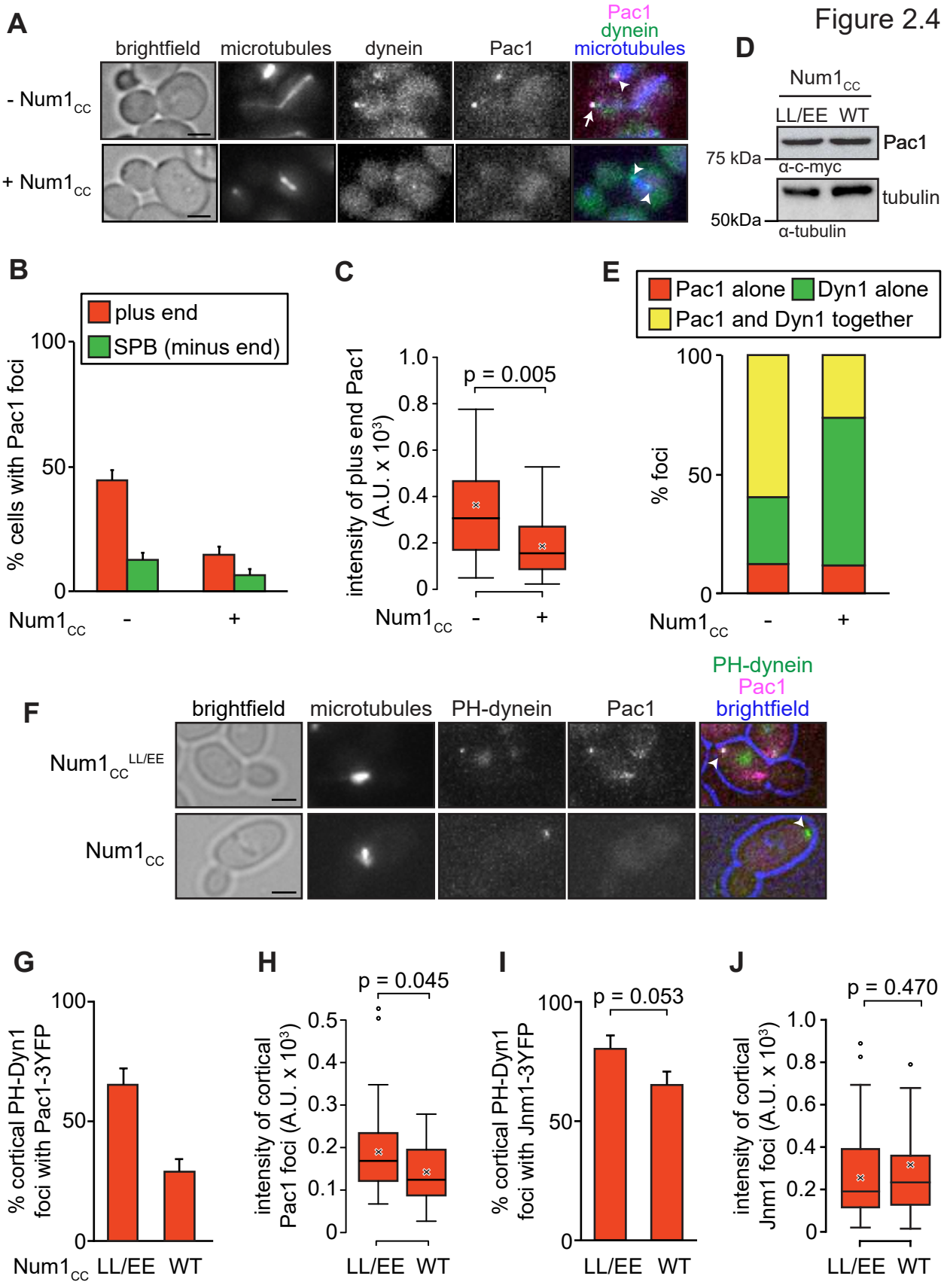
A
brightfield
microtubules
dynein
Pac1
Pac1
dynein
microtubules
- Num1CC
+ Num1CC
D
Num1CC
LL/EE WT
Pac1
75 kDa
α-c-myc
tubulin
50kDa
α-tubulin
B
plus end
SPB (minus end)
% cells with Pac1 foci
100
50
0
Num1CC - +
C
intensity of plus end Pac1 (A.U. x 10³)
1.0
0.8
0.6
0.4
0.2
0
p = 0.005
Num1CC - +
E
Pac1 alone
Dyn1 alone
Pac1 and Dyn1 together
% foci
100
50
0
Num1CC - +
F
brightfield
microtubules
PH-dynein
Pac1
PH-dynein
Pac1
brightfield
Num1CC LL/EE
Num1CC
G
% cortical PH-Dyn1 foci with Pac1-3YFP
100
50
0
Num1CC LL/EE WT
H
intensity of cortical Pac1 foci (A.U. x 10³)
0.5
0.4
0.3
0.2
0.1
0
p = 0.045
LL/EE WT
I
% cortical PH-Dyn1 foci with Jnm1-3YFP
100
50
0
p = 0.053
LL/EE WT
J
intensity of cortical Jnm1 foci (A.U. x 10³)
1.0
0.8
0.6
0.4
0.2
0
p = 0.470
LL/EE WT

Figure 2.4. Overexpression of Num1$_{CC}$ depletes Pac1 from plus ends and disrupts dynein-Pac1 interaction. (A) Representative images of *GAL1p:num1$_{CC}$* cells expressing mTurquoise2-Tub1, Pac1-3mCherry and Dyn1-3YFP used for quantitation in panels B, C and E. Arrow indicates plus end focus, and arrowheads indicate SPB foci. (B) The percentage of cells that exhibit plus end (red) or SPB (green) fluorescent Pac1-3mCherry foci is plotted for the cells shown in panel A. Error bars represent standard error of proportion (n ≥ 122 cells). (C) Box plot of fluorescence intensity values of plus end associated Pac1-3mCherry (n ≥ 26 foci). (D) Western blot of Pac1-13myc-expressing *GAL1p:num1$_{CC}$* or *GAL1p:num1$_{CC}^{LL/EE}$* cells (as indicated) grown in galactose-containing media, with loading control (anti-alpha-tubulin). (E) The extent of Pac1-3mCherry and Dyn1-3YFP colocalization is plotted for the indicated cells (n ≥ 61 fluorescent foci). (F) Representative images of *GAL1p:PH-DYN1-3mCherry* cells expressing Pac1-3YFP, and either Num1$_{CC}$ or Num1$_{CC}^{LL/EE}$. Arrowheads indicate cortical foci. (G and I) The percentage of cortical PH-Dyn1-3mCherry foci that colocalize with either (G) Pac1-3YFP (n ≥ 49 foci) or (I) Jnm1-3YFP (n ≥ 55 foci) is plotted for cells expressing either Num1$_{CC}$ or Num1$_{CC}^{LL/EE}$. (H and J) Box plot of fluorescence intensity values for either cortical (H) Pac1-3YFP (n ≥ 25 foci) or (J) Jnm1-3YFP foci (n ≥ 44 foci; one outlier was omitted from the plot for display purposes only). For all box plots, the whiskers define the range of data, boxes encompass the 25th to 75th quartiles, the line depicts the median value, and the "x" depicts the mean value. All images are maximum intensity projections of a 2-µm Z-stack of wide-field images. Scale bars correspond to 2 µm. See also Figure S1.4.

An enhanced Pac1 affinity mutant of dynein, or Pac1-overexpression reduces the extent of Num1$_{CC}$-mediated plus end depletion of dynein

If a Num1$_{CC}$-mediated Pac1 unbinding event is the cause for plus end depletion of dynein-dynactin complexes, we reasoned that we could reduce the extent of Num1$_{CC}$ mediated dynein depletion from microtubule plus ends by two different means: (1) enhancing the affinity of dynein for Pac1, or (2) overexpression of Pac1. To test the former, we used a yeast strain expressing a well characterized, motility competent dynein mutant (Dyn1$_{HL3}$) that exhibits higher affinity for Pac1 than wild-type dynein (Figure 2.5A) (Markus and Lee, 2011). We predicted that Dyn1$_{HL3}$ and Pac1 would be less susceptible to Num1$_{CC}$-mediated plus end depletion as a result of their higher affinity. Consistent with our hypothesis, induction of Num1$_{CC}$ overexpression reduced the frequency of observing Dyn1$_{HL3}$-3YFP and Pac1-3mCherry plus end foci by 40% and 22%, respectively (Figure 2.5B and C), much less than what we observed in wild-type *DYN1* cells (respective 81% and 67% reduction; compare to Figure 2.1E and 2.4B). Fluorescence intensity measurements revealed no significant change in the number of Dyn1$_{HL3}$ or Pac1 molecules at

Figure 2.5

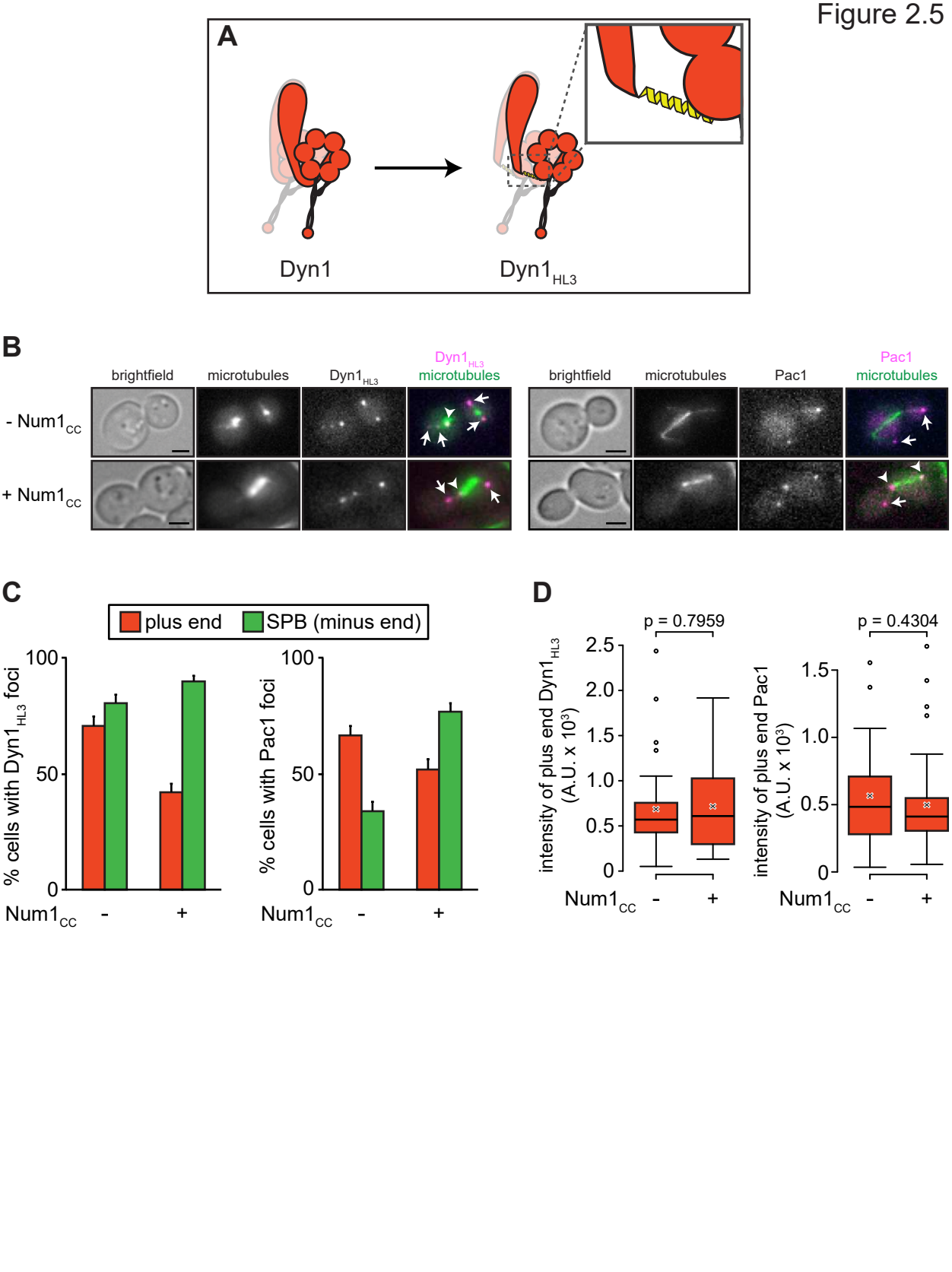
A
Dyn1
Dyn1HL3
B
brightfield
microtubules
Dyn1HL3
Dyn1HL3 microtubules
brightfield
microtubules
Pac1
Pac1 microtubules
- Num1CC
+ Num1CC
C
plus end
SPB (minus end)
% cells with Dyn1HL3 foci
% cells with Pac1 foci
100
50
0
Num1CC - +
D
p = 0.7959
p = 0.4304
intensity of plus end Dyn1HL3 (A.U. x 10³)
intensity of plus end Pac1 (A.U. x 10³)
2.5
2.0
1.5
1.0
0.5
0
Num1CC - +

Figure 2.5. Dyn1 $_{HL3}$ is less susceptible to Num1$_{CC}$-mediated plus end depletion. Diagram depicting Dyn1$_{HL3}$ high Pac1 affinity mutant, in which a helical linker has been inserted between the dynein tail and motor domains (Markus and Lee, 2011). (B) Representative images of *GAL1p:num1$_{CC}$* cells expressing mTurquoise2-Tub1, and either Dyn1$_{HL3}$-3YFP (left), or Dyn1$_{HL3}$ and Pac1-3mCherry (right) used for quantitation in panels C and D. Each image is a maximum intensity projection of a 2-µm Z-stack of wide-field images. Arrows indicate plus end foci, and arrowheads indicate SPB foci. Scale bars correspond to 2 µm. (C) The percentage of cells that exhibit plus end (red) or SPB (green) fluorescent Dyn1$_{HL3}$-3YFP (left), or Pac1-3mCherry (right) foci is plotted for the cells shown in panel B. Error bars represent standard error of proportion (n ≥ 119 cells). (D) Box plot of fluorescence intensity values of plus end associated Dyn1$_{HL3}$-3YFP or Pac1-3mCherry (n ≥ 33 foci). Whiskers define the range of data, boxes encompass the 25th to 75th quartiles, the line depicts the median value, and the "x" depicts the mean value. See also Figure S1.5.

plus ends upon Num1$_{CC}$ overexpression (Figure 2.5D). Thus, both Pac1 and Dyn1$_{HL3}$ are less susceptible to plus end depletion by Num1$_{CC}$ overexpression in *dyn1$_{HL3}$* cells.

To test whether overexpression of Pac1 could rescue plus end depletion, we replaced the native *PAC1* promoter with the *GAL1* promoter, which is sufficient to induce greater than 10-fold higher Pac1 expression levels when compared to wild-type cells (Markus et al., 2011). To establish a baseline for Pac1 overexpression-mediated enhancement of dynein plus end targeting, we first assessed dynein localization in cells overexpressing Pac1 and Num1$_{CC}^{LL/EE}$, the latter of which has no discernible effect on dynein targeting (see Figure 2.2B and C). In these cells, we observed an increase both in frequency and mean fluorescence intensity of plus end dynein by 44% and 170%, respectively (Figure 2.6B and D), when compared to cells overexpressing Num1$_{CC}^{LL/EE}$ and expressing native levels of Pac1. In comparison, overexpression of Pac1 and wild-type Num1$_{CC}$ reduced the frequency of plus end dynein by 47% ($p < 0.0001$; compare *GAL1p:PAC1 num1$_{CC}^{LL/EE}$* to *GAL1p:PAC1 num1$_{CC}$*), while the mean fluorescence intensity was not reduced significantly (30%; $p = 0.1636$; Figure 2.6B and D). These values are significantly less than the respective 78% and 37% reduction in frequency and intensity we observed when Num1$_{CC}$ alone was overexpressed (when compared to Num1$_{CC}^{LL/EE}$; Figure 2.6C and E). Thus, Pac1 overexpression reduces the extent by which Num1$_{CC}$ depletes dynein from microtubule plus ends.

If Num1$_{CC}$ depletes dynein from plus ends by inducing Pac1 release, then we reasoned that enhancing dynein plus end targeting by a Pac1-independent means would not be able to rescue plus end depletion to the same extent as Pac1 overexpression. To test this, we overexpressed Kip2, a kinesin-7 family member that affects steady-state microtubule length (see Figure 2.6A, bottom), and plays a role in transporting dynein to microtubule plus ends (Carvalho et al., 2004; Markus et al., 2009; Roberts et al., 2014a). As with Pac1, we first established a baseline by which Kip2 overexpression enhances dynein plus end localization by imaging Dyn1-3mCherry in *GAL1p:KIP2 GAL1p:num1$_{CC}^{LL/EE}$* cells. Consistent with a role for Kip2 in transporting dynein away from minus ends and towards plus ends, overexpression of Kip2 enhanced the frequency of dynein plus end-targeting by 19%, and reduced the frequency of SPB targeting by 83% ($p = 0.0019$; Figure 2.6B). Fluorescence intensity measurements revealed a robust 147% increase in the number of dynein molecules per plus end (Figure 2.6D). When both Kip2 and wild-type Num1$_{CC}$ were overexpressed, the frequency and mean fluorescence intensity of plus end dynein was reduced by 59% ($p < 0.0001$) and 63% ($p = 0.0012$), respectively, when compared to *GAL1p:KIP2 GAL1p:num1$_{CC}^{LL/EE}$* cells (Figure 2.6B – E). The extent by which Kip2 overexpression reduces Num1$_{CC}$-mediated plus end dynein depletion is therefore less than that of Pac1. Taken together, these data are consistent with our hypothesis, and suggest that Num1$_{CC}$ and Pac1 are competing for binding to dynein-dynactin complexes. It is interesting to note that Pac1 binds to dynein within the C-terminal motor domain (Huang et al., 2012; Markus et al., 2009; Reck-Peterson et al., 2006; Toropova et al., 2014), while Num1 associates with dynein via the N-terminal tail domain (Markus et al., 2009). Thus, interference with Dyn1-Pac1 binding by Num1$_{CC}$ likely occurs by an allosteric mechanism.

Num1$_{CC}$ colocalizes with dynein-dynactin

Previous data indicate that Num1$_{CC}$ interacts with dynein at SPBs, and is found in the cytoplasm as bright foci (presumably aggregates; see Figure S1.5A, open arrows, and S2.5B, "cytoplasm") (Tang et al., 2012). We found that localization of Num1$_{CC}$ to the SPB is largely

Figure 2.6

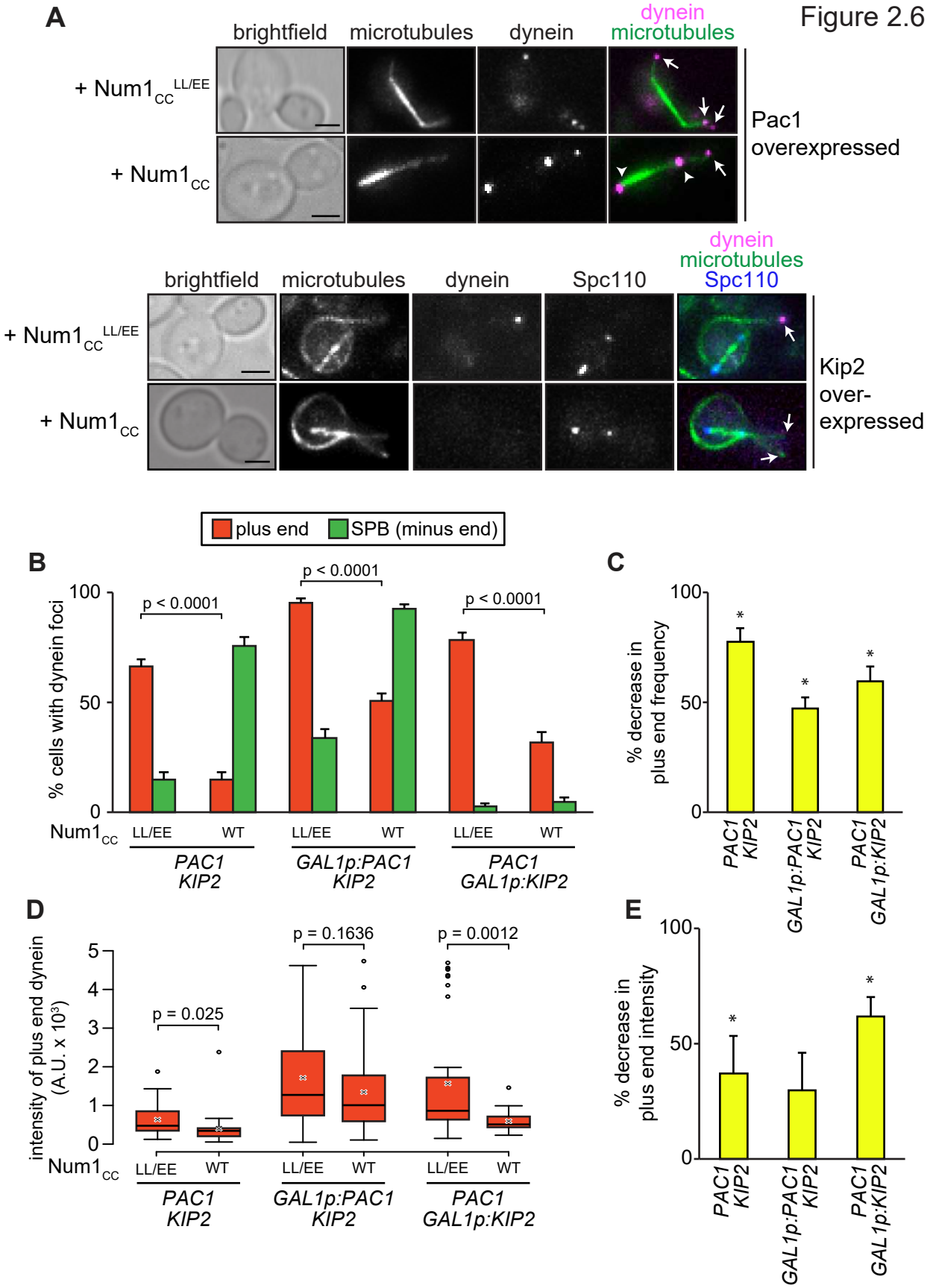
A
brightfield
microtubules
dynein
dynein
microtubules
+ Num1CC LL/EE
+ Num1CC
Pac1
overexpressed
brightfield
microtubules
dynein
Spc110
dynein
microtubules
Spc110
+ Num1CC LL/EE
+ Num1CC
Kip2
over-
expressed
plus end
SPB (minus end)
B
% cells with dynein foci
p < 0.0001
p < 0.0001
p < 0.0001
Num1CC
LL/EE
WT
PAC1
KIP2
GAL1p:PAC1
KIP2
PAC1
GAL1p:KIP2
C
% decrease in
plus end frequency
PAC1
KIP2
GAL1p:PAC1
KIP2
PAC1
GAL1p:KIP2
D
intensity of plus end dynein
(A.U. x 10³)
p = 0.025
p = 0.1636
p = 0.0012
E
% decrease in
plus end intensity

Figure 2.6. Overexpression of Pac1 reduces the extent of by which $Num1_{CC}$ depletes plus end dynein. (A) Representative images of cells expressing mTurquoise2-Tub1, Dyn1-3mCherry, either $Num1_{CC}$ or $Num1_{CC}^{LL/EE}$, and either overexpressing Pac1 or Kip2, as indicated. Due to the distorted spindle phenotype in Kip2-overexpressing cells, Spc110-Venus was used to mark SPBs. All cells were grown in galactose-containing media to induce overexpression of Pac1, Kip2, $Num1_{CC}$, or $Num1_{CC}^{LL/EE}$, as indicated. Each image is a maximum intensity projection of a 2-µm Z-stack of wide-field images. For top row (Pac1 overexpressed), arrows indicate plus end foci, and arrowheads indicate SPB foci. For bottom row (Kip2 overexpressed), arrows indicate plus ends with, or without foci. Scale bars correspond to 2 µm. (B) The percentage of cells that exhibit plus end (red) or SPB (green) Dyn1-3mCherry foci is plotted for cells shown in panel A, and for cells shown in Figures 1D and 2B. Error bars represent standard error of proportion (n ≥ 113 cells). (C) Extent by which $Num1_{CC}$ overexpression reduced the frequency of observing dynein plus end foci when compared with respective *PAC1 KIP2* isogenic parent strain overexpressing $Num1_{CC}^{LL/EE}$. Asterisks indicate statistically significant percent decrease (see panel B for p values). (D) Box plot of fluorescence intensity values of plus end associated Dyn1-3mCherry (n ≥ 31 foci). Whiskers define the range of data, boxes encompass the 25th to 75th quartiles, the line depicts the median value, and the "x" depicts the mean value. (E) Extent by which $Num1_{CC}$ overexpression reduced the number of dynein molecules (i.e., fluorescence intensity) at plus ends when compared with isogenic *PAC1 KIP2* parent strain overexpressing $Num1_{CC}^{LL/EE}$. Asterisks indicate statistically significant percent decrease (see panel D for p values). See also Figure S1.5.

dependent on dynein, and more specifically, the microtubule-binding domain of dynein (Figure S1.5A and B). Furthermore, cells in which dynein plus end-targeting is restored – by overexpression of Pac1, deletion of the dynein microtubule-binding domain, or use of Dyn1HL3 – exhibit $Num1_{CC}$ at plus ends, albeit at a low frequency (Figure S1.5A – C). These data indicate that $Num1_{CC}$ can bind plus end dynein (as well as the $Dyn1_{\Delta MTBD}$ and $Dyn1_{HL3}$ mutants) and suggest that Num1 and Pac1 binding to dynein are not entirely mutually exclusive. The latter is consistent with the observation that $Dyn1_{HL3}$-Pac1 complexes can offload together to Num1 cortical sites (Markus and Lee, 2011).

Direct observation of minus end-directed motion of dynein along astral microtubules

In budding yeast, dynein is targeted to microtubule plus ends by two distinct mechanisms: (1) direct recruitment from the cytoplasm, and (2) Kip2-mediated plus end-directed transport along astral microtubules (Carvalho et al., 2004; Markus et al., 2009). Evidence of the latter is apparent by the movement of fluorescent dynein speckles along astral microtubules toward plus ends (see

Figure 2.7A and Video S2.2) (Markus et al., 2009). In budding yeast, dynein is never observed moving in the opposite direction – toward the minus ends of astral microtubules. Minus end-directed activity is only apparent when cortically anchored dynein motors move the spindle through interactions with astral microtubules. If depletion of dynein-dynactin from microtubule plus ends is a consequence of these motors being switched "on," then we reasoned that cells overexpressing $Num1_{CC}$ would exhibit dynein molecules moving in a directed manner toward the minus ends of astral microtubules, as was recently observed in fission yeast expressing a $Mcp5_{\Delta PH}$ (Num1 homolog) fragment (Ananthanarayanan et al., 2013).

In uninduced cells (*i.e.*, not expressing any $Num1_{CC}$), or in those induced to express $Num1_{CC}^{LL/EE}$, only plus end-directed motility of dynein (or $dynein_{\Delta MTBD}$) molecules was ever observed (Figure 2.7A and Video S2.2). We were unable to observe minus end-directed motility of dynein molecules in cells overexpressing $Num1_{CC}$, likely due to the robust depletion of dynein from microtubule plus ends in these cells. Thus, we chose to focus on cells in which $Num1_{CC}$ mediated depletion of dynein plus end-binding was partially restored: *GAL1p:KIP2* and *GAL1p:PAC1* cells. Strikingly, we observed numerous instances of minus end-directed motility of dynein in cells overexpressing Kip2 or Pac1 in addition to $Num1_{CC}$ (Figure 2.7B and C, and S2.5D; see Videos S2.3 and S2.4). The mean velocity of minus end-directed dynein molecules along astral microtubules in *GAL1p:KIP2* cells was slightly higher than that in *GAL1p:PAC1* cells (55.3 nm/sec, n = 22; versus 41.7 nm/sec, n = 9; Figure 2.7D); however, the values from both strains were very similar to the velocity of single molecules of purified dynein (~70-100 nm/s (Huang et al., 2012; Markus and Lee, 2011; Reck-Peterson et al., 2006)) and dynein-mediated spindle movements in this organism (41 nm/sec (Markus et al., 2011)). Thus, overexpression of $Num1_{CC}$ depletes dynein from microtubule plus ends by activating its minus end-directed motility.

Although we were able to see $Num1_{CC}$-mediated minus end motility of dynactin (Jnm1-3YFP) in *GAL1p:KIP2* cells (Figure 2.7Biii), we were unable to observe examples of either Pac1 or $Num1_{CC}$ moving toward the minus ends. The reason for the latter is unclear, but may be due

Figure 2.7

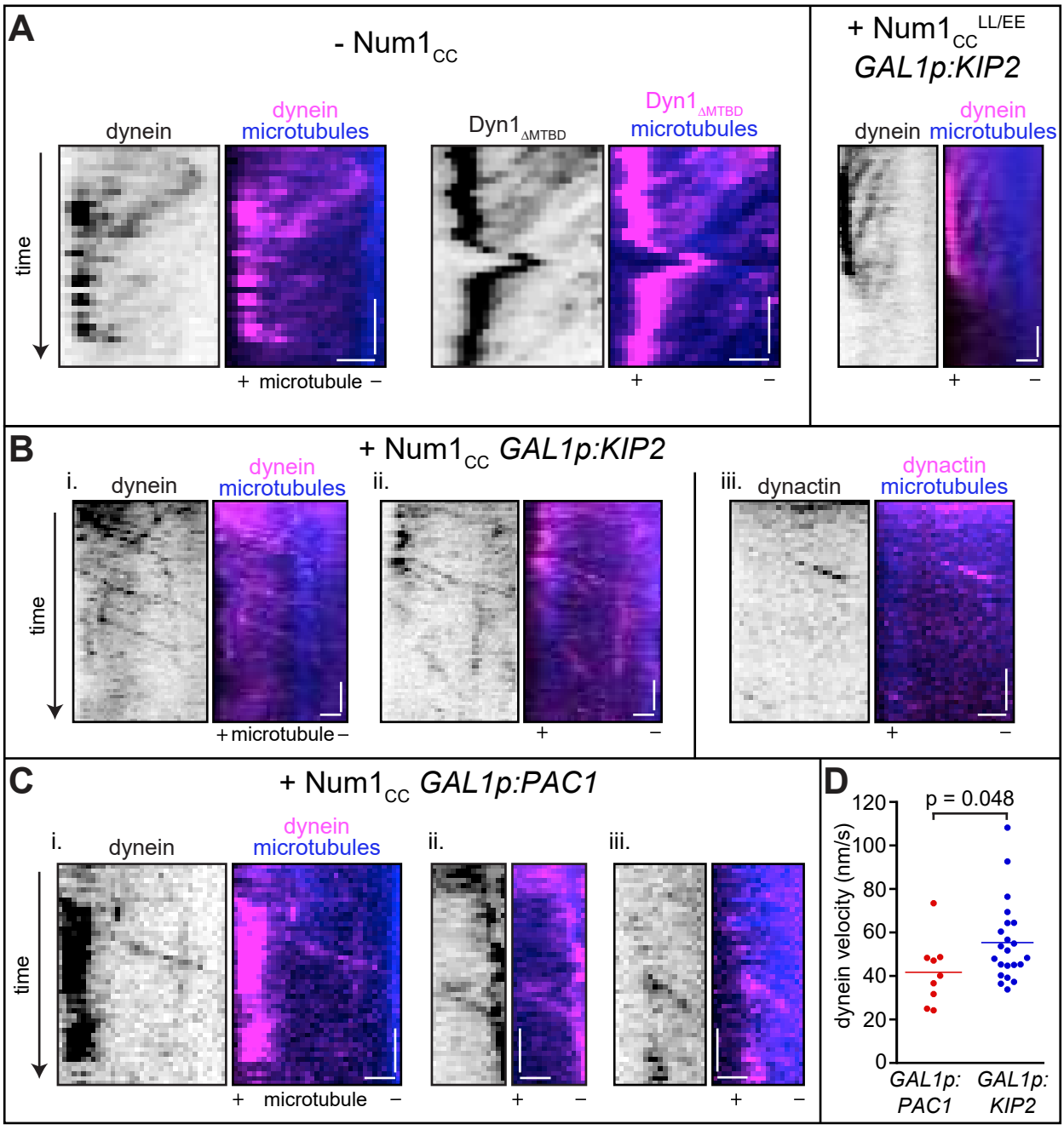
A
- Num1CC
dynein
dynein microtubules
Dyn1ΔMTBD
Dyn1ΔMTBD microtubules
time
+ microtubule −
+ −
+ Num1CC LL/EE
GAL1p:KIP2
dynein
dynein microtubules
+ −
B
+ Num1CC GAL1p:KIP2
i. dynein
dynein microtubules
ii.
iii. dynactin
dynactin microtubules
time
+ microtubule −
+ −
+ −
C
+ Num1CC GAL1p:PAC1
i. dynein
dynein microtubules
ii.
iii.
time
+ microtubule −
+ −
+ −
D
p = 0.048
dynein velocity (nm/s)
120
100
80
60
40
20
0
GAL1p: PAC1
GAL1p: KIP2

Figure 2.7. Direct observation of $Num1_{CC}$-mediated minus end motility of dynein and dynactin. (A) Example kymographs of plus end-directed motility of dynein molecules along astral microtubules observed in uninduced *GAL1p:num1$_{CC}$* cells (left; "- $Num1_{CC}$"), or in cells overexpressing $Num1_{CC}^{LL/EE}$ and Kip2 (right). (B and C) Example kymographs depicting minus end-directed motility of dynein or dynactin (*i.e.*, Jnm1) along astral microtubules in cells overexpressing $Num1_{CC}$ and either (B) Kip2, or (C) Pac1. Kymographs were generated from time-lapse images acquired using HILO microscopy (see Materials and Methods). Scale bars correspond to 1 minute (vertical bar) and 1 μm (horizontal bar). (D) Velocity values for minus end-directed dynein runs observed in either Pac1- or Kip2-overexpressing cells. See also Videos S2.2, S2.3, and Figure S1.5.

to disengagement of $Num1_{CC}$ from dynein subsequent to activation. Taken together with the lack of Pac1 accumulation at SPBs in $Num1_{CC}$-overexpressing cells, the reduced colocalization of Dyn1 and Pac1 (in *DYN1* and *PH-DYN1* cells), and the ability of Pac1 overexpression to rescue Dyn1 plus end-targeting, the lack of minus end-directed Pac1 molecules further suggest that $Num1_{CC}$ activates plus end dynein by relieving Pac1-mediated inhibition.

2.3 DISCUSSION

When purified from various sources, including budding yeast and animal tissue, dynein motors are active as apparent from ATPase and microtubule gliding assays. Yeast dynein requires no additional factors for processive single molecule motility (Reck-Peterson et al., 2006), whereas dynein isolated from animal tissue requires a combination of dynactin and various adaptor proteins that link dynein to dynactin (McKenney et al., 2014; Schlager et al., 2014). This latter phenomenon helps explain how dynein activity is recruited to different vesicular or organellar compartments in animal cells, and thus how dynein activity is regulated with spatial precision. For instance, one of these adaptors, BicD2, binds to Rab6 on various vesicular cargoes, and thereby recruits dynein-dynactin complexes, which allows for minus end-directed movements of these vesicular cargoes (Matanis et al., 2002). Although mechanistically distinct, we have identified a similar mechanism at play in budding yeast. Specifically, Num1-mediated recruitment of dynein-dynactin complexes to the cell cortex is sufficient to: (1) anchor dynein-dynactin complexes at their site of activity; and, (2) activate dynein for its spindle orientation function. Unlike animal cells,

however, association with dynactin is not sufficient to activate dynein motility in yeast cells. Rather, our studies indicate that a Num1-mediated Pac1 dissociation event is responsible for switching dynein from being “off” at microtubule plus ends, to “on” at the cell cortex.

Our results revealed a small but significant $Num1_{CC}$-mediated enhancement in the apparent dynein-dynactin interaction at plus ends (see Figure 2.3H). Although this effect appears to be minor when compared to that of $Num1_{CC}$ on the dynein-Pac1 interaction, it is possible that, like the human adaptor proteins (*e.g.*, BicD2, Spindly), Num1 also plays a role in stabilizing the dynein-dynactin complex. If so, it may be that Num1 may further promote dynactin-mediated processivity enhancement of dynein in a manner reflective of the human adaptor proteins (McKenney et al., 2014; Schlager et al., 2014). Future studies will be needed to directly test this in a reconstituted system.

Although dynactin does not activate yeast dynein motility *per se*, it is interesting to note that dynein-dynactin binding is a rate-limiting step during the dynein offloading process. Quantitative fluorescence microscopy revealed a three-fold excess of dynein relative to dynein-dynactin complexes at microtubule plus ends (Markus et al., 2011). Given the reliance of dynein on dynactin for offloading to Num1 receptor sites (Lee et al., 2003b), the limiting nature of dynactin at plus ends effectively restricts dynein pathway activity by limiting the number of cortical dynein-dynactin complexes. Increasing the number of intact dynein-dynactin complexes at plus ends by deletion of She1, which regulates their interaction *in vivo* (Woodruff et al., 2009), results in an increased number of cortical dynein-dynactin complexes, as well as enhanced dynein pathway activity (Markus et al., 2011). Thus, through mechanistically distinct processes, dynactin effectively activates dynein-mediated processes both in animal and yeast cells.

It is well established that Pac1 plays a central role in targeting dynein-dynactin to microtubule plus ends in yeast (Lee et al., 2003b). Given the ability of Pac1 to reduce dynein motility *in vitro* (Huang et al., 2012; Markus and Lee, 2011), it has been postulated that Pac1 may hold dynein at plus ends in part by preventing its minus end-directed motility. At some point

following or concomitant with dynein offloading, Pac1 dissociates from dynein, and is never observed at cortical Num1 sites in wild-type cells (Lee et al., 2003b). Given the observations presented here, we hypothesize that Num1 binding to dynein-dynactin triggers the dissociation of Pac1 from dynein. The fact that $Dyn1_{\Delta MTBD}$ is insensitive to $Num1_{CC}$ overexpression suggests that microtubule-binding by dynein is a requisite for Pac1 dissociation. This suggests a mechanism whereby Num1 binding to the dynein tail domain (Markus et al., 2009) communicates allosteric changes to the motor head that, following microtubule-binding, induces Pac1 dissociation from its binding site (at the junction between AAA3 and AAA4 (Toropova et al., 2014)), and consequently permits minus end-directed motility (see Figure 2.8). The requisite microtubule-binding by dynein for $Num1_{CC}$-mediated Pac1 dissociation likely explains the plus end colocalization of $Dyn1_{\Delta MTBD}$ with $Num1_{CC}$ (Figure S1.5A –C) and Pac1 (not shown).

It is interesting to note the apparent discrepancies between the requirements for plus end binding of yeast and human dynein. In budding yeast, the dynein motor domain, Pac1, and Bik1 are absolutely essential (Lee et al., 2003b; Markus et al., 2009; Sheeman et al., 2003), but dynactin is dispensable for this process (Lee et al., 2003b). However, recent *in vitro* reconstitution experiments with human dynein revealed a distinct plus end-binding complex that requires EB1, the $p150^{Glued}$ subunit of dynactin, and the full-length dynein complex (*i.e.*, the motor domain is not sufficient) (Duellberg et al., 2014). These latter observations –which did not describe any minus end-directed dynein motility – suggest that dynein and dynactin (or, at least $p150^{Glued}$) can interact at plus ends in the absence of the recently characterized adaptor proteins (*e.g.*, Hook3, Spindly, BicD2) (McKenney et al., 2014; Schlager et al., 2014), and furthermore suggest that their interaction is not sufficient for dynein motility.

Our observation that the microtubule-binding domain of dynein is dispensable for plus end-targeting was surprising and changes our understanding by which dynein recognizes and binds to microtubule plus ends. In light of this observation, we propose that dynein does not directly contact the plus end, but rather associates with plus ends indirectly through its interactions

with Pac1 and Bik1 (see Figure 2.1B). Evidence indicates that Pac1 enables dynein tip-tracking in part by linking it to the plus end-binding protein Bik1 (Roberts et al., 2014a; Sheeman et al., 2003). Thus, the ability of Pac1 (and LIS1) to permit prolonged encounters between dynein and microtubules (Huang et al., 2012; McKenney et al., 2010) is likely unrelated to plus end binding by dynein in this organism. However, it is conceivable that by maintaining dynein in an "off" state at plus ends, Pac1 may prevent minus end motility of dynein motors that are in very close proximity to the microtubule. Upon binding of $Num1_{CC}$, dynein may pivot (likely in a stochastic manner) such that it may contact the plus end directly through its MTBD, subsequently release Pac1, and then walk towards the minus end. An analogous situation may take place in wild-type cells: following offloading to Num1 receptor sites at the cortex, dynein is well positioned to contact the microtubule to initiate spindle movements, which in turn may trigger Pac1 dissociation (Figure 2.8). Recent structural studies support such a possibility: upon microtubule binding, conformational changes within the microtubule-binding domain affect corresponding changes within the motor ring (Schmidt, 2015). These changes, which are propagated by the anti-parallel coiled-coil that lead from the microtubule-binding domain to the motor ring (via AAA4), could presumably affect Pac1 binding at the AAA3-AAA4 junction (see Figure 2.8) (Toropova et al., 2014).

Consistent with Num1 affecting the dynein-Pac1 interaction, the dynein mutant with higher than normal affinity for Pac1 ($Dyn1_{HL3}$) was much less susceptible to $Num1_{CC}$-mediated plus end depletion. It is unclear why $Dyn1_{HL3}$ exhibits higher affinity for Pac1. This mutant was engineered such that a helical linker was inserted between the tail and motor domains (Markus and Lee, 2011). In the context of the tertiary structure of the dynein motor, this region lies in close proximity to the Pac1-binding site (between AAA3 and AAA4; see Figure 2.5A). Taken together with an apparent enhanced affinity of a tail-less dynein construct (motor domain only) for Pac1 (Markus et al., 2009; Reck-Peterson et al., 2006), it stands to reason that the tail domain plays a negative

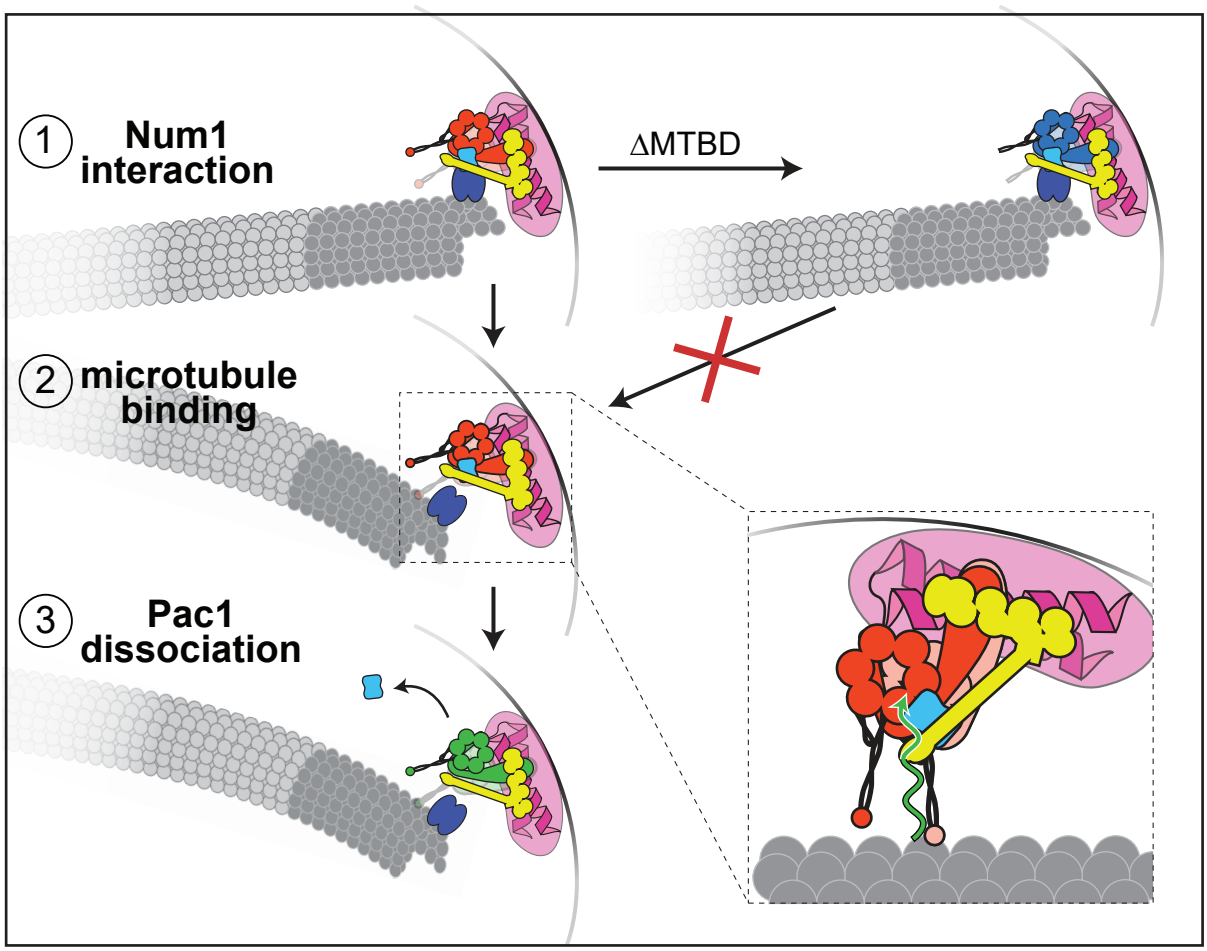

Figure 2.8. Model for Num1-mediated activation of dynein-mediated spindle positioning. Our data suggest that at the moment of offloading (step 1), contact between dynein–dynactin and cortical Num1 triggers a cascade of events that ultimately leads to Pac1 dissociation (step 3); however, the MTBD (deletion of which interrupts this process) is required to make contact with the microtubule to initiate Pac1 dissociation (step 2).

regulatory role in affecting Pac1 binding. Thus, whatever allosteric conformational change Num1$_{CC}$-dynein tail binding induces is likely interrupted by insertion of the helical HL3 linker.

The nature of the Num1$_{CC}$-dynein-dynactin interaction is currently unknown; however, a recent structural study has revealed how human dynein-dynactin interacts with the coiled coil-containing adaptor protein BicD2 (Urnavicius et al., 2015). Given the importance of the Num1 coiled-coil domain in the dynein-dynactin interaction, and the observation that Num1 – like BicD2 – only interacts with intact dynein-dynactin complexes (Splinter et al., 2012), it maybe that Num1 exhibits a similar mode of binding (*i.e.*, direct contact with the dynein tail domain, and the Arp1 filament). Future high-resolution structural studies of the dynein tail domain within the context of the Num1$_{CC}$-dynein-dynactin complex will be necessary to understand the network of interactions that define this enormous protein complex, and also how the tail domain may possibly affect Pac1-motor domain binding.

2.4 MATERIALS AND METHODS

Media and strain construction

All strains are derived from YEF473A (Bi and Pringle, 1996) and are listed in Table S1. We transformed yeast strains using the lithium acetate method (Knop et al., 1999a). Strains carrying null mutations or fluorescently tagged components were constructed by PCR product-mediated transformation (Longtine et al., 1998b) or by mating followed by tetrad dissection. Strains expressing mTurquoise2-Tub1 were generated as described (Markus et al., 2015). Transformants were clonally purified by streaking to individual colonies on selective media. Proper tagging was confirmed by PCR, and in some cases sequencing. Yeast synthetic defined (SD) media was obtained from Sunrise Science Products (San Diego, CA).

To generate a yeast strain with point mutations in Num1$_{CC}$ (L167E L170E; Figure 2.2A), we used the site-specific genomic mutagenesis approach (Gray et al., 2004a). Briefly, after integration of the *URA3* cassette into the *num1$_{CC}$* locus (replacing nucleotides 499 to 510, corresponding to amino acids L167 to L170), a PCR product amplified from pSM37 (see below)

containing the desired nucleotide substitutions was transformed into the *URA3*-integrated strain, and subsequently selected on 5-fluoroorotic acid (5-FOA)-containing plates. 5-FOA resistant colonies were selected, and confirmed by colony PCR and sequencing of the genomic DNA region. A similar method was used to delete the MTBD (residues 3102-3225) from *DYN1*.

To generate a yeast strain expressing the *GAL1p:PH-DYN1* allele, a cassette containing *KANR::GAL1p:PH* was amplified from pFA6a-kanMX6-pGAL1-PH (see below) and used for integration immediately upstream of the *DYN1-3mCherry* locus.

Plasmid construction

Using isothermal assembly (Gibson et al., 2009), we generated a plasmid in which the L167E L170E point mutations were engineered into a plasmid encoding $Num1_{CC}^{(95\text{-}303)}$ -PCNS-TEV-ZZ (pBSG02) (Tang et al., 2012). Briefly, primers were used to separately amplify the N-terminal (nucleotides 283-498, corresponding to amino acids 95-166) and C-terminal (nucleotides 511-909, corresponding to amino acids 171-303) portions of $Num1_{CC}$ such that the desired nucleotide substitutions were included in the reverse primer for the N-terminal portion, and the forward primer for the C-terminal portion. After amplification, the 3' and 5' ends of the PCR products corresponding to the N- and C-terminal regions, respectively, contained 20 nucleotides of sequence identity with each other, while the 5' and 3' ends of the N- and C-terminal regions, respectively, contained 20 nucleotides of sequence identity with the NcoI and NotI-digested pBSG02 vector. After digesting pBSG02 with NcoI and NotI (to excise $Num1_{CC}^{(95\text{-}303)}$ wild-type), the gel purified PCR products and digested vector were assembled *in vitro* as described (Gibson et al., 2009). Proper assembly was verified by restriction digest and DNA sequencing, and resulted in pSM37 (encoding $Num1_{CC}^{(95\text{-}303)LL/EE}$-PCN-S-TEV-ZZ).

To generate a plasmid with which to N-terminally tag Dyn1 with a PH domain, the PH domain of Num1 (amino acids 2563-2692) was amplified using a forward primer flanked with an XmaI site, and a reverse primer flanked with a SalI site. The PCR product was digested with XmaI

and SalI, and ligated into pFA6a-kanMX6-PGAL1 (Longtine et al., 1998b) digested similarly, yielding pFA6a-kanMX6-PGAL1-PH.

Image acquisition, analysis, and dynein motility assay

Yeast cultures were imaged after growth at 30°C to mid-log phase in synthetic defined media supplemented with either 2% glucose (SD + glucose), or 2% galactose plus 2% raffinose (SD + gal/raf; the latter for induction of $Num1_{CC}$, Pac1, or Kip2, as indicated). To assess the effects of $Num1_{CC}$ on localization of dynein pathway components, *GAL1p:num1$_{CC}$* cells were induced in SD + gal/raf for 6 hours prior to mounting cells for fluorescence microscopy. For wide-field fluorescence microscopy, yeast cells were imaged on an agarose pad containing 50 mM potassium phosphate buffer (pH 7), and images were collected at room temperature using a 1.49 NA 100X objective on a Nikon Ti-E inverted microscope equipped with a Ti-S-E motorized stage, piezo Z-control (Physik Instrumente), SOLA SM II LE LED light engine (Lumencor), motorized filter cube turret, and an iXon X3 DU897 cooled EM-CCD camera (Andor). The microscope system was controlled by NIS-Elements software (Nikon). A step size of 1 µm was used to acquire Z-stack images 2 µm thick. Sputtered/ET filter cube sets (Chroma Technology) were used for imaging mTurquoise2 (49001), GFP (49002), YFP (49003), and mCherry (49008) fluorescence.

Image analysis was performed using ImageJ (kymographs in Figure 2.7 were generated with the MultipleKymograph plugin). Plus end and SPB foci were identified in two (or three) color movies, and scored accordingly. Specifically, plus end molecules were recognized as those foci that localized to the distal tips of dynamic microtubules (identified via mTurquoise2-Tub1 imaging), while SPB molecules were recognized as those foci that localized to one of the spindle poles. Cortical molecules (*e.g.*, in PH-Dyn1-expressing cells) were identified as those foci not associated with an astral microtubule plus end that remained stationary at the cell cortex for at least 3 frames. Two datasets were considered statistically significant if a student's *t*-test (assuming unequal variance) returned a p value < 0.05.

For highly inclined and laminated optical sheet (HILO) microscopy (Tokunaga et al., 2008), samples were prepared and imaged as above, except 488 and 561 nm lasers were used to excite YFP and mCherry, respectively. The laser illumination angle was adjusted individually for each sample to achieve the maximum signal-to-noise ratio. Emission filters were 525/50 nm for YFP and 600/50 for mCherry.

Purification of TAP (S tag-ZZ)-Dyn1-EGFP, and the single-molecule motility assay (Figure S1.1 and Video S2.1) were performed as previously described (Markus et al., 2012; Markus and Lee, 2011).

Cell lysis and immunoblotting

For western blotting, yeast cultures were grown at 30°C in 3 ml of either SD + glucose, or SD + gal/raf, and harvested. Equal numbers of cells were pelleted and resuspended in 0.2 ml of 0.1 M NaOH and incubated for 5 minutes at room temperature as described (Kushnirov, 2000). Following centrifugation, the resulting cell pellet was resuspended in sample buffer and heated to ~100°C for 3 minutes. Lysates were separated on a 10% SDS polyacrylamide gel and electroblotted to PVDF in 25 mM Tris, 192 mM glycine supplemented with 0.05% SDS and 10% methanol for 30 minutes. Rabbit anti-c-Myc polyclonal (GenScript) or anti-alpha-tubulin (Applied Biological Materials, Inc.) monoclonal antibodies, and HRP-conjugated goat anti-rabbit or anti-mouse antibody (Jackson ImmunoResearch Laboratories) were used at 1:1000, 1:1000, 1:3000, or 1:3000, respectively. Chemiluminescence signal was acquired on an ImageQuant LAS 500 gel documentation system. Immunoblots were exposed without saturating the camera's pixels.

CHAPTER 3

INVESTIGATING THE ROLE OF NDL1/NUDE IN DYNEIN ACTIVATION[3]

3.1 INTRODUCTION

To reach its site of activity- the cell cortex- dynein must be targeted to astral microtubules first. If this step is bypassed and dynein reaches the cortex independently, defects in spindle positioning accrue (Markus and Lee, 2011; Marzo et al., 2019b). Therefore, this step is essential for dynein function and is regulated by Pac1/Lis1 and Ndl1/NudE. Although Ndl1/NudE has been identified in this role, its exact function is not completely understood. Ndl1/NudE was first identified in an *Aspergillus nidulans* (filamentous fungus) screen as a protein important for proper nuclear distribution, along with dynein and Pac1/Lis1. In budding yeast, loss of Ndl1/NudE causes an increase in binucleate cells and Ndl1/NudE defects can be rescued by overexpression of Pac1/Lis1 in both fungi and metazoa, suggesting that it works upstream of Pac1/Lis1 or may enhance Pac1/Lis1 function (Li et al., 2005; Efimov, 2003; Wang and Zheng, 2011). Mutations in Ndl1/NudE in mammalian systems cause neurodevelopmental defects, similar to loss of Pac1/Lis1 function (Bradshaw et al., 2013). Loss of Pac1/Lis1 function was originally discovered as the cause of the neurodevelopmental disease, lissencephaly or “smooth brain” (Reiner et al., 1993). Neuronal stem cells prematurely enter asymmetric divisions due to defects in dynein localization (Yingling et al., 2008).

Because of structural data, more is known about how Pac1/Lis1 interacts with dynein than Ndl1/NudE but how it effects dynein motility is still unclear. Pac1/Lis1 exists as a dimer with each monomer containing an β propeller domain that can interact between AAA3 and AAA4 of the

[3] This work was done in collaboration with the McKenney Lab at UC Davis (see Discussion section). Damian Garno contributed to experimental design and data analysis.

dynein ATPase ring or through a secondary binding site near AAA5 (Figure 5.1; (Huang et al., 2012; Toropova et al., 2014; DeSantis et al., 2017). By interacting with the motor domain, Pac1/Lis1 may regulate dynein by uncoupling ATP hydrolysis from microtubule binding, therefore inhibiting dynein motility (Huang et al., 2012; Toropova et al., 2014). However, recent work in our lab and others suggests that Pac1/Lis1 binding actually prevents dynein from entering an autoinhibitory state- promoting activity- rather than acting as an inhibitor (Marzo et al., 2019a; Elshenawy et al., 2019b; Htet et al., 2019; Qiu et al., 2019a). Although Pac1/Lis1 is well established as a recruitment factor for dynein plus end localization, its effect on dynein motility is conflicting.

In vitro studies demonstrate that the mechanism of how Pac1/Lis1 and Ndl1/NudE work together and individually to regulate dynein is complex and even contradictory in some events. Using purified components and single molecule approaches, Pac1/Lis1 has been shown to inhibit dynein motility on microtubules (Yamada et al., 2008; Huang et al., 2012; Wang et al., 2013; Torisawa et al., 2011) and increase dynein stall time under load (McKenney et al., 2010; Yi et al., 2011; Reddy et al., 2016). In contrast, Ndl1/NudE alone appears to cause dynein dissociation from microtubules, yet the addition of Ndl1/NudE with Pac1/Lis1 inhibits dynein motility and enhances the persistence of dynein force production, even allowing dynein to adapt its ability to handle high load (Yamada et al., 2008; Torisawa et al., 2011; McKenney et al., 2010; Huang et al., 2012; Reddy et al., 2016). Although their individual effects differ, the current model of regulation considers Ndl1/NudE as a tether that interacts with dynein through its globular C-terminus and extends its coiled-coil N-terminus to bind to Pac1/Lis1 and aid Pac1/Lis1 binding to the motor domain (Figure 3.6B) (Sasaki et al., 2000; Niethammer et al., 2000; Liang et al., 2004; Feng et al., 2000; Efimov and Morris, 2000; Stehman et al., 2007). However, the presence of the dynein activating complex, dynactin, adds complexity to this regulation. Human dynein requires dynactin and an adapter protein such as BicD2 to be motile on microtubules (McKenney et al., 2014; Schlager et al., 2014). Dynactin and the adapter bind in the tail domain and align the motor

domains to improve dynein walking efficiency. Studies have determined that dynactin and Ndl1/NudE compete for an overlapping binding site on the accessory chains that bind the tail domain (intermediate chain and LC8) (Stehman et al., 2007; McKenney et al., 2011), which developed the hypothesis that Ndl1/NudE and dynactin cannot regulate dynein simultaneously. Because dynactin is associated with processive “active” dynein, studies suggest that Ndl1/NudE and Pac1/Lis1 regulation may be used to recruit dynein to microtubule plus ends and initiate transport but be competed off by dynactin for motility events (McKenney et al., 2011; Egan et al., 2012; Jha et al., 2017). Surprisingly though, in single molecule experiments of dynein-dynactin-BicD2 (DDB), the addition of Lis1 increased DDB velocity at high concentrations and in rare cases was seen moving with the complex, contrary to its ability to increase the stall force of dynein alone in optical trapping experiments (Gutierrez et al., 2017; Baumbach et al., 2017; Jha et al., 2017). These data suggest that Lis1 can affect DDB complexes in the absence of Ndl1/NudE and may have an unexplored role regulating dynein individually. In budding yeast, Pac1/Lis1 can function alone to target dynein to microtubules, yet the presence of Ndl1/NudE appears to be required for ideal levels of dynein to be recruited for error free spindle positioning and cell division.

Many questions remain surrounding Ndl1/NudE function: How does the presence of Ndl1/NudE improve dynein plus end targeting? Does Ndl1/NudE enhance Pac1/Lis1-mediated dynein targeting through a tethering mechanism? Does it play a role in dynein targeting or activity as well? This study aimed to better define the role of Ndl1/NudE in dynein spindle positioning and the mechanism in which it may foster Pac1/Lis1 effects on dynein in budding yeast. I determined that Ndl1/NudE and dynein share an overlapping binding site on Pac1/Lis1, which leads us to support the model that Ndl1/NudE enhances Pac1/Lis1 role in recruiting dynein to plus ends through a tethering mechanism and allows us to speculate that Ndl1/NudE plays a role in releasing Pac1/Lis1 from the dynein-dynactin complex before offloading. These two seemingly opposing functions depend on the presence of dynactin and demonstrates that the context in which these regulators affect dynein is important. The data presented here provides an exciting

example of how the balance of dynein regulators ensures that temporal and spatial regulation occurs accurately for important cellular processes.

3.2 RESULTS

Dynein plus end localization decreases in the absence of Ndl1/NudE

To dissect the role of Ndl1 in dynein regulation, I first observed the localization of dynein in NDL1 null cells. Using fluorescently-labelled dynein, I measured the fluorescence intensity and counted the frequency of molecules at astral microtubule plus ends, SPB (spindle pole body; equivalent to centrosome), and the cortex. In the dynein pathway, dynein is targeted to the plus end first, and then is offloaded to the cortex. It also accumulates at the SPB, where it can be delivered to the plus end via a kinesin (Kip2). In the absence of Ndl1, I observed a significant decrease in dynein frequency at plus ends (70.5% WT; 19.0% NDL1 null) and the cortex (6.3% WT; 0.9% NDL1 null) and no change in SPB accumulation (Figure 3.1A, D). Fluorescence intensity measurements revealed that significantly fewer molecules of dynein were at plus ends and SPB in the absence of Ndl1 (Figure 3.1C). These results are consistent with the first observations of NDL1 null cells (Li et al., 2005), even though I did not see a significant decrease in cortical intensity. This difference is likely due to the infrequency of total cortical patches observed (6 in WT; 1 in NDL1 null).

Next, I overexpressed Ndl1 to determine if excess Ndl1 had any effect on dynein localization. Dynein intensity at plus ends, SPB, and the cortex was not changed, but the frequency of dynein foci at plus ends and the cortex increased significantly (Figure 3.1B, E-F). To overexpress Ndl1, I used a galactose inducible promotor (GAL1) that is repressed when cells are grown in glucose. The increase in localization frequency in the treatment (grown in galactose) compared to control (grown in glucose) may be exaggerated because the comparison is more similar to an overexpression and a “null” phenotype rather than overexpression compared to wild type levels of Ndl1. These results suggest that overexpression of Ndl1 only has a small effect on dynein localization in contrast to overexpression of Pac1 which increases dynein localization and

Figure 3.1

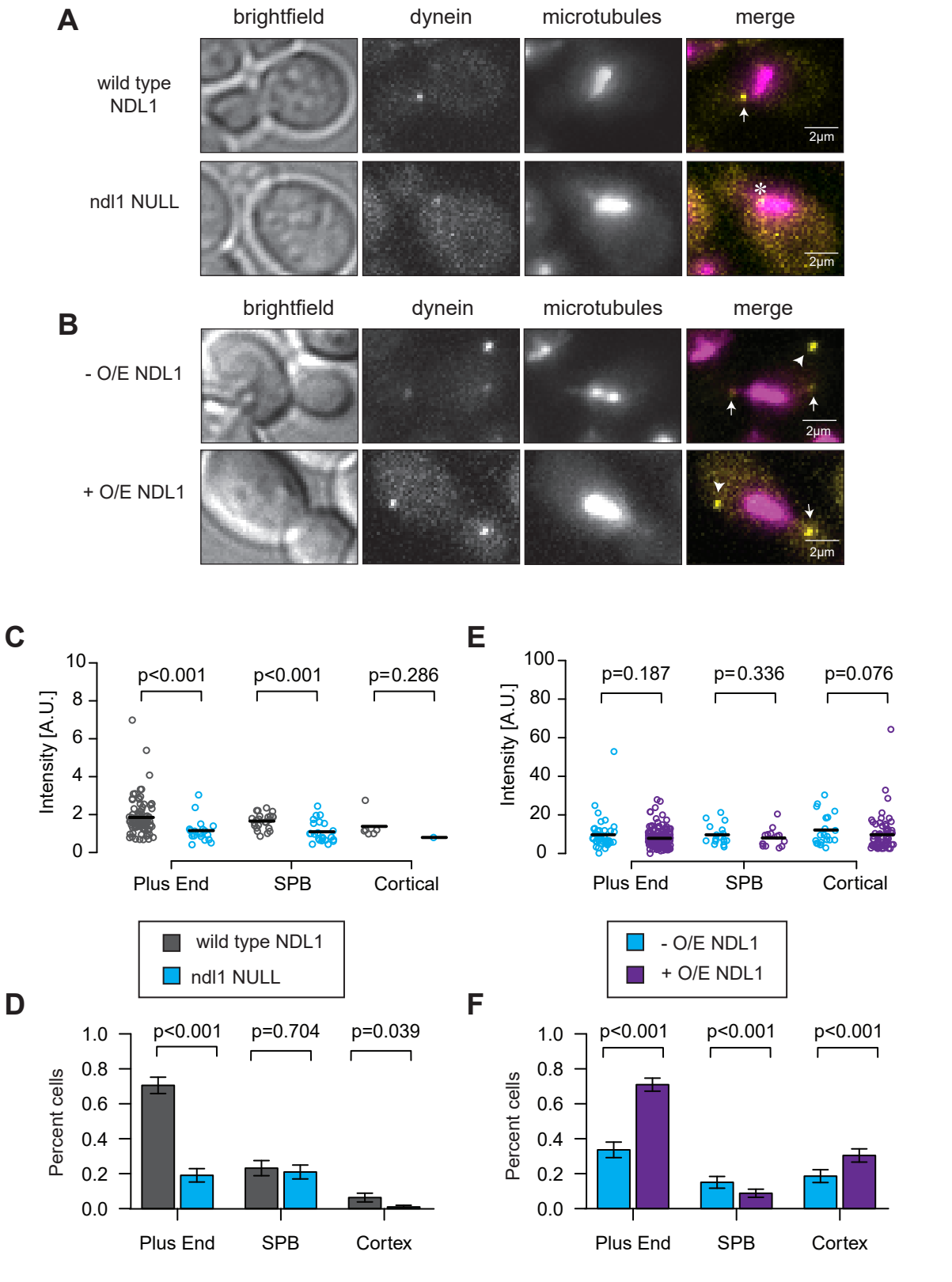
A
brightfield
dynein
microtubules
merge
wild type NDL1
ndl1 NULL
2μm
B
- O/E NDL1
+ O/E NDL1
C
Intensity [A.U.]
p<0.001
p<0.001
p=0.286
Plus End
SPB
Cortical
wild type NDL1
ndl1 NULL
D
Percent cells
p<0.001
p=0.704
p=0.039
Plus End
SPB
Cortex
E
p=0.187
p=0.336
p=0.076
- O/E NDL1
+ O/E NDL1
F
p<0.001
p<0.001
p<0.001

Figure 3.1. Loss of Ndl1/NudE reduces dynein plus end localization. (A) Representative images of wild-type NDL1 or ndl1 NULL cells expressing mTurquoise2-Tub1 (α-tubulin) and Dyn1-3YFP used for quantification in C and D. Cells were grown to approximately the first cell division in SD media supplemented with glucose. (B) Representative images of GAL1p:NDL1 cells expressing mTurquoise2-Tub1 (α-tubulin) and Dyn1-3GFP used for quantification in E and F. Cells were grown to approximately the first cell division in SD media supplemented with glucose (uninduced; -O/E NDL1) or galactose plus raffinose (induced; + O/E NDL1). In both A and B, only cells in mitosis were counted. Plus end, SPB, or cortical Dyn1 foci were identified in two-color movies and scored accordingly (see Materials and Methods). Each image is a maximum-intensity projection of a 2-µm Z-stack of wide-field images. Bars, 2 µm. Arrows indicate plus end foci, arrowheads indicate cortical foci, and white flower indicates SPB focus. (C) Scatter plots represent the fluorescence intensity distribution of each type (plus end, SPB, or cortical) Dyn1-3YFP foci in either WT or ndl1 NULL cells (n ≥ 44 foci). Mean is represented by a black line. (D) The percentage of cells that exhibit plus end, SPB, or cortical Dyn1-3YFP foci is plotted for the strains shown in A. Error bars represent the standard error of proportion (n ≥ 95 cells). (E) Scatter plots represent the fluorescence intensity distribution of each type (plus end, SPB, or cortical) Dyn1-3GFP foci for strains in B (n ≥ 82 foci). (F) The percentage of cells that contain Dyn1-3GFP foci is plotted for the strains shown in B. Error bars represent the standard error of proportion (n ≥ 113 cells).

intensity significantly (Markus et al., 2011). Together with NDL1 null observations, my results support previous conclusions that Ndl1 is a factor in dynein recruitment to plus ends and must work upstream of Pac1 (Li et al., 2005).

Loss of Ndl1/NudE reduces dynein-mediated spindle movements in budding yeast

Observing that loss of Ndl1 reduces dynein accumulation at plus ends and the cortex, I wanted to further characterize how this may cause nuclear segregation defects (Li et al. 2005). To assess how Ndl1 may affect spindle movements driven by dynein, I performed a spindle dynamics assay adapted for our lab (Moore et al., 2009). The assay conditions require the KAR9 pathway be disrupted to ensure only dynein-mediated spindle movements are observed. The KAR9 pathway acts upstream of dynein to orient the spindle via actin/myosin so that it can be pulled through the mother-bud neck by cortically anchored dynein motors. With this pathway removed, cells are arrested with the DNA synthesis inhibitor, hydroxyurea (HU), in premetaphase which results in many dynein-mediated spindle movements - oscillating back and forth between the mother and bud (Figure 3.2A). I deleted the NDL1 gene and assessed the dynamics of the

fluorescently labelled spindle over time by time lapse imaging. Spindle movements generated by cortically-anchored dynein were distinguished from diffusion by hand (see Materials and Methods) and called sliding events. NDL1 null cells had fewer sliding events ($p = 0.003$) and were half as active as wild-type cells (time active: 29.48% WT vs. 16.31% NDL1 null; Figure 3.2B (i and iii)). When the spindle crosses the mother-bud neck more force is required to pull the nucleus through the narrow space. For this reason, I used neck crossing events as a readout of dynein force generation. NDL1 null cells crossed the neck less frequently (60.5 ± 7.65% WT; 40.9 ± 9.76% NDL1 null; $p<.05$), suggesting that dynein is producing less force when NDL1 is deleted (Figure 3.2B (ii)). Additionally, each pulling event was overall slower and the total spindle displacement was significantly less than wild type (Figure 3.2B (iv and v)). At cortical patches, dynein is thought to act as an ensemble- many motors interacting with the microtubule at once and working together. In vitro dynein ensembles of four motors or more have a higher velocity and travel for longer distances than single motors because the probability of at least one dynein remaining engaged with the microtubule at one time is higher (Derr et al., 2012). Since deleting NDL1 results in fewer motors at the cortex (Figure 3.1D), then fewer dynein may be engaged with the microtubule at one time to explain the decreased spindle displacement and force generation (neck crosses) measurements. These data support further the hypothesis that Ndl1 is involved in dynein recruitment and is required for the correct amount of dynein to reach the cortex and generate enough force on microtubules for mitosis to occur normally.

Although overexpression of NDL1 had little effect on dynein localization, I wanted to determine if it had any effect on dynein activity by observing dynein-mediated spindle movements. I incorporated a galactose inducible promoter (GAL1p) upstream of the NDL1 gene locus through homologous recombination (see Materials and Methods). Because growth in galactose can have unexpected effects, I grew the wild-type control in galactose and compared the results to a strain containing GAL1p:NDL1 for consistency. When NDL1 was overexpressed, the number of sliding events and time actively engaged in moving the spindle was not changed (Figure 3.3A (i and iii)).

Figure 3.2

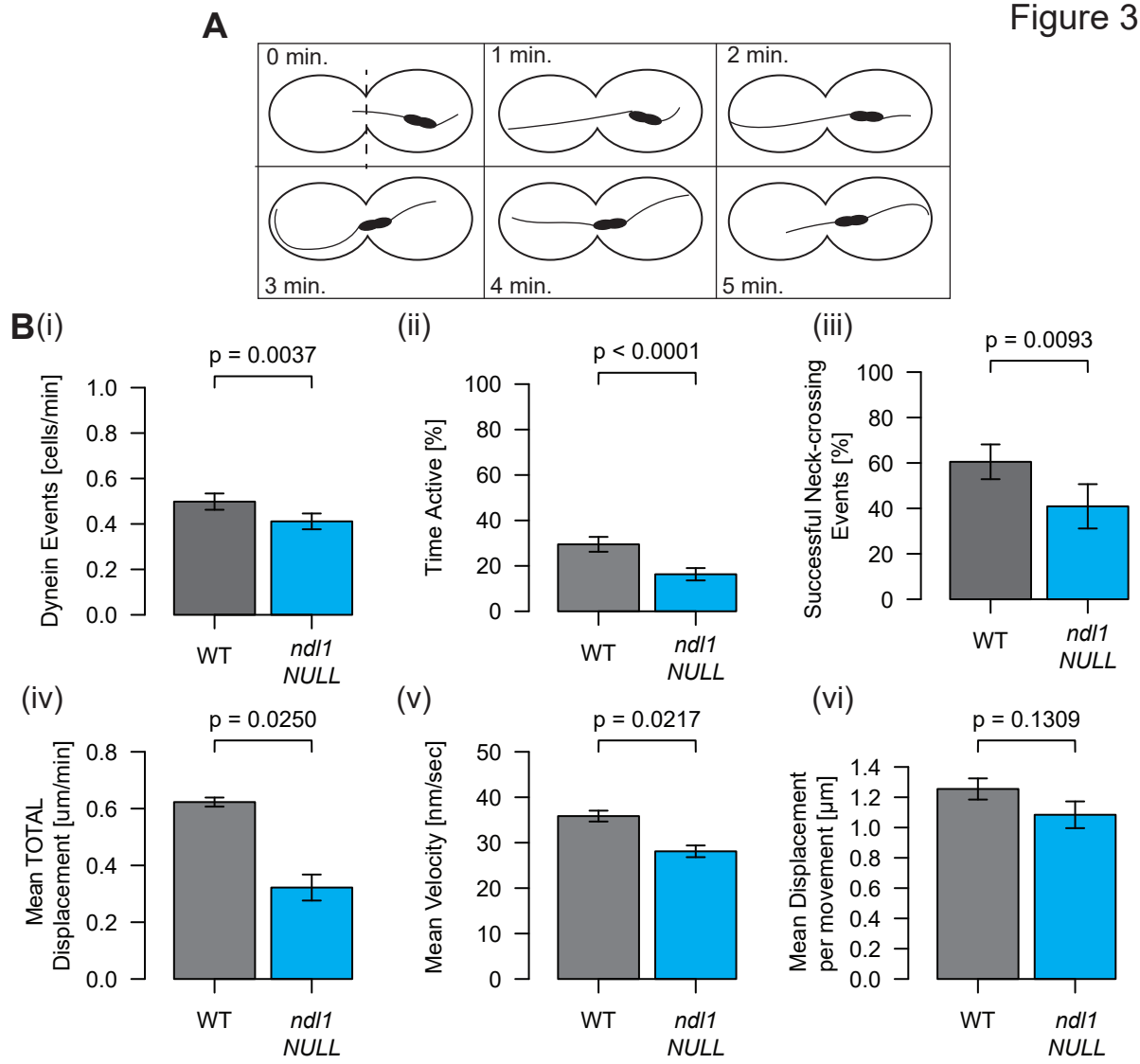

Figure 3.2. Loss of Ndl1/NudE reduces dynein-mediated spindle movements (A) Cartoon of the spindle dynamics assay. Mitotic spindle movements are directed by astral microtubule interactions with cortical dynein (not shown) between mother and daughter cells over time. Dashed line indicates the mother-bud neck. In this assay cells express GFP-Tub1 (α-tubulin) to visualize the mitotic spindle and astral microtubules. The center of the spindle was tracked with a MatLab code (see Materials and Methods) to measure its displacement over the course of a 10 minute movie. Combined with these measurements, dynein-mediated pulling events were determined by hand to calculate the following parameters. (B) Wild type or ndl1 NULL cells were grown to mid-log phase in SD media supplemented with glucose and arrested in 200µM Hydroxyurea (HU). Cells were immobilized on agarose pads containing 200µM HU for the duration of imaging. (i) The average number of dynein-mediated pulling events over the course of the movie. (ii) Percent of successful attempts that the spindle crossed the mother-bud neck. (iii) Percent time dynein was actively pulling the spindle. (iv) Average total displacement per minute of all dynein-mediated spindle movements. (v) Average velocity of dynein-mediated spindle movements. Error bars in (i-iii) represent the standard deviation of the weighted average (n ≥ 2 experiments). Error bars in (iv) and (v) represent the standard error of mean (n ≥ 36 cells).

The only parameter that changed significantly was an increase in velocity of spindle movements (32.1 ± 1.87 nm/sec WT; 38.1 ± 1.61 nm/sec GAL1p:NDL1; Figure 3.3A (v)). Recall that NDL1 overexpression increased dynein frequency at plus ends and the cortex, although the intensity at these foci did not increase (Figure 3.1E-F). This indicates that the small increase in dynein delivered to the cortex under this condition was enough to increase the spindle velocity, but not enhance the force generated or total spindle displacement. The results from the spindle dynamics assay demonstrate that Ndl1 affects dynein force generation (successful neck crosses) and overall activity, but through a role in dynein recruitment and not a direct effect on motor activity.

To test the hypothesis that Ndl1 acts upstream of Pac1, I attempted to rescue the NDL1 null defects by overexpressing Pac1. In unarrested, normally growing cells, overexpression of Pac1 increases dynein accumulation at plus ends and the cortex, and microtubule sliding events occur more frequently (Markus et al., 2011). Additionally, NDL1 null defects are rescued by the overexpression of Pac1 (Li et al., 2005; Efimov, 2003), therefore I expected the spindle dynamics assay to have similar results. Surprisingly, control cells (GAL1p:PAC1 with wild-type NDL1) had few sliding events, and zero successful neck crosses (Figure 3.3A (i and ii)). GAL1p:PAC1 did not rescue the spindle oscillation defects observed from NDL1 null cells. The number of sliding events remained unchanged as did the time dynein was active (Figure 3.3A (i and iii)). Neck crosses remained at zero and the velocity and total displacement of the spindle were unchanged. The number of sliding events actually decreased, and each event was shorter when Ndl1 was deleted and Pac1 was overexpressed (Figure 3.3A (ii-vi)). These results appear to contradict previous findings; however, I noted an unusual number of broken microtubules pulled out of the SPB and floating in the cell under these conditions. Broken microtubules were also observed by Markus et al. 2011. To cross the mother-bud neck, high dynein pulling forces are required to successfully move the nucleus through the narrow passage. If GAL1p:PAC1 microtubules break

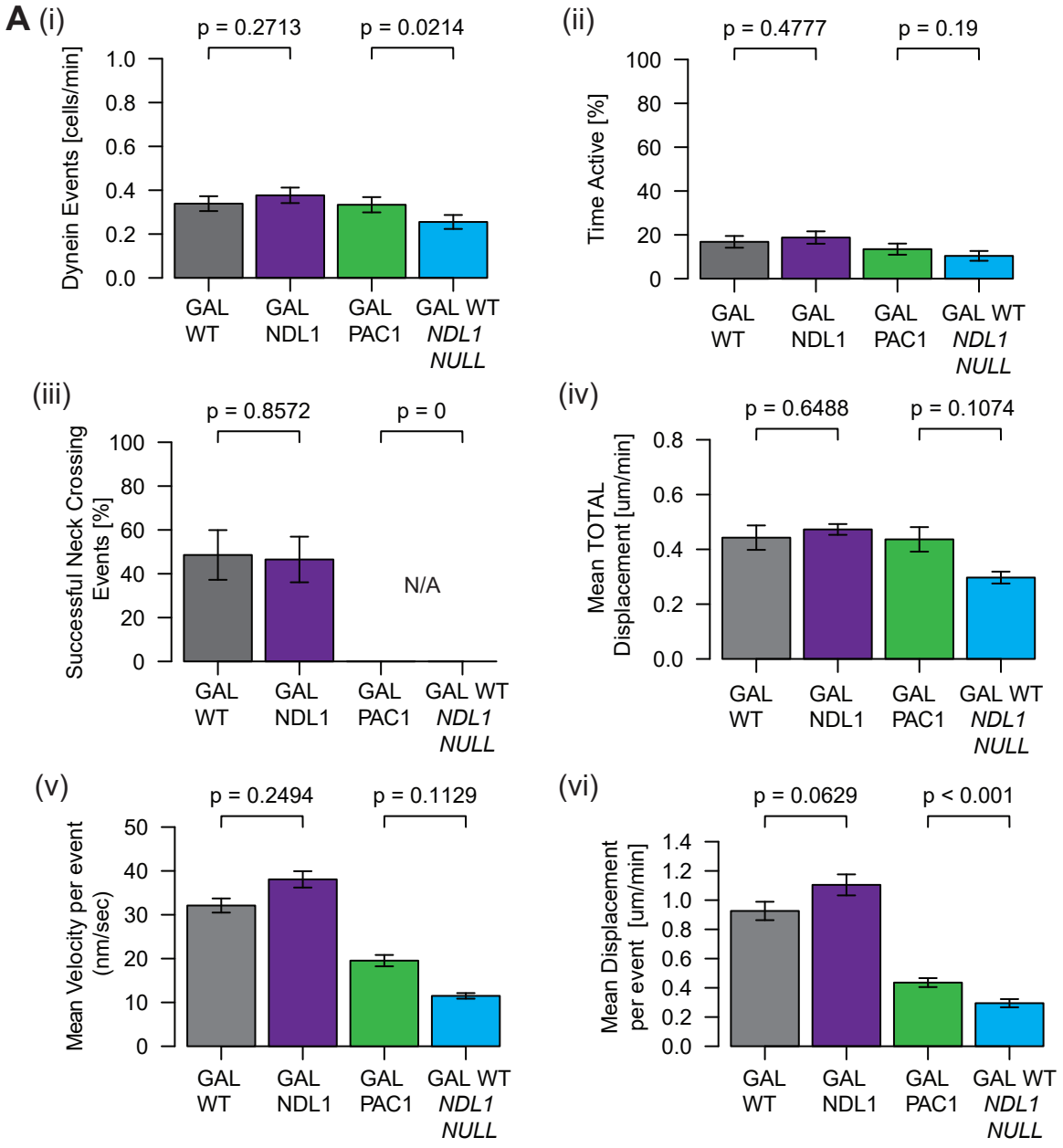

Figure 3.3. Overexpression of Ndl1/NudE has little effect on spindle dynamics. Spindle dynamics assay as described in Figure 3.2. (A) Cells were grown to mid-log phase in SD media supplemented with raffinose and arrested in SD media containing galactose and 200μM Hydroxyurea (HU) to overexpress either GAL1p:Ndl1, or GAL1p:Pac1. Cells were immobilized on agarose pads containing galactose and 200μM HU for the duration of imaging. (i) The average number of dynein-mediated pulling events over the course of the movie. (ii) Percent of successful attempts that the spindle crossed the mother-bud neck. (iii) Percent time dynein was actively pulling the spindle. (iv) Average total displacement per minute of all dynein-mediated spindle movements throughout each movie. (v) Average velocity of dynein-mediated spindle movements. Error bars in (i-iii) represent the standard deviation of the weighted average (n = 2 experiments). Error bars in (iv) and (v) represent the standard error of mean (n ≥ 36 cells).

more often, then it makes sense that neck crosses were not observed. Additionally, Markus et al. 2011 included cells in G1 that have not formed a bud, explaining why more sliding events may have been seen in the presence of Pac1 overexpression. Because of this unexpected effect on microtubules, overexpression of Pac1 is not a viable rescue experiment for NDL1 null mutants in *this particular assay.*

Ndl1/NudE must interact with dynein to enhance Pac1/Lis1-mediated dynein plus end targeting

The current model for Ndl1/NudE function predicts that Ndl1/NudE enhances Pac1/Lis1-mediated dynein targeting to plus ends by tethering Pac1/Lis1 to the motor (McKenney et al., 2010). Ndl1/NudE has been shown to interact with both Pac1/Lis1 and in the dynein tail domain with the intermediate chain and LC8 (Efimov and Morris, 2000; Niethammer et al., 2000; Sasaki et al., 2000; Liang et al., 2004; Stehman et al., 2007; McKenney et al., 2011). To determine whether or not an interaction with dynein is required for Ndl1 function, I disrupted the potential Ndl1-binding site on dynein by expressing a fluorescently labelled fragment of dynein that contains only the motor domain with the tail deleted ($dyn1_{MOTOR;}$ Markus et al., 2009). As a result of the tail deletion, monomeric $dyn1_{MOTOR}$ fragments accumulate at plus ends at high levels because they cannot associate with dynactin and be offloaded to the cortex. In these cells, I then deleted or overexpressed NDL1 to determine what effect Ndl1 would have on dynein localization.

I predicted that the presence or absence of Ndl1 would have no effect on $dyn1_{MOTOR}$ localization because Ndl1 would not be able to “enhance” binding or tether Pac1 to the motor without interacting with dynein. Unexpectedly, when NDL1 was deleted the fluorescence intensity of $dyn1_{MOTOR}$ at plus ends significantly increased (Figure 3.4C), which contrasts the results seen with full-length dynein (Figure 3.1C). In accordance with fluorescence intensity, the frequency of plus ends with $dyn1_{MOTOR}$ increased in the absence of Ndl1 (Figure 3.4D). These data suggest that wild-type Ndl1 levels (control cells) may sequester Pac1 from binding $dyn1_{MOTOR}$ and when

Figure 3.4

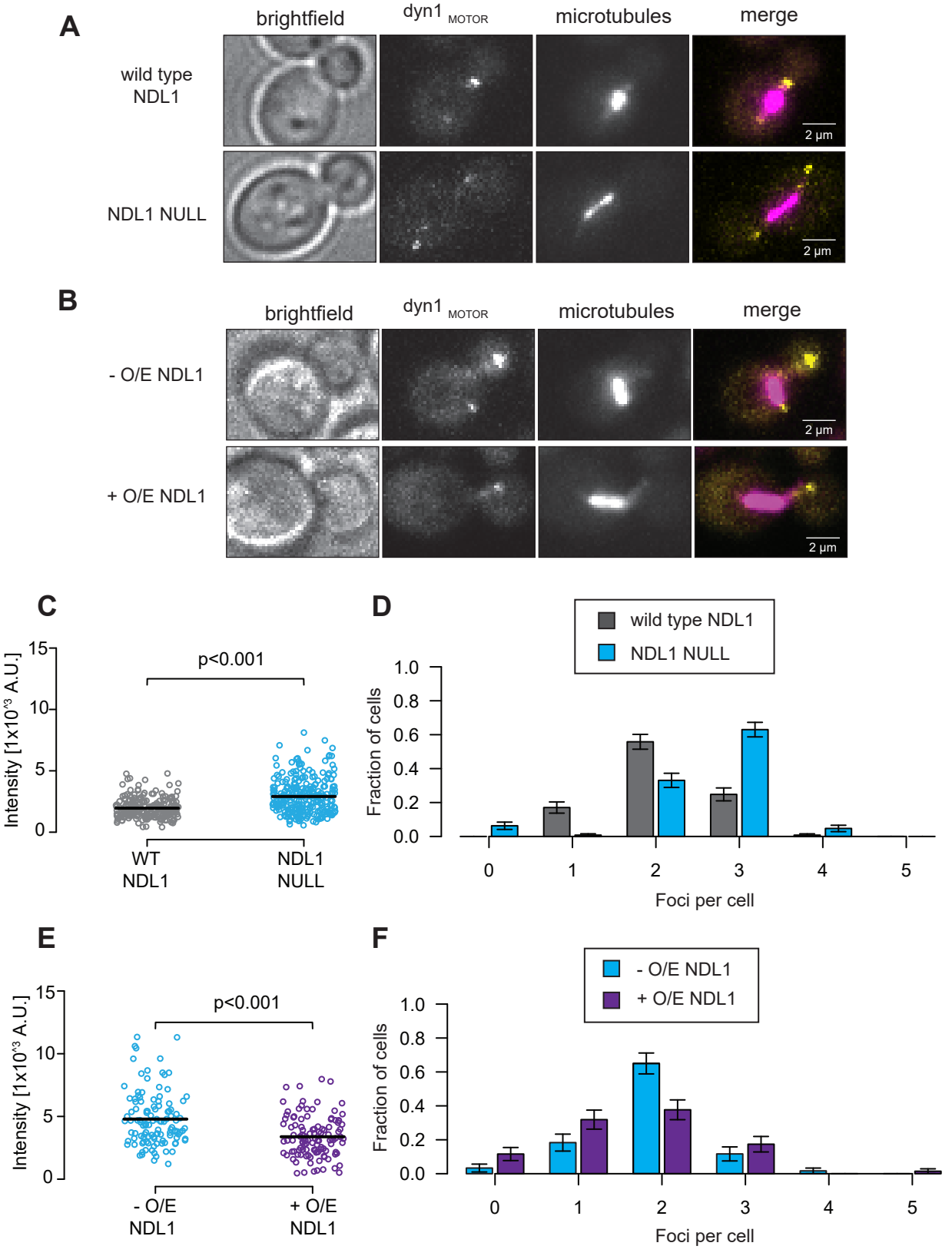
A
brightfield
dyn1 MOTOR
microtubules
merge
wild type NDL1
NDL1 NULL
2 µm
B
brightfield
dyn1 MOTOR
microtubules
merge
- O/E NDL1
+ O/E NDL1
2 µm
C
Intensity [1x10^3 A.U.]
p<0.001
WT NDL1
NDL1 NULL
D
wild type NDL1
NDL1 NULL
Fraction of cells
Foci per cell
E
Intensity [1x10^3 A.U.]
p<0.001
- O/E NDL1
+ O/E NDL1
F
- O/E NDL1
+ O/E NDL1
Fraction of cells
Foci per cell

Figure 3.4. Overexpression of Ndl1/NudE depletes dyn1$_{MOTOR}$ from plus ends. (A) Representative images of wild-type NDL1 or ndl1 NULL cells expressing mTurquoise2-Tub1 (α-tubulin) and dyn1$_{MOTOR}$-3YFP used for quantification in C and D. (B) Representative images of GAL1p:NDL1 cells expressing mTurquoise2-Tub1 (α-tubulin) and dyn1$_{MOTOR}$-3YFP used for quantification in E and F. Cells were grown to approximately the first cell division in SD media supplemented with glucose (uninduced; -O/E NDL1) or galactose plus raffinose (induced; +O/E NDL1). (C) Scatter plots represent the fluorescence intensity distribution of dyn1$_{MOTOR}$-3YFP plus end foci (n ≥ 225 foci) shown in A. (D) The percentage of cells that exhibit plus end dyn1$_{MOTOR}$-3YFP foci is plotted for the strains shown in A. Error bars represent the standard error of proportion (n ≥ 127 cells). (E) Scatter plots represent the intensity distribution of dyn1$_{MOTOR}$-3YFP plus end foci shown in B (n ≥ 40 foci). (F) The percentage of cells that exhibit plus end dyn1$_{MOTOR}$-3YFP foci is plotted for the strains shown in B. Error bars represent the standard error of proportion (n ≥ 60 cells). The black line in C and E represents the mean and statistical significance (p ≤ .05) was determined with a Mann-Whitney test because the data points do not fit a normal gaussian distribution (based on a Shapiro-Wilk analysis).

Ndl1 is absent, more Pac1 becomes available to bind and recruit dyn1$_{MOTOR}$ to plus ends. To investigate further if Ndl1 competes with dyn1$_{MOTOR}$ for Pac1 binding, I overexpressed Ndl1. I now

expected to see lower levels of dyn1$_{MOTOR}$ at plus ends than in wild-type Ndl1 cells because excess Ndl1 would bind Pac1 and prevent it from interacting with dyn1$_{MOTOR}$. As expected, Ndl1 overexpression significantly decreased fluorescence intensity of dyn1$_{MOTOR}$ and decreased the number of dynein plus end foci in each cell (Figure 3.4E-F). Due to Pac1 dependency on dynein for localization to plus ends (Markus et al., 2011), these results are also as a readout of Pac1 levels and support the hypothesis that Pac1 is sequestered by excess Ndl1, therefore decreasing dyn1$_{MOTOR}$ at plus ends. From these experiments, I conclude that the dynein tail domain is required for Ndl1 to increase dynein plus end accumulation. Further, excess Ndl1 reduces dyn1$_{MOTOR}$ localization at plus ends and the cortex, most likely by sequestering Pac1 and preventing dyn1$_{MOTOR}$ from being targeted to the plus end.

Pac1/Lis1 has an overlapping binding site for Ndl1/NudE and dynein

To determine if the decrease in dyn1$_{MOTOR}$ plus end localization is due to Ndl1 binding and sequestering Pac1, I used a FLAG-bead pulldown assay. I bound purified Pac1-1xFLAG-SNAP (construct from S. Reck-Peterson) to anti-FLAG beads and incubated with equal amounts of GST-

Dyn1^{331KDa}. This dynein construct was used to eliminate the potential Ndl1 binding site by replacing the tail domain with GST to dimerize the motor domains (Figure 3.5A) (Reck-Peterson et al., 2006). With increasing concentrations of purified Ndl1, GST-Dyn1^{331KDa} protein levels decreased in the bead bound fraction and increased in the flow-through, signifying that dynein was no longer bound to Pac1-FLAG beads (Figure 3.5). In controls, Ndl1 bound to Pac1-FLAG beads demonstrating a direct interaction that has not been shown before (Figure 3.5A (i)). Size exclusion chromatography was used to confirm the interaction between Ndl1 and Pac1, but was inconclusive (Figure 3.6A). These data demonstrate that Ndl1 competes off GST-Dyn1^{331KDa} from Pac1 likely through a direct interaction with Pac1. This indicates that dynein and Ndl1 share an overlapping binding site on Pac1.

3.3 DISCUSSION

In summary, the in vivo and in vitro data presented here demonstrate that Ndl1/NudE enhances the amount of Pac1/Lis1-mediated dynein that is targeted to microtubule plus ends for optimal spindle positioning. In the absence of the dynein tail domain, Ndl1/NudE cannot enhance dynein localization and even causes a decrease in dynein accumulation at plus ends and the cortex. Further, my in vitro results suggest that this decrease in dynein accumulation is due to Ndl1/NudE competing for an overlapping binding site on Pac1/Lis1. Therefore, Ndl1/NudE must interact with both dynein and Pac1/Lis1 to improve dynein targeting- likely acting as a tether between the two. Together these data present a compelling argument that Ndl1/NudE can either enhance Pac1/Lis1-mediated dynein targeting or prevent Pac1/Lis1-dynein interaction depending on the context.

Considering the multi-step path dynein takes to reach its site of activity- the cortex- it is interesting that dynein must be targeted to the plus end first and then be delivered to the cell cortex rather than associating directly from the cytoplasm (Lee et al., 2003b, 2005; Sheeman et al., 2003). Experiments done to bypass the plus end have shown that dynein exists in a “masked” or inhibited state that requires the regulatory steps of targeting to the plus end to become active

Figure 3.5

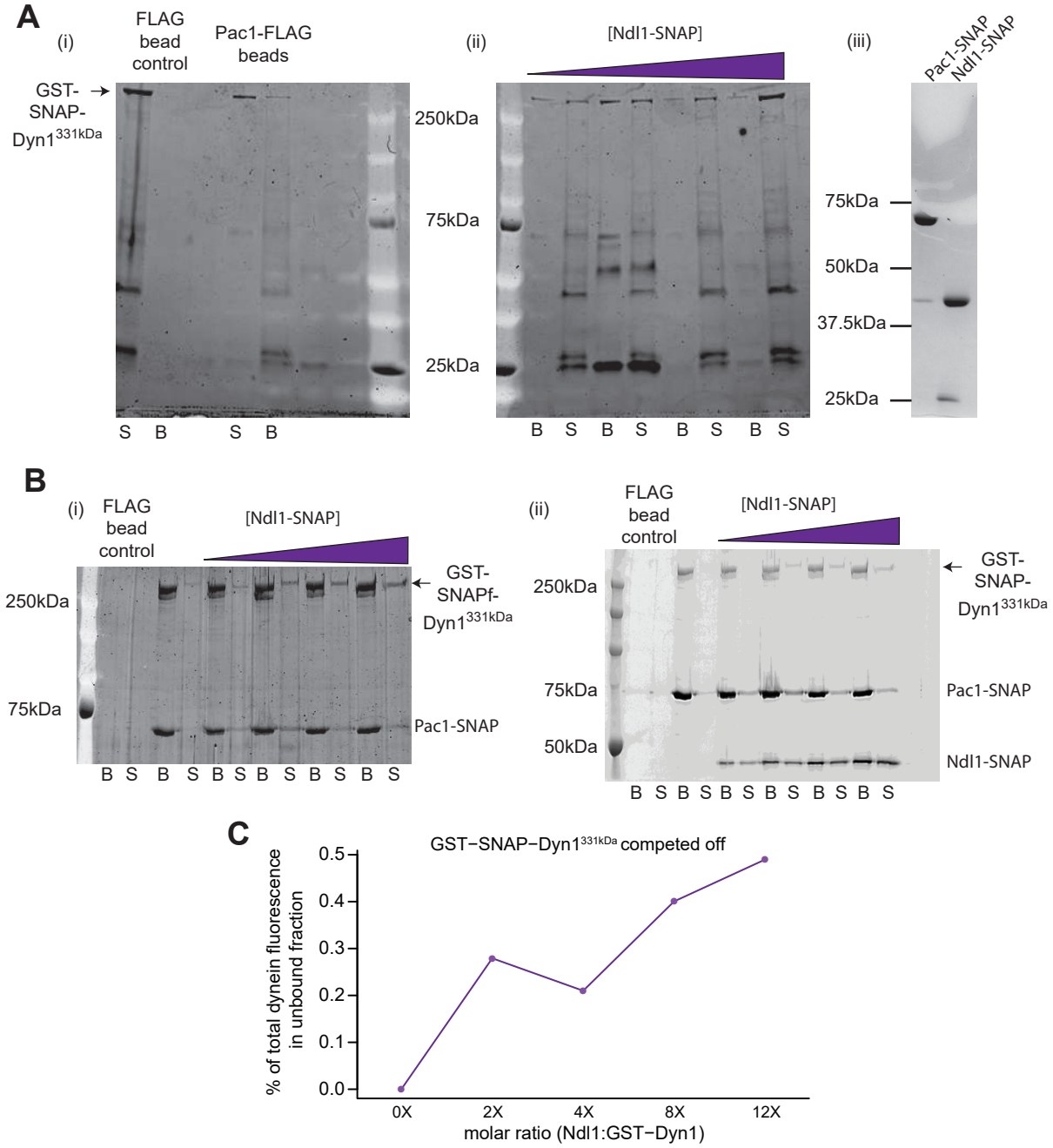

Figure 3.5. Pac1/Lis1 has a single binding site for Ndl1/NudE and dynein. Pac1-1XFLAG-SNAP coated FLAG beads incubated with either GST-SNAP-Dyn1^{331kDa} or GST-SNAP-Dyn1^{331kDa} with some concentration of Ndl1-SNAP. After washing (unbound fraction; S), Pac1 was competed off beads with FLAG epitope (bound fraction; B) and ran on 7.5% SDS-PAGE gels. (A) Gels stained with Sypro-Ruby (Thermo Fisher Scientific). (i) Control beads with no Pac1 bound or Pac1-FLAG beads alone. (ii) Pac1-FLAG beads incubated with GST-Dyn1^{331kDa} and increasing concentrations of Ndl1 (0X, 2X, 4X, 8X, 12X approx. molar ratio Ndl1:GST-Dyn1^{331kDa}) (iii) Pac1-SNAPf and Ndl1-SNAPf purification. (B) Repeat of experiment in A. (i) Sypro ruby stain of gel. (ii) Fluorescence scan of SNAPf-660 labeled proteins from same gel as (i). (C) GST-Dyn1^{331kDa} unbound fraction (S) fluorescence values quantified from A on the left and B on the right with ImageJ and normalized and averaged togeher. Increasing concentrations of Ndl1 resulted in increased GST-Dyn1^{331kDa} in the unbound fraction.

to pull on astral microtubules and position the spindle (Markus et al., 2009; Markus and Lee, 2011; Marzo et al., 2019b). My work in Chapter 2 addresses the possibility that release of Pac1/Lis1 binding by associating with the cortical anchor Num1 is a critical step in dynein activation, yet recent work in our lab suggests Pac1/Lis1 may have an additional role. Marzo et al. (2019 preprint) was able to fully reconcile the hypothesis that dynein is "masked" by showing that dynein forms an autoinhibitory conformation called the 'phi particle' due its structure looking like the Greek letter phi, previously thought not to occur in yeast (Zhang et al., 2017). Marzo et al. (2019 preprint) re-evaluated the effect of Pac1/Lis1 on dynein motility and determined that Pac1 surprisingly improved motility in contrast to its accepted effect as a dynein inhibitor (Huang et al., 2012). In light of these results, the initial role of Pac1/Lis1 may be to 'open' dynein by physically preventing it from returning to its 'closed' or autoinhibitory state.

However, the process of Pac1/Lis1 binding to dynein in the cytoplasm may be inefficient: in the 'closed' state Pac1/Lis1 is precluded from binding and must wait for dynein to randomly sample the 'open' conformation. For this reason, it is possible that the role of Ndl1/NudE is to enhance the efficiency of Pac1/Lis1 binding to dynein because of this autoinhibitory conformation (Qiu et al., 2019b). Ndl1/NudE may be able to access the tail domain more easily and recruit a high, local concentration of Pac1/Lis1 to be available when dynein randomly releases from its autoinhibition. Because overexpression of Pac1/Lis1 can rescue the loss of Ndl1/NudE, it is conceivable that Ndl1/NudE acts 'upstream' to interact with dynein first and recruit high levels of Pac1/Lis1 to the vicinity. When Pac1/Lis1 is bound between AAA3 and AAA4, the autoinhibitory conformation is physically prevented, and an 'open' dynein is targeted to astral microtubule plus ends (Marzo et al., 2019a; Elshenawy et al., 2019b; Htet et al., 2019; Qiu et al., 2019b). At plus ends, dynein associates with dynactin and although yeast dynein is motile without it, dynactin is required for offloading to the cortical receptor Num1 and spindle positioning (Reck-Peterson et al., 2006; Sheeman et al., 2003). Pac1/Lis1 holding dynein in an 'open' state conformation may improve dynactin recruitment (Wang et al., 2013; Dix et al., 2013).

Interestingly, Pac1/Lis1 is not associated with dynein-dynactin complexes at Num1 cortical sites (Lee et al., 2003b; Markus et al., 2011) zand was the basis of my hypothesis in Chapter 2 that Pac1/Lis1 release from dynein-dynactin is required for activation and is triggered by Num1 binding. While my work in Chapter 2 determined that Num1 binding plays a major role in Pac1/Lis1 release, the results here suggest Ndl1/NudE may be involved as well. The plus end is where all the dynein regulators meet and exchange: Ndl1/NudE and Pac1/Lis1 target dynein to the microtubule, where dynactin is recruited and finally, only dynein-dynactin complexes are offloaded to Num1 cortical patches. The exchange between Ndl1/NudE and Pac1/Lis1 regulation for dynactin likely begins at the overlapping binding site between Ndl1/NudE and dynactin on the intermediate chain in the tail domain (Stehman et al., 2007; McKenney et al., 2011). When Ndl1/NudE cannot interact with dynein either because its binding site is missing (Figures 3.4 and 3.5) or obstructed by dynactin, it will compete for Pac1/Lis1 binding with dynein. I can speculate that the recruitment of dynactin at plus ends may trigger Pac1/Lis1 release via Ndl1/NudE competition and interaction with Num1.

To determine if the competition between Ndl1/NudE and dynein for Pac1/Lis1 binding was relevant in other systems, I collaborated with the McKenney laboratory at UC Davis to test if Pac1/Lis1 also had an overlapping binding site for Ndl1/NudE and dynein in humans. Most work measuring the in vitro effects of Ndl1/NudE and Pac1/Lis1 has been done on dynein alone, but the McKenney lab used dynein-dynactin-BicD2 (DDB) complexes in a single molecule motility assay to determine the effect of NudEL (NudE-like) on processive dynein complexes. Since NudEL and dynactin share a binding site on dynein, it was not surprising that NudEL had little to no effect on the velocity or diffusion rates of DDB. At the same time, NudEL did reduce the number of DDB complexes along microtubules- like it does with dynein alone (Yamada et al., 2008; McKenney et al., 2011). These new data suggest that the microtubule dissociation effect is not caused by direct interaction and therefore may not be relevant in cells. To test if NudEL binds to Lis1 at the same site as dynein, in vitro colocalization experiments showed that NudEL interacts

wild type Lis1, but not with Lis1 mutants that prevent dynein binding (R316A and W340A) (Toropova et al., 2014; Gutierrez et al., 2017). These results suggest that NudEL binds to Lis1 at the same site as dynein. Next, my collaborators performed a competition assay on microtubules and observed that NudEL can compete off Lis1 bound to DDB complexes. Combined with my yeast data, we show that Pac1/Lis1 has one binding site for both Ndl1/NudE and dynein. I propose that to switch between regulation by Pac1/Lis1 to dynactin, Ndl1/NudE can compete off Pac1/Lis1 from motor complexes.

The results in this study suggest that Ndl1/NudE has two roles: 1. recruiting Pac1/Lis1 to dynein early in the cytoplasm and 2. contributing to Pac1/Lis1 removal from dynein-dynactin complexes during offloading (Figure 3.6B). In Chapter 2, I proposed a model that suggested the cortical receptor Num1 is required for dynein activation by either enhancing dynein-dynactin interaction or releasing Pac1/Lis1 binding, although the two mechanisms are not exclusive. Including Ndl1/NudE in this model, the mechanism for Pac1/Lis1 release may involve Ndl1/NudE competing off Pac1/Lis1 in the presence of dynactin. If we consider Num1 as an adapter protein such as BicD2 in humans, then Num1 may enhance the dynein-dynactin interaction in a way that encourages Ndl1/NudE to be competed off and bring Pac1/Lis1 with it (Figure 6.1).

If Ndl1/NudE plays a role in switching between Pac1/Lis1 and dynactin regulation, we must factor this into the spindle dynamics data. The NDL1 null phenotype can be explained by fewer dynein molecules reaching the cortex, which is supported by my localization data and Ndl1/NudE's first role in dynein targeting. However, if Ndl1/NudE competes off Pac1/Lis1 from dynein-dynactin complexes then I would expect to see Pac1/Lis1 localized at cortical patches when Ndl1/NudE is deleted, which is never seen in wild type cells (Lee et al., 2003b). Further, I would expect this is to greatly contribute to spindle movement defects. A dynein mutant described by Markus et al. (2011) that remains bound to Pac1/Lis1 at the cell cortex has a spindle mispositioning defect as severe as DYN1 null cells, yet NDL1 null defects are not nearly as severe as DYN1 null in the spindle dynamics assay (Marzo et al., 2019b). This suggests that Pac1/Lis1

Figure 3.6

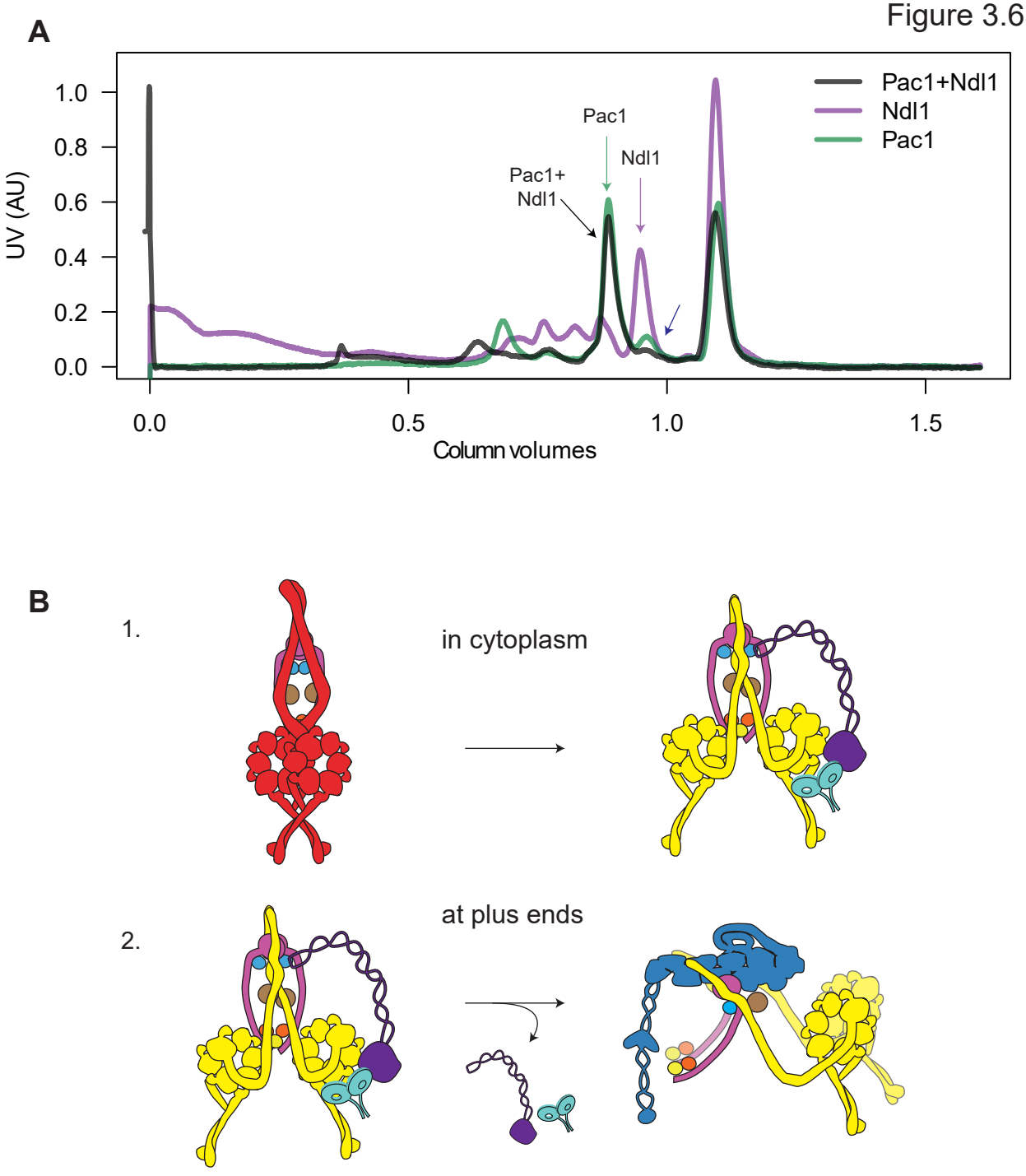

Figure 3.6. Size exclusion chromatography and model. (A) Elution profiles of Pac1-SNAP (green), Ndl1-SNAP (purple), and a mixture of both proteins (black) incubated for 10min on ice prior to loading (See Materials and Methods). Complex formation is indicated by the coelution of Pac1 and Ndl1 (black arrow) and depletion of Ndl1 (blue arrow). (B) Model of Ndl1/NudE function in yeast: 1. Ndl1/NudE (purple) aids in Pac1/Lis1 (teal) binding to open dynein conformation (from red to yellow). 2. Ndl1/NudE competes Pac1/Lis1 off dynein in the presence of dynactin.

release from dynein-dynactin is important for dynein activation and function at the cortex and secondly, Ndl1/NudE is not essential for this process. Although the data in this study support the model that Ndl1/NudE may contribute to Pac1/Lis1 release through competition, the mechanism for Pac1/Lis1 release is still not fully understood. My work strongly supports the model that Ndl1/NudE tethers Pac1/Lis1 to dynein for optimal dynein targeting to plus ends in the first step of the pathway. The results also show a shared binding site between Ndl1/NudE and dynein for Pac1/Lis1 that suggests a mechanism in which dynactin may compete Ndl1/NudE off dynein so that Ndl1/NudE can then compete Pac1/Lis1 off active dynein-dynactin complexes (Figure 3.6B). Switching between different regulatory proteins in different contexts must be important for dynein to be targeted to its proper location and activated at the correct time. This study presents Ndl1/NudE as an important player in both localizing dynein and contributing to switching between regulators.

3.4 FUTURE DIRECTIONS

The work in this chapter proposes two functions for Ndl1/NudE in budding yeast: to recruit Pac1/Lis1 to autoinhibited dynein and then to compete off Pac1/Lis1 in the presence of dynactin. To better understand these two functions, I suggest the following experiments. First, Pac1/Lis1 mutations should be used to determine if Ndl1/NudE and dynein compete for the same binding site. This experiment was done with human proteins by our collaborators with Lis1 and NudEL, but it was not done with yeast. Mutations that prevent Pac1 from binding dynein are known and can be tested easily (Toropova et al., 2014). Next, the location of the Ndl1/NudE binding site on dynein needs to be determined. The work in this study is currently lacking a control to confirm that Ndl1/NudE cannot bind the GST-Dyn1^{331KDa} construct. Point mutations in the dynein intermediate chain (Pac11) can be made and purified to examine their interaction with Ndl1/NudE in vitro. Pac11 (dynein intermediate chain) mutations that abolish dynein interaction have been determined (Siglin et al., 2013) and could be used to show whether Ndl1/NudE and dynactin share a binding site. It would be helpful to determine the binding affinities between Pac1/Lis1 and

dynein, and Pac1/Lis1 and Ndl1/NudE. If Pac1/Lis1 prefers one or the other it may help to understand how Pac1/Lis1 is released during the offloading step. Improvements to the pulldown assay should be made to better determine the amount of Ndl1/NudE required to compete dynein off Pac1-FLAG beads. These results will also improve our understanding of the affinities between the three proteins. Regarding Pac1/Lis1 release defects, fluorescently labelled Pac1/Lis1 should be imaged to determine if any Pac1/Lis1 is localized at the cortex. This would support the hypothesis that Ndl1/NudE contributes to Pac1/Lis1 release.

3.5 MATERIALS AND METHODS

Media and strain construction

All strains are derived from either YEF473A (Bi and Pringle, 1996)for imaging or W303 (constructed by Rodney J. Rothstein) for protein purification and are listed in Table 3.1 (Ralser et al., 2012). We transformed yeast strains using the lithium acetate method (Knop et al., 1999). Strains carrying null mutations, or the upstream GAL1 promoter were constructed by PCR product-mediated transformation (Longtine et al., 1998b) or by mating followed by tetrad dissection. Strains expressing mTurquoise2-Tub1 were generated as described (Markus et al., 2015). Transformants were clonally purified by streaking to individual colonies on selective media. Proper tagging was confirmed by PCR and, in some cases, sequencing. Yeast synthetic defined (SD) media were obtained from Sunrise Science Products.

Spindle Dynamics Assay and Imaging Analysis

Yeast cultures were grown overnight in SD media supplemented with 2% glucose (SD glucose) and diluted in the morning for 1 hour to mid-log phase. Cells were then arrested with 200µM hydroxyurea (HU) for 2.5 hours. Cells were mounted on 1.7% agarose pads with SD glucose containing 200µM HU for fluorescence microscopy. In strains containing a GAL1 promoter, cells were grown in SD raffinose overnight and the arrest phase was conducted in two steps: 1 hour in SD raffinose with 200µM HU and transferred to SD galactose with 200µM HU for 1.5 hours. This was to prevent an over-induction which we have observed to occur when cells

have grown in galactose containing media for more than 2.5-3 hours. The effect can revert to uninduced measurements potentially because the proteins begin to be degraded at such high levels.

Thirteen Z-stacks at 0.2µm spacing of GFP-labeled microtubules (GFP-Tub1) were acquired every 10 seconds for 10 minutes on a stage pre-warmed to 30ºC. Images were taken on a Nikon Ti-E microscope equipped with a 1.49 NA 100X TIRF objective, a Ti-S-E motorized stage, piezo Z-control (Physik Instrumente), an iXon DU888 cooled EM-CCD camera (Andor), a stage-top incubation system (Okolab), and a spinning disc confocal scanner unit (CSUX1; Yokogawa) with an emission filter wheel (ET525/50M for GFP, and ET632/60M for mRuby2; Chroma). The 488 nm laser housed in a LU-NV laser unit equipped with AOTF control (Nikon) were used. The microscope was controlled with NIS Elements software (Nikon).

To analyze the images, a custom MatLab (MathWorks) code was generated to track spindle movements throughout the movie. The code analyzed the spindle as a single Z stack projection and followed its midpoint through time. The data output included velocity and displacement of each spindle movement per frame. Each cell (n ≥ 16 cells per experiment) was then analyzed by hand to determine which movements were dynein-mediated pulling events and which were diffusive.

Wide-field image acquisition and data analysis

Yeast cultures were grown overnight in SD media supplemented with 2% glucose (SD glucose) or 2% raffinose (SD raffinose; strains containing a GAL1 promoter) and diluted in the morning to mid-log phase to maximize cells in mitosis. Cells grew in either SD glucose or for overexpression phenotypes, SD galactose. Cells were mounted on 1.7% agarose pads containing non-fluorescent SD media. Wide-field fluorescence images were collected using a 1.49 NA 100× objective on a Ti-E inverted microscope equipped with a Ti-S-E motorized stage (Nikon), piezo Z-control (Physik Instrumente), a SOLA SM II LE LED light engine (Lumencor), a motorized filter cube turret, and an iXon X3 DU897 cooled EM-CCD camera (Andor). The microscope system

was controlled by NIS-Elements software (Nikon). A step size of 0.5 µm was used to acquire 2-µm-thick Z-stack images. Sputtered/ET filter cube sets (Chroma Technology) were used for imaging mTurquoise2 (49001), GFP (49002), YFP (49003), and mCherry (49008) fluorescence.

Images were analyzed as single Z-stack maximum projections in Fiji software (ImageJ, National Institutes of Health). Only mitotic cells with a spindle length between 0.16µm and 0.4µm and a bud were considered for analysis. Plus end and SPB foci were identified in two color movies and scored accordingly. Specifically, plus end molecules were recognized as those foci that localized to the distal tips of dynamic microtubules (identified via mTurquoise2-Tub1 or mRuby-Tub1 imaging), whereas SPB molecules were recognized as those foci that localized to one of the spindle poles. Cortical molecules were identified as those foci not associated with an astral microtubule plus end that remained stationary near the cell cortex for at least three frames. Intensity measurements were determined by the integrated pixel density (ImageJ) of a 3 x 3 pixel box defining the focus. Two data sets were considered statistically significant if a Student's *t* test (assuming unequal variance) returned a p-value < 0.05.

Protein purification and pulldown assay

To purify 6xHis-GFP-3XHA-GST-DYN1^{331kD}-HALO and Ndl1-SNAPf yeast cells were grown in 3ml YPAD (YPA supplemented with 2% glucose) overnight, transferred to 25ml YPAD for the day, poured into 200ml YPA supplemented with 2% raffinose overnight and finally overexpressed in 1L YPA supplemented with 2% galactose for 24hrs. Cells were harvested by centrifugation, washed once with water and the resuspended cell pellet was then frozen by drops in liquid nitrogen. Lysis was performed by grinding the liquid nitrogen-frozen pellets with a coffee grinder (Hamilton Beach model 80374). The cell powder was melted in 0.2 volumes of 5X dynein lysis buffer (1X dynein lysis buffer: 30 mM HEPES (pH 7.2), 50 mM K-Acetate, 2 mM Mg-Acetate, 1 mM EGTA, 10% glycerol, 0.2% Triton X-100, 1 mM DTT, 0.5 mM Mg-ATP, 1 mM Pefabloc). Subsequent steps were at 4°C unless indicated. After lysis, the initial supernatant was centrifuged at 13,000 rpm for 15 min. The resulting supernatant was then incubated with IgG sepharose

(Amersham Pharmacia) for 1 hour. The IgG beads containing bound protein were then washed 2 times with dynein lysis buffer with 0.1% Triton X-100, and washed twice with 'modified' TEV cleavage buffer (10 mM Tris (pH 8.0), 150 mM K-Acetate, 2mM Mg-Acetate, 0.005% TritonX-100, 0.5 mM ATP, 1 mM DTT, 1 mM Pefabloc). The beads were then incubated with 1ul of 1mM SNAP-Alexa Fluor 647 substrate (New England Biolabs) for 10 minutes at room temperature in the dark. After washing 3-5 times with 'modified' TEV cleavage buffer, beads were resuspended in 0.1ml and incubated with TEV protease for 1 hour at 16°C. Ndl1 protein was similarly purified via its ZZ tag, with the exception that all buffers lacked Mg-ATP and TEV cleavage was left overnight at 4ºC in 0.3-0.4ml of 'modified' TEV cleavage buffer to increase efficiency. Approximate yield for 1L of $Dyn1_{331kD}$ was 0.20µM (0.13 mg/ml) while 8L of Ndl1 was prepped to yield 0.32 mg/ml (7.7µM).

Pac1-1xFLAG-SNAPf was purified via 8X-HIS and ZZ tags. Cells were grown, harvested, and lysed as above. Lysed cells were resuspended in 0.2 volumes of 5X Buffer A (1X Buffer A: 50 mM K-Phosphate [pH 8.0], 150 mM K-Acetate, 150 mM NaCl, 2 mM Mg-Acetate, 5 mM β-mercaptoethanol, 10% glycerol, 0.2% Triton X-100, 0.5 mM Pefabloc, and 1 mM PMSF) supplemented with 10 mM imidazole (pH 8.0). Note: Mg-Acetate will crash out at the 5X concentration so this component was added after diluting buffer into cell lysate. Subsequent steps were at 4°C unless indicated. The lysate was clarified by centrifugation at 13,000rpm for 20 min. The supernatant was incubated with Ni-NTA agarose (QIAGEN) for 1 hour, washed three times with Buffer A + 20 mM imidazole, and eluted with 10ml Buffer A + 250 mM imidazole. Eluted protein was then incubated with IgG sepharose beads (Amersham Pharmacia) for 1 hour and washed twice with Buffer A + 20 mM imidazole and once with 'modified' TEV cleavage buffer. Beads containing bound Pac1 were incubated with 1µl of 1mM SNAP-Alexa Fluor 647 substrate (New England Biolabs) for 10 minutes at room temperature in the dark. After washing 3-5 times with 'modified' TEV cleavage buffer, beads were resuspended in 0.3-0.4ml and incubated with TEV protease overnight at 4°C. Approximate yield for 8L of Pac1-SNAPf was 0.36 mg/ml (4.5µM).

For the pulldown assay excess Pac1 protein was pre-incubated with anti-FLAG M2 agarose beads (Sigma-Aldrich) rotating for 1 hour at 4ºC. The beads were washed 2 times with 'modified' TEV cleavage buffer (lacking DTT and Triton X-100 for the remainder of this assay). Each reaction contained 20µl of Pac1-bound beads and total volume of 30µl protein mixture. A constant concentration of GST-dyn1 was included in each reaction with different concentrations of Ndl1 as noted in Figure 3.5. These mixtures were incubated with the Pac1-bound anti-FLAG beads for 1.5 hours at 4ºC. The beads were centrifuged at 500 x g for 1 minute and the supernatant was collected as the 'unbound' fraction to be run on an SDS-PAGE gel. The remaining beads were washed twice with Wash Buffer (30mM Hepes pH 7.2, 200mM K-Acetate, 2mM Mg-Acetate, 2mM EGTA, 10% glycerol, 0.5mM Mg-ATP), and once with 'modified' TEV cleavage buffer. To elute Pac1 and any proteins bound to Pac1, 30µl of 'modified' TEV cleavage buffer with 1µl of 5mg/ml FLAG peptide was added to the beads for 30min at 4ºC. The beads were centrifuged at 500 x g and the supernatant was collected as the 'Pac1 bound' fraction. Both unbound and bound fractions were boiled in 1X SDS Sample Buffer and run on a 7.5% SDS-PAGE gel. The gels were scanned for Alexa-647 fluorescence with Typhoon FLA 9500 (GE Healthcare Life Sciences) and then stained with SYPRO Ruby protein stain (Thermo Fisher Scientific) for quantification.

Size exclusion chromatography

Proteins purified as described were ran on Superose 6 Increase 10/300 column using a NGC Chromatography System (Bio-Rad) that had been equilibrated with dynein assay buffer (50 mM Tris–HCl [pH 8.0], 150 mM potassium acetate, 2 mM magnesium acetate, 1 mM EGTA, 5% glycerol, and 1 mM DTT). Fractions (0.5ml) were collected and combined, but not concentrated. Protein concentration was determined using Bradford Reagent (Bio-Rad) and BSA standards. For binding experiments, indicated combinations of gel-filtered protein were pre-incubated at a concentration of 600nM each for 10 min at 4°C. Samples were fractionated on a Superose 6

Increase 3.2/300 column that had been equilibrated with dynein assay buffer. Fractions (0.5ml) were analyzed by SDS-PAGE and Sypro staining (Thermo Fischer Scientific).

Table 3.1. Strains used in this study.

Strain	*GENOTYPE*	*Source*
SMY404	*dyn1Δ::MOTOR-3YFP::TRP1 TUB1::HPH::HIS3p:mTurquoise2-Tub1 ura3-52 lys2-801 leu2-Δ1 his3-Δ200 trp1-Δ63*	*Lammers and Markus 2015*
SMY854	*Pac1-3YFP::LEU2 TUB1::HPH::HIS3p:mTurquoise2-Tub1 ura3-52 lys2-801 leu2-Δ1 his3-Δ200 trp1-Δ63*	*Lammers and Markus 2015*
SMY948	*Dyn1-3YFP::TRP TUB1::HPH::HIS3p:mRuby2-Tub1 ura3-52 lys2-801 leu2-Δ1 his3-Δ200 trp1-Δ63*	*this study*
SMY1786	*KAN::Gal1p:Ndl1 Dyn1-3GFP::TRP1 TUB1+3'UTR::HPH::HIS3p:mRuby2-TUB1 ura3-52 lys2-801 leu2-Δ1 his3-Δ200 trp1-Δ63*	*this study*
SMY1985	*KAN::Gal1p:Ndl1 dyn1Δ::MOTOR-3YFP::TRP1 TUB1+3'UTR::HPH::HIS3p:mRuby2-TUB1 ura3-52 lys2-801 leu2-Δ1 his3-Δ200 trp1-Δ63*	*this study*
SMY2115	*Dyn1-3YFP::TRP TUB1::HPH::HIS3p:mRuby2-Tub1 ndl1Δ::HPH ura3-52 lys2-801 leu2-Δ1 his3-Δ200 trp1-Δ63*	*this study*
SMY2157	*dyn1Δ::MOTOR-3YFP::TRP1 ndl1Δ::HIS3 TUB1::HPH::HIS3p:mTurquoise2-Tub1 ura3-52 lys2-801 leu2-Δ1 his3-Δ200 trp1-Δ63*	*this study*
SMY193	*GFP-Tub1 kar9Δ ura3-52 lys2-801 leu2-Δ1 his3-Δ200 trp1-Δ63*	*Markus et al. 2011*
SMY1921	*GFP-Tub1::LEU2 kar9Δ::KAN ndl1Δ::HIS3 ura3-52 lys2-801 leu2-Δ1 his3-Δ200 trp1-Δ63*	*this study*
SMY2110	*GFP-Tub1::LEU2 kar9Δ::KAN KAN::Gal1p:Ndl1 ura3-52 lys2-801 leu2-Δ1 his3-Δ200 trp1-Δ63*	*this study*
SMY2271	*GFP-Tub1::LEU2 kar9Δ::KAN KAN::GALp-PAC1 ura3-52 lys2-801 leu2-Δ1 his3-Δ200 trp1-Δ63*	*this study*
SMY2272	*GFP-Tub1::LEU2 kar9Δ::KAN KAN::GALp-PAC1 ndl1Δ::HIS3 ura3-52 lys2-801 leu2-Δ1 his3-Δ200 trp1-Δ63*	*this study*
SMY1008	*W303: pGAL-ZZ-TEV-6xHis-GFP-3XHA-GST-D6-DYN1-gsDHA-KanR prb1D his3-11,15 ura3-52 leu2-3,112 ade2-1 trp-1 pep4D::HIS5*	*S. Reck-Peterson*
SMY1616	*W303: GAL1p:Ndl1-ga-SNAPf-TEV-ZZ prb1D his3-11,15 ura3-52 leu2-3,112 ade2-1 trp-1 pep4D::HIS5*	*this study*
SMY287	*W303: GAL1p:8xHis-ZZ-TEV-Pac1-g-1xFLAG-gaSNAP dyn1Δ ndl1Δ prb1D his3-11,15 ura3-52 leu2-3,112 ade2-1 trp-1 pep4D::HIS5*	*S. Reck-Peterson*
Plasmid	**BACTERIAL EXPRESSION PLASMIDS**	*Source*
B842	*pBJ1153:ARSH/CEN-Gal1p:8xHis-ZZ-2xTEV-Pac1*	*this study*
B843	*pBJ1153:ARSH/CEN-Gal1p:8xHis-ZZ-2xTEV-Pac1 [R378A]*	*this study*
B844	*pBJ1153:ARSH/CEN-Gal1p:8xHis-ZZ-2xTEV-Pac1 [W419A]*	*this study*

CHAPTER 4

CONDITIONS FOR SINGLE MOLECULE DYNEIN-DYNACTIN MOTILITY

4.1 INTRODUCTION

The most notable dynein regulator is dynactin, a multi-subunit protein complex that is a processivity factor required for dynein activation. Originally discovered in a cytosolic fraction that activated purified dynein (Schroer and Sheetz, 1991), it has been used as a proxy for dynein activity and localization in the cell. Dynactin is essential for mammalian cells, and deletion of dynactin in yeast leads to loss of dynein function (Schroer, 2004; Sheeman et al., 2003; Moore et al., 2008). However, purified yeast dynein is processive independently of dynactin, while recombinant human dynein requires dynactin and an adapter protein for activity (Reck-Peterson et al., 2006; McKenney et al., 2014; Schlager et al., 2014). It is not clear how yeast dynactin impacts dynein activity or if an adapter is required for complex formation.

Both yeast and human dynactin comprise an Arp1 filament and a shoulder domain containing Jnm1/dynamitin, Ldb18/p24, and Nip100/p150^{glued} (Figure 4.2A) (Urnavicius et al., 2015; Moore et al., 2008). While human dynactin also includes additional proteins at both ends of the filament, Arp10 is the only subunit that binds the barbed end in yeast (Clark and Rose, 2006). The largest subunit, Nip100/p150^{glued}, dimerizes and contains a long extension that can interact with microtubules and +TIP proteins via a CAP-gly domain (Waterman-Storer et al., 1995). This domain is important for high force generation events such as nuclear positioning in neuronal development (Yan et al., 2015; Moore et al., 2009). Nip100/p150glued also interacts with the dynein intermediate chain (Vaughan and Vallee, 1995; King et al., 2003; Siglin et al., 2013). In addition, the major interaction between dynactin and dynein occurs between the Arp1 filament and the dynein tail domain (Figure 4.1A) (Urnavicius et al., 2015). However, the Arp1-tail

interaction only occurs in the presence of an adapter protein that slides in between the dynactin filament and the tail to hold the complex together (McKenney et al., 2014; Schlager et al., 2014).

Discovering the requirement of an adapter protein to form a processive human dynein-dynactin complex was paramount in understanding dynein activation. It had been shown that separating the motor domains removed autoinhibition and promoted processivity, but how this was regulated in cells was unclear (Torisawa et al., 2011). When the long coiled-coil adapters such as BicD2, Hook3, Spindly, or Rab11-FIP3 interact at the interface between dynein and dynactin, the motor domains are aligned in parallel to promote processive movement and decrease the frequency of dissociation (Urnavicius et al., 2015; Chowdhury et al., 2015; Olenick and Holzbaur, 2019). Forming this complex prevents dynein from reverting back to its autoinhibitory, phi-particle state (Zhang et al., 2017). Interestingly, some adapter molecules have a propensity to bind two dynein motors to one dynactin (Grotjahn et al., 2018; Urnavicius et al., 2018). These complexes have increased velocity along microtubules and may be important for specific functions. In contrast to mammalian systems, an adapter protein has not been identified in yeast, although I suggest that Num1 could fill this role (Chapter 2).

The functional homolog of Num1, NuMA in humans, has been suggested to potentially act as an adapter in addition to its cortical receptor role. NuMA contains a coiled-coil region and a Spindly-like motif that are required to activate dynein-dynactin at the cortex for spindle movements to occur (Okumura et al., 2018; Gama et al., 2017). Ectopically anchored dynein-dynactin is not sufficient to move the spindle but must interact with NuMA (Okumura et al., 2018). This supports my hypothesis that the coiled-coil region of Num1 may activate dynein by acting as an adapter. Additionally, Num1 could recruit multiple dyneins to one dynactin to increase force generation required for spindle positioning. To explore these possibilities, I established an in vitro motility assay that visualizes single molecule dynein motors. I determined the best conditions for purifying dynactin and Num1 to examine how they affect dynein motility.

4.2 RESULTS

Purification of dynein and dynactin

To investigate dynein regulation at the single molecule level, I established a dynein purification protocol by troubleshooting the original method developed by Reck-Peterson et al. (2006) and modified by Markus et al. (2011). To significantly improve protein yield, dynein was expressed from a different yeast genetic background called W303 and is used throughout the budding yeast community. Yeast background strains specifically used for protein purification have proteases deleted to prevent degradation. For reasons not completely understood, the W303 background produced significantly higher protein concentrations even though the previous strain was deficient in the same proteases. This new dynein strain contained a deletion of the dynactin subunit, Nip100, to ensure dynein was not purified with contamination from this regulator (from the Reck-Peterson Lab). To further prevent protein contamination, I deleted Num1 at its endogenous locus. In this strain, an affinity tag is attached at the N-terminus of dynein and a HaloTag is C-terminally expressed for fluorescent labeling (Dyn1-HALO; Figure 4.1A).

The purification protocol is detailed in the Materials and Methods section, but I will highlight two important modifications. First, I determined that the use of TritonX-100 detergent in the lysis and wash buffers affected dynein motility. After omitting the detergent in these steps, I reduced the concentration to 0.005% in the final storage buffer ('modified' TEV buffer). Next, the wash step that followed dynein binding to beads was changed to be less harsh. The lower salt wash was used to prevent accessory chains from dissociating. After considerable troubleshooting, the lab now consistently purifies good yields of dynein motor complexes.

I next attempted to purify the dynactin complex, which had been purified only once before by Kardon et al. (2009). Using the same yeast strain and purification strategy, I purified dynactin by using an affinity tag N-terminally fused to the Arp10 subunit and fluorescently labeled the complex with a HaloTag C-terminally fused to the Nip100 subunit (Figure 4.2A). By tagging two different subunits, only intact complexes were expected to be visualized. Each of the five subunits

were endogenously expressed to ensure the correct ratio of subunits formed complete complexes. Because the proteins were not overexpressed and likely cell cycle regulated, I determined the best cell density required for the highest protein yield. In live cells, I imaged fluorescently labeled dynactin (Jnm1-3mCherry; Table 4.1) accumulation at plus ends at different cell densities (not shown). At densities above an OD_{600} of 3.0 dynactin levels at plus ends began to decrease, therefore I limited cell growth to between 1.5 and 3.0 before harvesting. Finally, dynactin complexes were purified using the same protocol established for dynein, except that Triton X-100 concentrations were not limited (see Materials and Methods).

Protein concentrations of either dynein or dynactin were too low to visualize on SDS-PAGE. Therefore, to confirm purification of the complexes I modified the single molecule motility assay originally described by Reck-Peterson et al. (2006). Briefly, individual motor complexes were added to a flow chamber containing fluorescently labeled microtubules and visualized with TIRF microscopy (Figure 4.1A). Dynein motors (Dyn1-HALO) behaved as expected with velocities near 100nm/sec and run lengths near 2.0µm (Figure 4.1B-D) (Reck-Peterson et al., 2006; Markus and Lee, 2011; Marzo et al., 2019b). To image dynactin moving in complex with dynein, fluorescently labeled Nip100-HALO was mixed with unlabeled Dyn1-HALO motors (Figure 4.1B). I assumed that any moving dynactin molecules were in complex with dynein because they do not have any motile properties on their own (McKenney et al., 2014). Dual-color movies were attempted, but colocalized complexes were rarely, if ever observed. Unexpectedly, dynein-dynactin complexes had the same velocity and run length has dynein motors alone (Figure 4.1C-D). This result contradicts the only published data analyzing purified yeast dynactin, which show the addition of dynactin causes a two-fold increase in run length (Kardon et al., 2009). Perhaps the previous data contradict my results because their yeast strain contained Num1, which may act as a necessary adapter to form the dynein-dynactin complex. However, I performed the experiment with dynein strains containing both wild-type Num1 (not shown) and Num1 deleted (Figure 4.1) and saw identical results- dynactin does not have an effect on dynein motility.

Figure 4.1

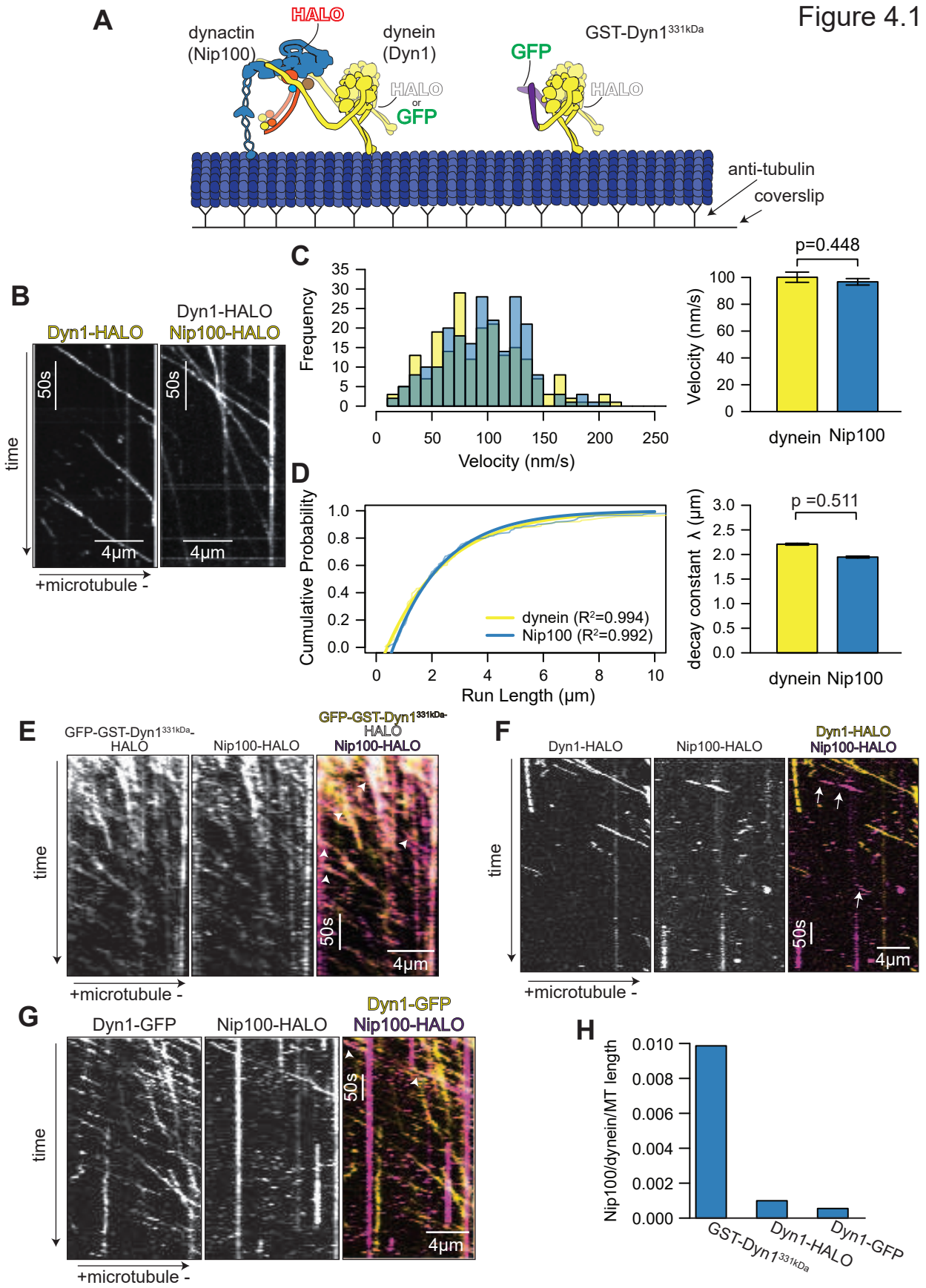
A
HALO
dynactin
(Nip100)
dynein
(Dyn1)
GST-Dyn1331kDa
GFP
HALO
or
GFP
HALO
anti-tubulin
coverslip
B
Dyn1-HALO
Dyn1-HALO
Nip100-HALO
time
50s
4μm
+microtubule -
C
Frequency
Velocity (nm/s)
p=0.448
dynein
Nip100
D
Cumulative Probability
dynein (R²=0.994)
Nip100 (R²=0.992)
Run Length (μm)
decay constant λ (μm)
p =0.511
dynein
Nip100
E
GFP-GST-Dyn1331kDa-HALO
Nip100-HALO
GFP-GST-Dyn1331kDa-HALO
Nip100-HALO
time
50s
4μm
+microtubule -
F
Dyn1-HALO
Nip100-HALO
Dyn1-HALO
Nip100-HALO
time
50s
4μm
+microtubule -
G
Dyn1-GFP
Nip100-HALO
Dyn1-GFP
Nip100-HALO
time
50s
4μm
+microtubule -
H
Nip100/dynein/MT length
GST-Dyn1331kDa
Dyn1-HALO
Dyn1-GFP

Figure 4.1. Dynactin has no effect on dynein motility. (A) Cartoon depiction of single molecule motility assay and protein constructs imaged. Dynactin was visualized with the Nip100 subunit labeled with HaloTag. Dynein was tagged with either a HaloTag or GFP and GST-Dyn1^{331KDa} contains an N-terminal GFP and a C-terminal HaloTag.(B and E-F) Kymographs for fluorescent protein indicated in bold color . HaloTag fusions were labeled with AlexaFluor 647 or TMR ligands and visualized on taxol- stabilized HiLyte 488 or 647-labeled MTs using time-lapse TIRF microscopy. Plus (+) and minus (−) indicate microtubule polarity. Kymographs represent motor complex location over time. In the y-axis, each pixel row represents a single time point and the x-axis is displacement. Each line is a single motor in time, with the inverse slope equaling the velocity. White arrows indicate examples of comigrating complexes. Motor complexes represented in B are two separate experiments: control Dyn1-HALO^{TMR} motors (left) and unlabeled Dyn1-HALO mixed with Nip100-HALO^{TMR} (right) quantified in C-D. Complexes in E and F are quantified in G. (C) Overlay of dynein and Nip100 velocity histograms (left) and mean velocity ± standard error bar plot (right). (D) Cumulative probability of run lengths of dynein and Nip100 with associated fits to a one-phase exponential decay (left) and bar plot of run length ± standard error of fit (right). R2 of fit values are displayed on cumulative probability plot. Data shown are from two independent experiments (n ≥ 214). P values were determined by Student's T-test for velocity and Mann-Whitney test comparing the fits for run length. Only those motor complexes that moved more than 3 frames were chosen for velocity and run length measurements. (G) Quantification of Nip100-HALO comigrating with either GFP-GST-Dyn1^{331KDa}-HALO or Dyn1-GFP. Buffer conditions in B and E included 150mM Potassium acetate, while 50mM Potassium acetate was used in F.

Fluorophore contamination leads to misidentification of dynactin complexes

To reconcile the difference in my results, I purified a dynein control that cannot interact with dynactin because it lacks the tail domain and instead is dimerized by GST (GST-dyn1^{331kDa}) (Reck-Peterson et al., 2006). The construct contains an N-terminal GFP as well as a C-terminal HaloTag (Figure 4.1A). Using the GFP to visualize motors and leaving the HaloTag empty, I incubated them with Nip100-HALO^{TMR} (Figure 4.1E). Strikingly, dynactin comigrated with the minimal motor domain almost 100% of the time (Figure 4.1G). These results suggest that the fluorescently labeled Nip100 subunit can interact with the motor domain, although in cells the tail domain and intermediate chain are required for Nip100 interaction (Siglin et al., 2013). Alternatively, excess HaloTag ligands from the dynactin purification could have contaminated the empty HALO substrates on GST-dyn1^{331kD} motors. I tested this hypothesis by purifying a full-length dynein construct that replaced the HaloTag fusion with GFP (Dyn1-GFP; Gennerich Lab).

In stark contrast to the robust motility seen in Fig. 4.1B-D, few dynactin complexes were seen comigrating with Dyn1-GFP molecules and only when buffer conditions were adjusted (Figure 4.1F-G; see below). Both the GST-dyn1^{331kD} and Dyn1-GFP controls prove that most dynactin complexes shown in Figure 4.1B-D are an artifact of HaloTag ligand contamination of empty HALO substrates. More importantly, the identical HaloTag fusion system was used in the published results by Kardon et al. (2009). My work shows that these published data are not representative of true dynein-dynactin complexes and a different experimental strategy is required.

Initially, I did not see any Nip100-HALO molecules in complex with Dyn1-GFP in the motility assay. This suggested that either dynactin complexes were not interacting with dynein or intact complexes were not purified. First, I reasoned that decreasing the ionic strength might enhance the interaction. Dynein and dynactin proteins were dialyzed into dynein assay buffer (DAB) that contained 50mM potassium acetate compared to the storage buffer (150mM potassium acetate; 'modified' TEV buffer). After dialysis, dynein and dynactin were incubated together and flowed into the chamber with microtubules. The comigrating complexes demonstrate that dynactin is being purified, yet the interaction between dynein and dynactin is weak due to the requirement for low salt (Figure 4.1F). Further, this purification strategy yields less dynactin than dynein molecules, and dynactin may require a different purification system.

Next, I confirmed that complete dynactin complexes were being purified. Nip100 has been shown to localize with dynein in the absence of other dynactin subunits, suggesting that Nip100 may not be a good proxy to visualize complete complexes in vitro (Moore et al., 2008). Whereas, the Arp10 subunit does not interact with dynein unless all subunits are present (Moore et al., 2008). To observe intact dynactin, I modified the fluorescent labeling system by obtaining a purification strain that included a SNAP tag (New England Biolabs) fusion protein on Arp10 in addition to Nip100-HALO (Figure 4.2A; from the Gennerich lab). Purified as before, dynactin complexes were labeled with both SNAP (Arp10) and HaloTag (Nip100) ligands. The different

fluorescent ligands cannot bind each other's substrate due to the chemistry involved (Stagge et al. 2013). Two color movies showed the frequency of dynactin complexes containing both Arp10-SNAP and Nip100-HALO subunits (Figure 4.2C). Dyn1-GFP was not imaged in these movies, but processive molecules indicated complex formation with the motor. Of the Nip100-HALO molecules observed, only 27.5% were colocalized with Arp10-SNAP suggesting that Nip100 can associate with dynein motors without an intact dynactin complex (Figure 4.2B). In contrast, Arp10-SNAP molecules colocalized with Nip100-HALO 74.1% of the time. These results demonstrate that Arp10 is the better proxy for complete dynactin formation.

Finally, I imaged Arp10-SNAP migrating under the lower salt conditions to determine the effect dynactin has on dynein motility. However, high concentrations of Dyn1-GFP were required to visualize few dynactin molecules and individual dynein runs were difficult to see at these high concentrations. Therefore, only Arp10-SNAP molecules were measured compared to a diluted Dyn1-GFP control (Figure 4.2D). These dynein-dynactin complexes had a slight, but significant increase in velocity, and no change in run length compared to dynein alone- the opposite results of the original study (Figure 4.2E-F) (Kardon et al., 2009). This supports findings that dynactin improves dynein processivity in mammalian systems (McKenney et al., 2014; Schlager et al., 2014). However, the low number of dynactin molecules affects the statistical significance between the two groups (n = 35). It will be important to increase the sample size and include other techniques to confirm that intact complexes are purified and determine if dynactin improves dynein motility.

Num1$_{CC}$ does not improve dynein-dynactin motility

Because dynactin does not have a dramatic effect on dynein, I tested the possibility that Num1 is required to form processive dynein-dynactin complexes. Recently, the Num1 functional homolog, NuMA, was characterized as an adapter with a Spindly-like motif (Okumura et al., 2018). Although Num1 does not share much sequence homology to NuMA, I compared the coiled-coil region with other NuMAs and human adapters and found a potential Spindly-like motif in amino

Figure 4.2

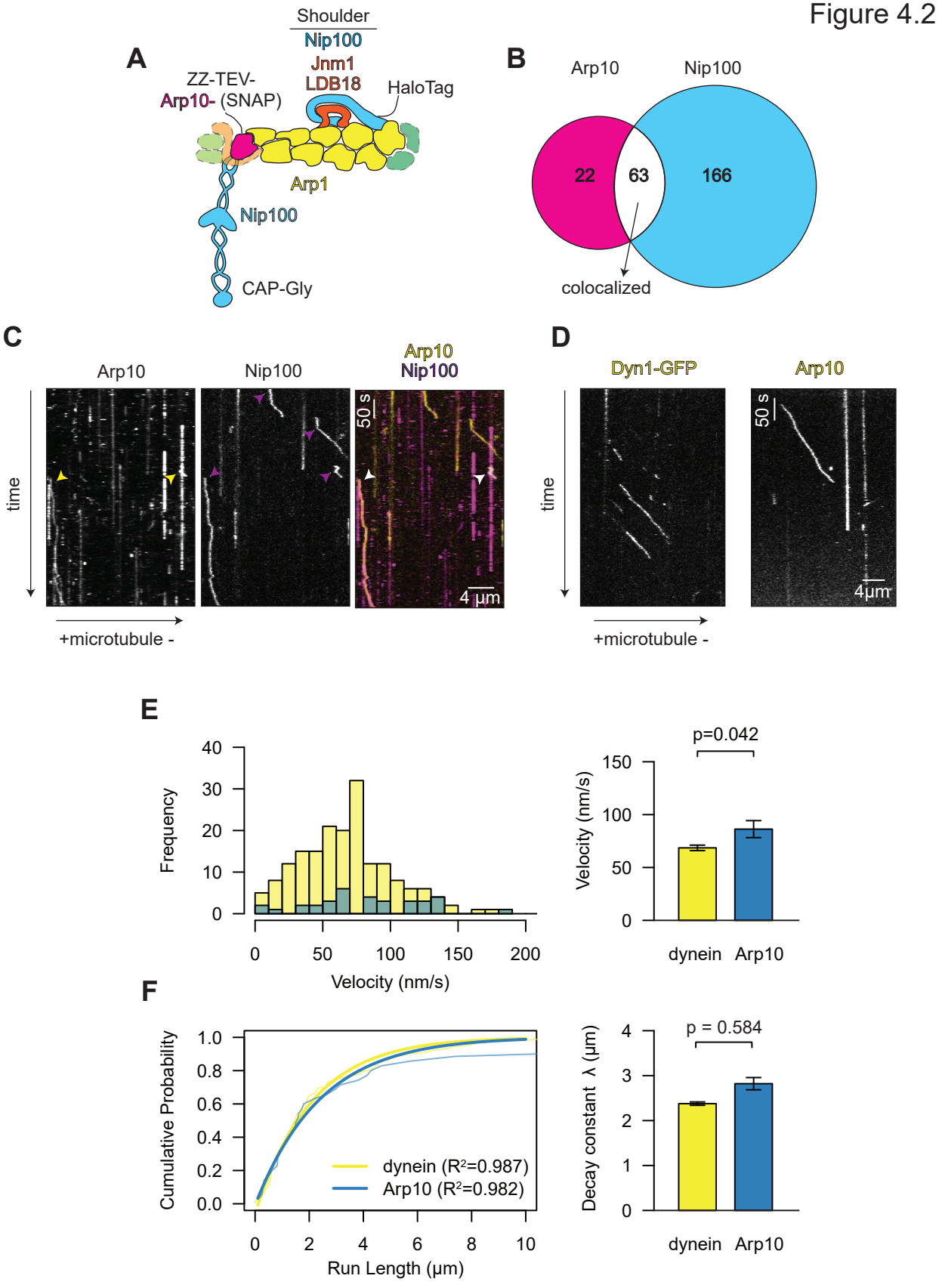
A
Shoulder
Nip100
Jnm1
LDB18
HaloTag
ZZ-TEV-
Arp10- (SNAP)
Arp1
Nip100
CAP-Gly
B
Arp10
Nip100
22
63
166
colocalized
C
Arp10
Nip100
Arp10
Nip100
time
50 s
4 µm
+microtubule -
D
Dyn1-GFP
Arp10
time
50 s
4µm
+microtubule -
E
Frequency
Velocity (nm/s)
p=0.042
Velocity (nm/s)
dynein
Arp10
F
Cumulative Probability
dynein (R²=0.987)
Arp10 (R²=0.982)
Run Length (µm)
p = 0.584
Decay constant λ (µm)
dynein
Arp10

Figure 4.2. Identification of complete dynactin complexes. (A) Cartoon diagram of yeast dynactin subunits and locations of affinity and fluorescent tags. Subunits in dashed lines are part of the human dynactin complex, but are not associated in yeast (Moore et al., 2009). Nip100 is part of the shoulder domain and forms an extension with a CAP-Gly domain. (B) Venn diagram showing the fraction of comigration between dynactin subunits. Nip100 subunits were seen migrating most often without Arp10. (C) Kymographs of Nip100-HALO^{TMR} alone (purple arrows; panel 2) or Arp10-SNAP^{647} comigrating with Nip100-HALO^{TMR} (white arrows; panel 3). Yellow arrows indicate Arp10-SNAP^{647} molecules. Dyn1-GFP used in these experiments cannot distinguished from taxol-stabilized HiLyte 488-labeled microtubules. (D) Kymographs of a control Dyn1-GFP experiment (left) compared to Arp10-SNAP^{647} molecules (right). Imaged on X-Rhodamine-labeled microtubules. Quantified in E and F. (E) Overlay of velocity histograms (left) and mean velocity bar plot ± standard error (right) for Dyn1-GFP or Arp10-SNAP. (F) Cumulative probability of run lengths of Dyn1 or Arp10 with associated fits to a one-phase exponential decay (left) and (right) bar plot of mean run length ± standard error of fit determined by λ (decay rate constant). Data shown are from one experiment (n ≥ 38).

acids 274-279 (Figure 4.3D). Using the predicted structure of Num1, amino acids 274-279 are in the dimerization domain between two Num1$_{CC}$ molecules (Tang et al., 2012). This region is not close to the known Num1-dynein disruption mutation, L167E and L170E (Tang et al., 2012), but still may be important in dynein-dynactin interaction.

Before the Spindly-like motif could be characterized, two different truncations of Num1 were purified to include in the motility assay. Tang et al. (2012) determined that the minimal domain required to recruit dynein-dynactin to Num1 patches on the cell cortex included amino acids 95-303 (Num1$_{CC}^{95-303}$; Figure 4.3A). The slightly larger construct containing amino acids 1-325 (Num1$_{CC}^{1-325}$; Figure 4.3A) also maintained the ability to pull down dynein from cells (Tang et al., 2012). For purification, I designed bacterial plasmids to express the HaloTag fusion on either the N- or C-terminus of Num1$_{CC}^{95-303}$. To determine if the HaloTag would affect function, I cloned the constructs at the endogenous locus of Num1 in cells expressing Dyn1-3mCherry and fluorescently labeled microtubules. Using the GAL1 promoter for overexpression of the constructs, I observed whether the constructs increased dynein accumulation at SPBs (minus ends) as expected (Chapter 2). I found that the C-terminally tagged Num1$_{CC}$ had higher levels of dynein SPB localization, while the N-terminal tag cells remained low (Figure 4.3B). These results

Figure 4.3

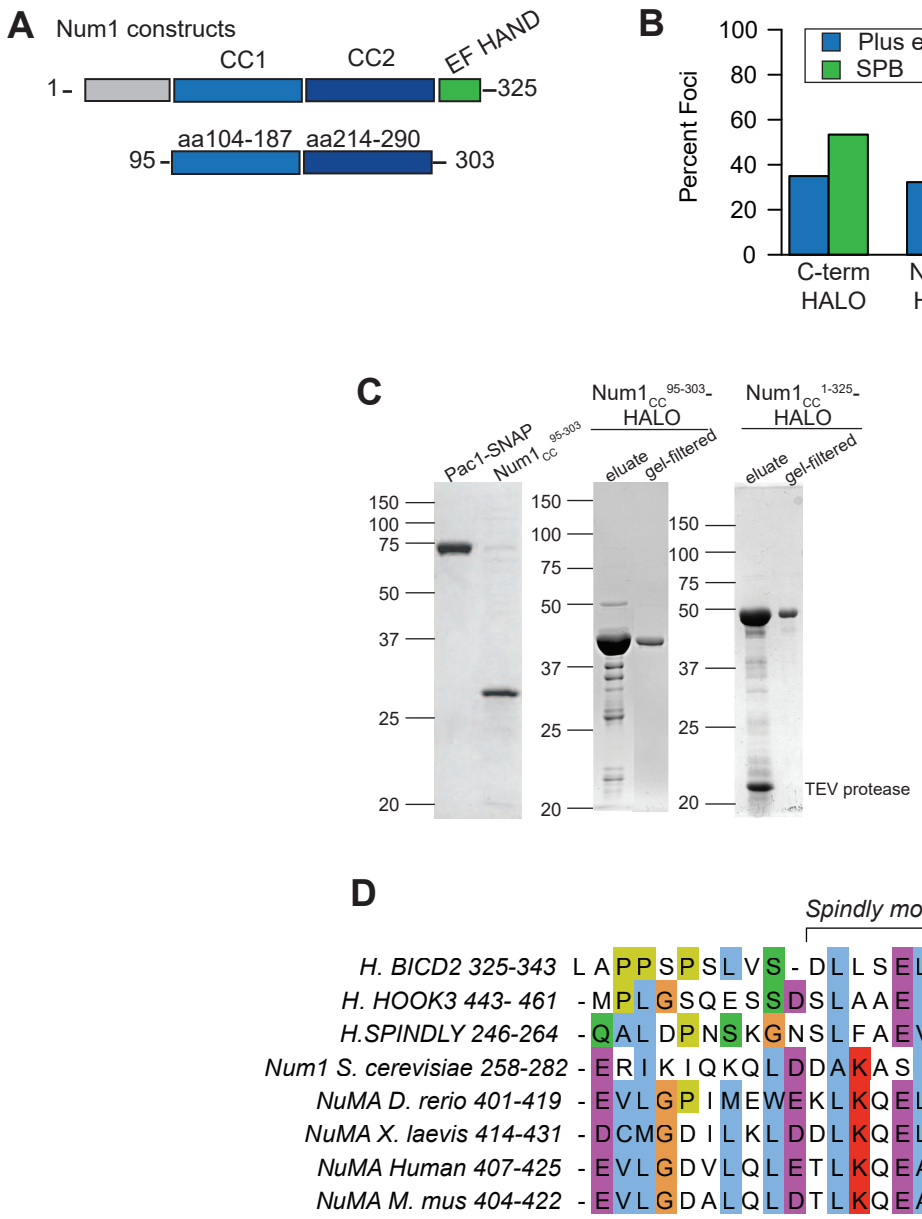

Figure 4.3. Num1$_{CC}$ construct building and characterization. (A) Diagram of constructs Num1$_{CC}$ amino acids1-325 and 95-303. (B) Percent dynein (Dyn1-3mCherry) foci at plus ends (blue) or SPB (green) in the presence of either HALO-Num1$_{CC}^{95-303}$ or Num1$_{CC}^{95-303}$-HALO overexpression. C-terminal HALO resulted in increased dynein at the SPB as expected for a functional Num1$_{CC}$ construct. (C) SDS-PAGE coomassie gels showing purifed proteins: Pac1-SNAP, Num1$_{CC}^{95-303}$, Num1$_{CC}^{95-303}$-HALO, and Num1$_{CC}^{1-325}$-HALO. (D) ClustalWS amino acid alignment of Spindly-motif regions of Num1, adapters, and NuMA homologs.

suggest that the N-terminal HaloTag may interfere with $Num1_{CC}$'s ability to activate dynein and were not used in further experiments.

Although $Num1_{CC}^{95-303}$ is sufficient for dynein cortical localization in cells, it is possible that a longer section is important for dynein-dynactin activation. In humans, the adapter Hook3 has been shown to have a minimal domain that interacts with dynein-dynactin but is not capable of activating processivity (Schroeder and Vale, 2016). Therefore, I also designed a bacterial plasmid to express and purify $Num1_{CC}^{1-325}$-HALO (Figure 4.3C). $Num1_{CC}^{1-325}$ was also the truncation used in Chapter 2, so I tested this construct first to determine its effect on dynein-dynactin motility.

Incubating $Num1_{CC}^{1-325}$-HALO with dynein alone resulted in comigration of the construct with the motor (Figure 4.4A). This was unexpected because in cell lysates lacking the Nip100 subunit of dynactin, dynein is not pulled down by $Num1_{CC}$ (Tang et al., 2012). Since my experiments were performed with Dyn1-HALO, cross-contamination between fluorophores could be a factor even though two-color molecules were observed. Looking at the motility properties, $Num1_{CC}^{1-325}$ had a slight negative effect on velocity, but no effect on run length (Figure 4.4B-C). It is possible that the decrease in velocity of dynein-$Num1_{CC}^{1-325}$ (DN) motor complexes may correlate with $Num1_{CC}$ interacting with slower moving motors or creating drag. Most likely these data suggest that $Num1_{CC}$ interacts non-specifically with dynein. To confirm this, I imaged $Num1_{CC}^{1-325}$ binding to GST-$Dyn1^{331KDa}$ that lacks the tail domain. An interaction was observed, but it was reduced with increasing concentrations of potassium acetate in the motility buffer (Figure 4.4E-F). This suggests that $Num1_{CC}^{1-325}$ weakly binds dynein non-specifically and colocalization is not due to cross-contamination between HaloTag ligands.

Finally, I examined the effect of $Num1_{CC}^{1-325}$ on dynein-dynactin motility. If $Num1_{CC}$ acts as an adapter, I expected to see an increase in either velocity or run length compared to dynein-dynactin alone. $Num1_{CC}^{1-325}$-HALO was gel filtered in the low salt DAB (50mM potassium acetate) to remove any excess HaloTag ligand from the purification so that the empty Nip100-HALO substrates could not be contaminated in the assay (Figure 4.3C). Dyn1-GFP could not be

Figure 4.4

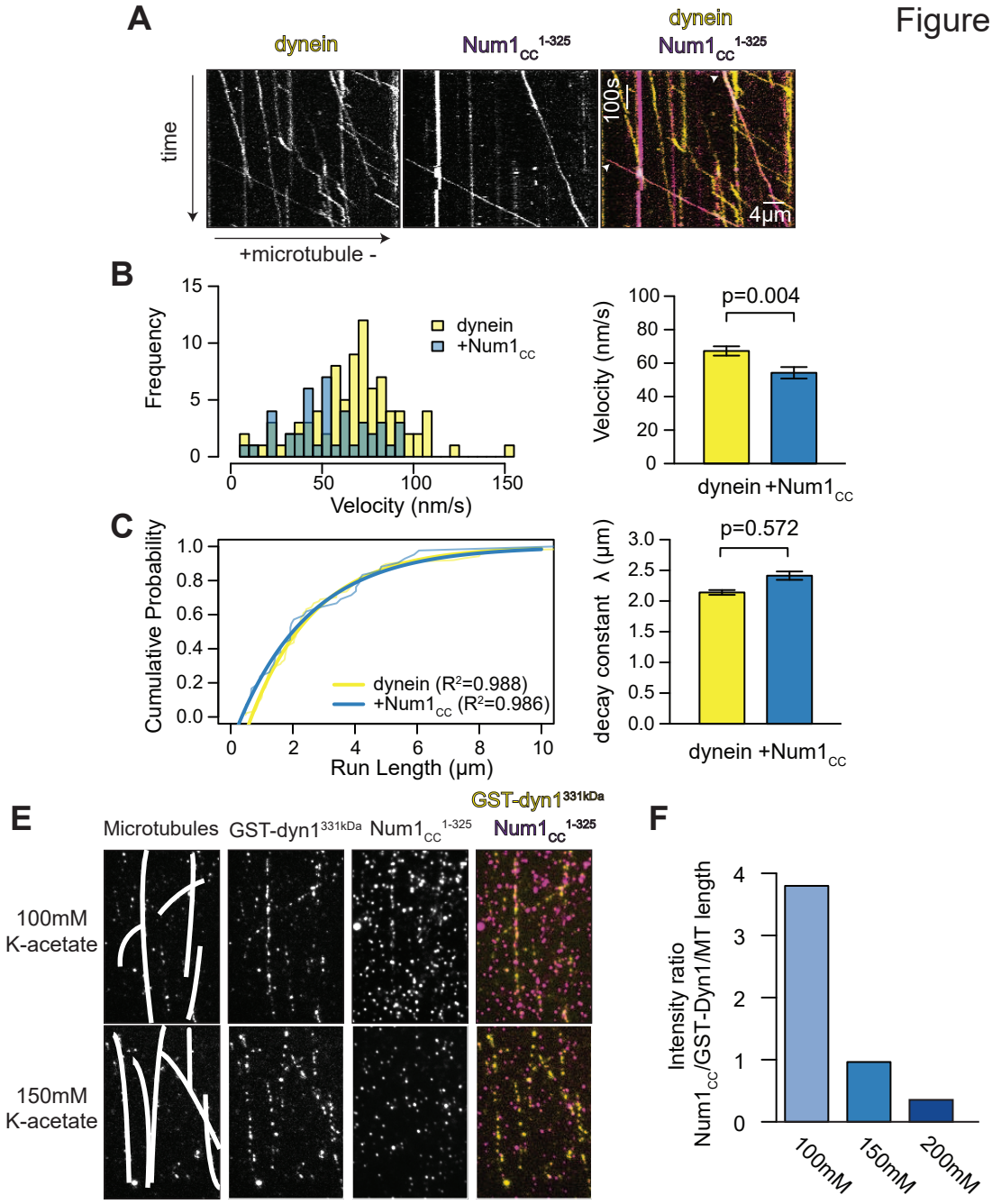

Figure 4.4. Num1$_{CC}$ interacts with, but has not effect on dynein. (A) Kymographs of comigrating Dyn1-HALO^{647}-Num1$_{CC}^{1-325}$-HALO^{TMR} proteins labeled with AlexaFluor 647 or TMR ligands, respectively and visualized on taxol-stabilized HiLyte 488-labeled MTs. (B) Overlay of velocity histograms (left) and mean velocity (right) of dynein alone or with Num1$_{CC}^{1-325}$ measured in the same movie in the presence of 250nM Num1$_{CC}$ (dimer concentration). (C) Cumulative probability of run lengths with associated fits to a one-phase exponential decay (left) and (right) bar plot of mean run length determined by λ (decay rate constant). Data shown are from one experiment (n ≥ 42). (E) Representative images of GST-Dyn1 with Num1$_{CC}^{1-325}$ showing that Num1$_{CC}^{1-325}$ binds less frequently in high salt conditions, quantified in F. (F) The fluorescence intensity ratio of Num1$_{CC}^{1-325}$-HALO^{TMR} to GST-dyn1^{331kDa}-HALO^{647} per microtubule length shows a decrease in Num1$_{CC}$ bound at higher salt conditions.

observed because its fluorescence overlapped with green microtubules. Num1$_{CC}^{1-325}$-HALO comigrated with Arp10-SNAP, but unexpectedly, dynein-dynactin-Num1$_{CC}$ (DDN) complexes moved slower than dynein-dynactin (DD) complexes observed in the same movie, while run lengths remained unchanged (Figure 4.5). Because Num1$_{CC}$ can interact with dynein non-specifically, it is possible that native DDN complexes did not form, and Num1$_{CC}$ introduces drag or negatively affects motility in some way.

To reduce non-specific binding of Num1$_{CC}$ and test if Num1$_{CC}$ can facilitate dynein-dynactin formation at closer to physiological salt conditions, I incubated the three proteins in 125mM potassium acetate DAB. A few Num1$_{CC}$ molecules were observed moving on microtubules, but not in complex with dynactin molecules (data not shown). This experiment suggests that the Num1$_{CC}^{1-325}$ construct is not sufficient to form intact DDN complexes in physiological salt conditions. I next tested the shorter Num1$_{CC}^{95-303}$ construct because I qualitatively observed that it has a lower frequency of non-specific binding to GST-Dyn1^{331KDa}. At salt conditions near 60mM potassium acetate, some dynein-dynactin molecules were seen, but not comigrating with Num1$_{CC}^{95-303}$ (not shown). Other conditions that were tested included varying salt and pH buffer conditions and yielded no improvement in DDN complex formation.

Alternatively, I implemented an approach that has been successful in purifying processive human DDX complexes (McKenney et al., 2014). Briefly, recombinant adapter protein was bound to beads and incubated with cell lysate containing fluorescently labeled dynein and dynactin. The adapter was then competed off the beads and the eluate contained adapter bound to dynein-dynactin forming native, processive complexes. In my experiments, bacterially expressed Num1$_{CC}^{95-303}$-HALO was bound to beads and incubated with control cell lysates that contained Dyn1-GFP with dynactin deleted (Nip100 deletion) or a strain that contained Nip100-EGFP and wild-type dynein. The complexes were eluted and imaged on microtubules (data not shown). Unexpectedly, Num1$_{CC}^{95-303}$ pulled out active dynein motors in controls cells lacking dynactin. This was surprising because western blots have shown the opposite, that Num1$_{CC}^{95-303}$ does not

Figure 4.5

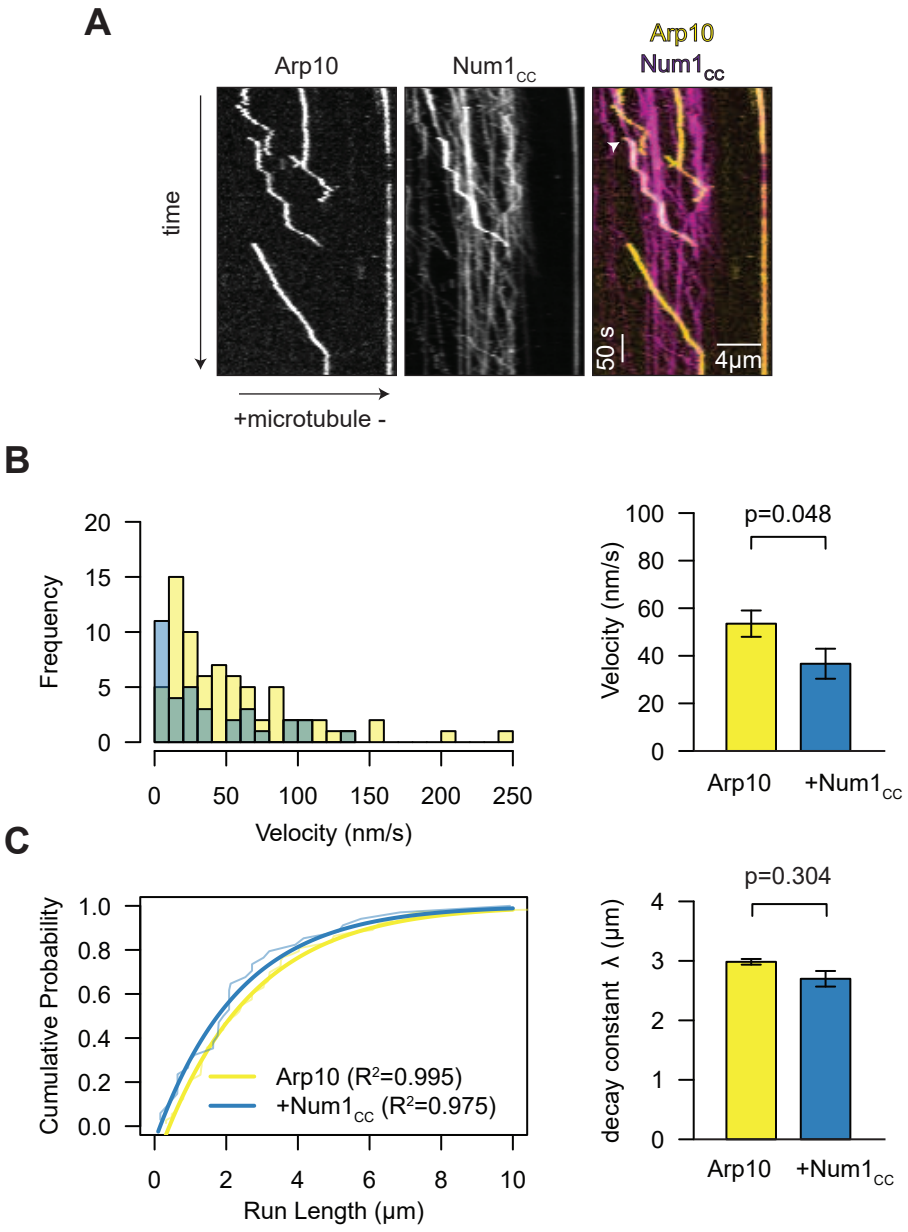

Figure 4.5. $Num1_{CC}$ has no effect on dynein-dynactin motility. (A) Kymographs of $Num1_{CC}^{1-325}$-$HALO^{647}$ comigrating with Arp10-$SNAP^{TMR}$ motor complexes. Complexes contained Dyn1-GFP, but dynein was not visualized. Single molecules were imaged on taxol-stabilized HiLyte 488-labedled MTs. White arrows point to comigrating motor complexes. (B) Overlay of velocity histograms (left) and mean velocity bar plot ± standard error (right). (C) Cumulative probability of run lengths with associated fits to a one-phase exponential decay (left) and (right) bar plot of mean run length± standard error of fit determined by λ (decay rate constant). Data shown are from one experiment (n ≥ 34).

interact with dynein in the absence of Nip100 (Tang et al., 2012). Control beads confirmed that dynein did not non-specifically bind, which suggests that dynein interacts with recombinant $Num1_{CC}^{95-303}$ independently of dynactin. Further, no dynactin molecules were observed in the motility assay from this experiment. Overall, these results demonstrate that native DDN complexes are not forming and alternative methods are required.

Pac1/Lis1 inhibits dynein, but binds to microtubules

Besides enhancing the dynein-dynactin interaction, Num1 is involved in releasing Pac1/Lis1 from dynein complexes to promote motility (Chapter 2). To analyze this mechanism, I first purified Pac1/Lis1 from yeast and determined its effect on dynein motors (Figure 4.3C). According to the initial Pac1/Lis1 function studies, Pac1/Lis1 is considered an inhibitor of dynein motility (Huang et al., 2012; Toropova et al., 2014). My results agreed with these findings and showed Pac1/Lis1 decreased dynein velocity by 26.8% (Figure 4.6A-B). Next, I observed that Pac1/Lis1 had the same inhibitory effect on DN complexes as dynein alone (Figure 4.6C-D). Comparing internally, dynein and DN had reduced velocities of 41.1±1.93 nm/s and 47.4±4.14 nm/s, respectively in the presence of 220nM Pac1/Lis1. Run lengths were not significantly different between the two, suggesting that Pac1/Lis1 affects them equally. These results are not surprising given that the interaction between dynein and $Num1_{CC}^{1-325}$ is non-specific and indicates that $Num1_{CC}$ binding to dynein has no regulatory effect.

To observe Pac1/Lis1 in complex with dynein, I fluorescently labeled Pac1-SNAP molecules and incubated them with Dyn1-HALO. Instead of visualizing comigrating complexes, Pac1-SNAP coated microtubules (Figure 4.6E). This striking effect looked similar to the yeast dynein effector She1 that prevents dynein motility by acting as a roadblock on microtubules (Ecklund et al., 2017). She1 loses its effect on dynein motility when the C-terminal tails of tubulin are removed by a non-specific protease, subtilisin. I treated microtubules with subtilisin and determined that Pac1/Lis1 binding could be reduced as well (Figure 4.6E). However, the protease treatment causes short microtubules that make it difficult to measure dynein motility under these

conditions. Most recently, our lab alternatively used high salt to prevent Pac1/Lis1 binding to microtubules and determined that the inhibitory effect was an artifact of microtubule binding (Marzo et al., 2019a). Instead, Pac1/Lis1 has a role in promoting motility by preventing the dynein autoinhibitory, phi-particle state and encouraging dynactin interaction in both fungi and humans (Marzo et al., 2019a; Qiu et al., 2019b; Htet et al., 2019; Elshenawy et al., 2019a).

I hypothesized that if Pac1/Lis1 contributes to a dynein conformation that is more favorable for dynactin interaction, Pac1/Lis1 may be involved in the formation of DDN complexes. In the single molecule assay, I incubated dynein with Pac1/Lis1 before mixing in dynactin and $Num1_{CC}^{95-303}$ (not shown). However, no incubation combination in solution or on microtubules gave promising results. In summary, different techniques are needed to explore the questions of how Num1 contributes to dynein-dynactin activation and Pac1/Lis1 release.

4.3 DISCUSSION AND FUTURE DIRECTIONS

In summary, I established conditions required to understand the regulatory effects of dynactin, $Num1_{CC}$ and Pac1/Lis1 on dynein motility. Significantly, I identified a problem with the currently published method of visualizing dynein-dynactin complexes (Kardon et al., 2009). The fluorescent labeling system used to visualize individual dynein and dynactin molecules resulted in cross-contamination of HaloTag ligands between the two protein complexes. Dynein-dynactin complexes could be distinguished from dynein motors. I addressed this problem by establishing a different tagging system to visualize intact dynein-dynactin complexes. Colocalized dynein-dynactin complexes however, had the same processivity as individual dynein motors.

The biggest challenge of this study involved the low levels of dynein and dynactin purified. I was not able to confirm that all components of the complexes were purified by standard biochemical assays such as gel electrophoresis, or size exclusion chromatography. Therefore, developing a purification method to improve protein yields is an important next step. The Markus lab recently established a yeast strain that overexpresses the dynein heavy chain and all its accessory chains to purify quantities high enough for negative stain EM (Marzo et al., 2019a).

Figure 4.6

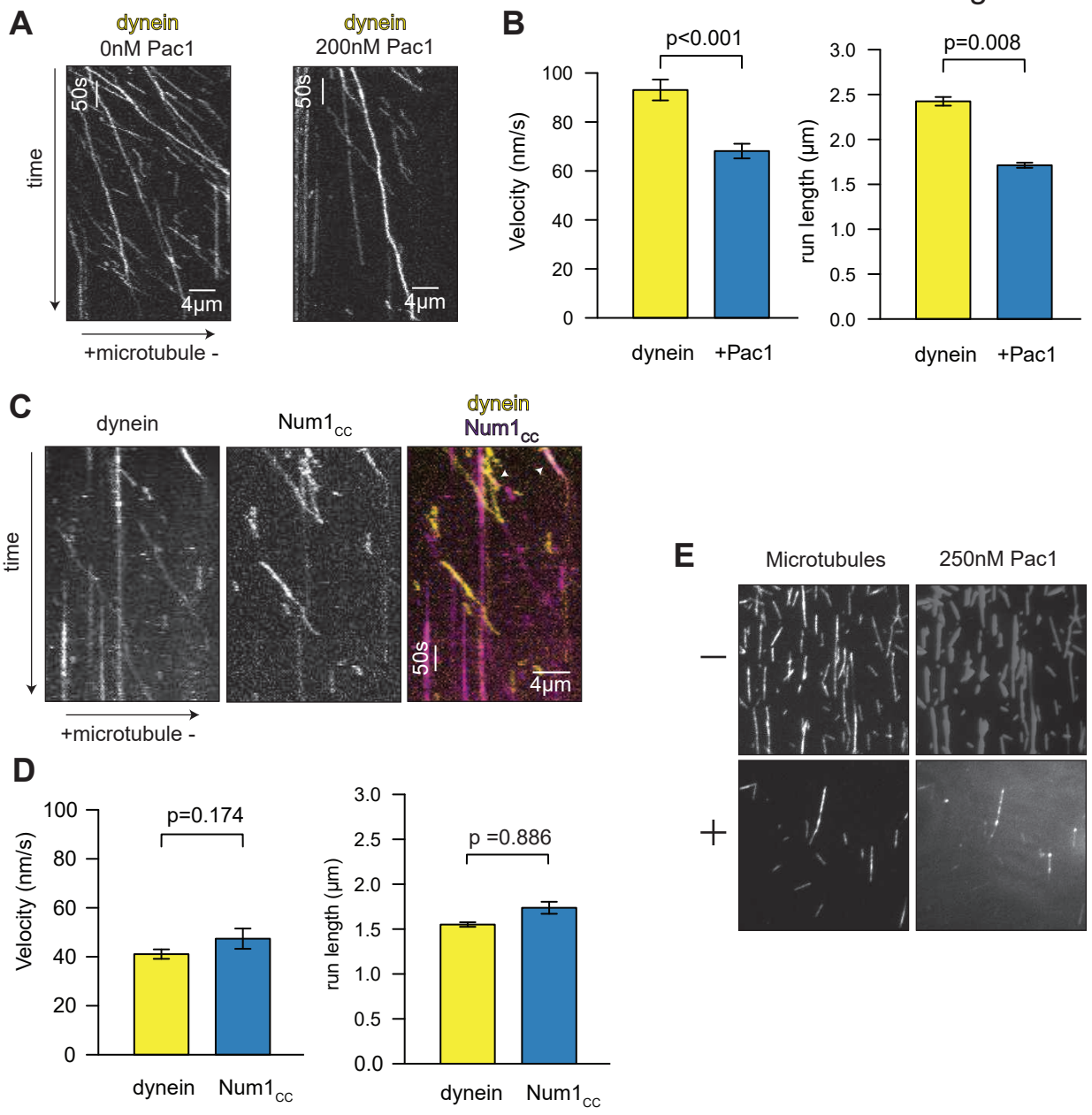

Figure 4.6. Pac1/Lis1 affects dynein and dynein-Num1$_{cc}$ equally. (A) Kymographs of dynein or dynein with 200nM Pac1-SNAP (dimer concentration). Dyn1-HALO^{TMR} motors were visualized on taxol-stabilized HiLyte 647-labedled MTs. (B) Dynein with Pac1 bar plot of mean velocity ± standard error (left) and (right) bar plot of mean run length ± standard error of fit represented by λ (decay rate constant). Data shown are from one experiment (n ≥ 105). (C) Kymographs of Dyn1-HALO^{TMR} and motors comigrating with Num1$_{CC}^{1-325}$-HALO^{647} in the presence of 220nM Pac1. White arrows indicate comigration. (D) Dynein alone or with Num1$_{CC}$ measured in the same movie. Bar plot of mean velocity ± standard error bar (left) and (right) bar plot of mean run length ± standard error of fit represented by λ (decay rate constant). Data shown are from one experiment (n ≥ 36). (E) 488-HiLyte labeled microtubules untreated (-) or treated with (+) substilisin protease and incubated with 250nM Pac1-SNAP. Pac1 affinity for microtubules decreases dramatically after substilisin treatment.

A similar dynactin strain was designed but has not yet yielded results. Overexpression of the Arp1 protein may cause problems in cells due to its ability to self-assemble. This could affect the Arp1 filament from forming properly and dynactin assembly. To address this potential problem, I designed plasmids to express dynactin in insect cells based on the SmartBac baculovirus expression system (Zhai et al., 2019). Briefly, the final expression plasmid contains all 5 subunits of dynactin, but under two different promoters. Arp1 is expressed by the commonly used polyhedrin (PH) promoter at high levels at a late stage of growth. Whereas, all other subunits (Jnm1, LDB18, Nip100, and Arp10) are controlled by an earlier promoter that expresses at lower levels. This approach worked well for assembling human dynactin by promoting the correct ratio of subunits into intact complexes (Zhai et al., 2019). Although this system was successful, the protein complex yields were still very low and therefore, this method is currently cost prohibitive.

Considered an activating complex, dynactin would be expected to enhance either velocity or run length of dynein. In humans, dynactin binding reorients the motor domains to prevent autoinhibition and aligns them in parallel to improve coordination along microtubules (Urnavicius et al. 2015; Chowdhury et al. 2015; Zhang et al. 2017). However, dynactin requires an adapter protein to have this effect (McKenney et al. 2014; Schlager et al. 2014). I assessed the possibility that dynactin required $Num1_{CC}$ to bridge its interaction with dynein but did not see any increase in velocity or run length. This indicates that native dynein-dynactin-$Num1_{CC}$ complexes are not forming under these conditions, despite this $Num1_{CC}$ construct being sufficient to activate dynein in cells (Chapter 2).

Another approach to obtain native DDN is to pull out intact complexes from cell lysates. In this method, endogenous $Num1_{CC}$ has an N-terminal affinity tag and is expressed in cells with fluorescently labeled dynactin. Moving dynactin complexes were observed using this method, but protein gels could not verify that all components were present (Dilsaver, 2019). Alternatively, an in vivo approach to assess whether $Num1_{CC}$ acts as an adapter complex may be an option. Dynein needs to be anchored to the cell cortex independently of Num1 to test whether spindle movements

require Num1 for activation or simply for cortical localization. Okumura et al. 2018 answered a similar question of NuMA in humans cells by ectopically linking dynein to the cell cortex using light-induced hetero-dimerization system (iLID) (Guntas et al., 2015). In these cells, dynein-dynactin was only active to produce spindle movements when NuMA was expressed, even though sufficient levels of dynein-dynactin were anchored to the cortex. This and other evidence proved that NuMA activates the motor complex by acting as an adapter. Using a similar idea, yeast dynein can be ectopically anchored to the cortex via an N-terminally expressed PH domain and dynein function can be assessed by observing spindle movements and positioning. It would be important that enough dynein is recruited to the cell cortex to rule out concentration as the problem for spindle position defects. Next, $Num1_{CC}$ would be overexpressed to determine if spindle movements are rescued, indicating that dynein has been activated. Although a similar experiment was done in Chapter 2 (Figure 2.4I-J) to examine if $Num1_{CC}$ affected dynactin association at these ectopic sites, activation (spindle movements) was not addressed. This experimental set up would be suitable to test if the Spindly-motif residues affect dynein activation by mutating them to alanine. Although the residues determined in the ClustalX alignment (Figure 4.3D) may reside in the dimerization region of Num1 predicted by Tang et al. 2012, the exact structure and organization of Num1 is unknown. To test if Num1 acts as an adapter in another way, Marzo et al. 2019a (preprint) used a dynein mutant that bypasses the need for Pac1/Lis1 to reach the cortex (D2868K) and determined that cortical association and spindle movements depend on Nip100 (dynactin). This supports the hypothesis that Num1 acts as an adapter interacting with both dynein-dynactin.

Ideally, an in vitro system would be used to answer many questions about the role of Num1 and the mechanisms of dynein activation. Some interesting questions include whether Num1 can recruit multiple dyneins to one dynactin and how Pac1/Lis1 could be involved. My work here shows that Pac1/Lis1 binds to microtubules in vitro which led our lab to determine that Pac1/Lis1 does not act as an inhibitor, but instead prevents dynein from forming its autoinhibitory

state (Marzo et al., 2019a). Similar studies in humans additionally showed that Pac1/Lis1 encourages the assembly of two dyneins to one dynactin (Elshenawy et al., 2019a; Htet et al., 2019). In yeast, Markus et al. 2011 determined that the ratio of dynein to dynactin is 2:1 at the cortex, suggesting that two dyneins may be bound to one dynactin when anchored to Num1. It is possible that Num1 facilitates multiple dyneins to one dynactin to increase force production to pull the spindle. In humans, adapters such as Hook3 allow for and prefer two dyneins to interact with one dynactin to enhance velocity (Urnavicius et al., 2018; Grotjahn et al., 2018). How Pac1/Lis1 and Num1 coordinate to form active DD complexes will continue to be an exciting question to unravel.

Testing the force generation properties of dynein with dynactin is also an important question. In vivo results suggest that this might be the main function of dynactin- to increase dynein force production to pull the spindle (Moore et al., 2009). A collaboration with the Gennerich lab at Albert Einstein University would use optical trapping to answer these types of questions. For example, the CAP-gly domain of Nip100 has been shown to impact dynein force generation to pull the spindle through the bud-neck (Moore et al., 2009). Similarly, loss of the dynein effector, She1, prevents spindle neck-crosses and enhances the ratio of dynein to dynactin at plus ends (Ecklund et al., 2017; Woodruff et al., 2009; Markus et al., 2011). Because She1 interacts with dynein at the microtubule-MTBD interface, She1 may also affect the CAP-gly domain of dynactin. Therefore, examining how She1 and dynactin work to affect dynein force generation and motility in vitro would give insight into how dynein is regulated to generate high pulling forces. Notably, all in vitro experiments in the Markus lab have used bovine tubulin, which could affect the results of dynein-dynactin motility. It is possible that yeast dynein has significantly different motility properties on native yeast microtubules and dynactin also may play a larger role in this context. The Markus lab has recently established a protocol to purify yeast tubulin and assemble microtubules. Using this tool will be exciting to observe native phenomena in vitro. Overall,

building tools to observe dynein regulation in vitro will be powerful in understanding the regulation of this complex motor protein.

4.4 MATERIALS AND METHODS

Media and strain construction

All strains are derived from either YEF473A (Bi and Pringle, 1996) for imaging or W303 (constructed by Rodney J. Rothstein) for protein purification and are listed in Table 4.1 (Ralser et al., 2012). We transformed yeast strains using the lithium acetate method (Knop et al., 1999b). Strains carrying null mutations or HALO-tag deletions were constructed by PCR product-mediated transformation (Longtine et al., 1998a). Transformants were clonally purified by streaking to individual colonies on selective media. Proper tagging was confirmed by PCR and, in some cases, sequencing. YPA media contains yeast extract, peptone and adenine hemisulfate (Sunrise Science Products).

Plasmid construction and expression

To fluorescently label $Num1_{CC}$ [95-303aa] in the bacterial expression vector pBSG02 (Tang et al. 2012) with a HaloTag (Promega), the HaloTag PCR fragment was amplified from pBJ090-HALO (derived from Longtine et al. 1998) with primers flanked with NotI and BamHI restriction sites. The PCR fragment and vector were digested with restriction enzymes and ligated together to insert the HaloTag at the C-terminus of $Num1_{CC}$ and before the precission protease cleavage site (PCN) to maintain the purification tags. An N-terminally Halo tagged $Num1_{CC}$ [95-303aa] vector was constructed by digesting pBSG02 with XbaI and NcoI and ligating with the HaloTag PCR product without its stop codon.

To generate the bacterial expression vector for purification of GST-2XTEV-$Num1_{CC}$ [1-325]-HALO, pGEX-KG (Guan and Dixon, 1991) digested with SalI and BamHI was used as the backbone. A fragment containing aa 1-325 of Num1 was amplified from genomic DNA using a forward primer including a 20 nucleotide overlap with pGEX-KG starting at the SalI site and two copies of the TEV protease cleavage site (GAGAATCTTTATTTTCAGGGC). HaloTag was

amplified from pBJ090-HALO with a forward primer that contained a 20 nucleotide overlap with the 3' end of the $Num1_{CC}$ fragment and the reverse primer contained a 20 nucleotide overlap starting at the BamHI site in pGEX-KG. The two PCR products were ligated into pGEX-KG using isothermal assembly and named B534. Similarly, an expression vector containing only 2XTEV-$Num1_{CC}$ [1-325] with no HaloTag was generated.

To express proteins from bacterial vectors, plasmids were transformed into BL21 pLysS cells (Promega; made competent by Jeanne Mick) and induced with IPTG using the LacO/LacI operon system.

Protein Purification

To purify dynein or dynactin strains were grown in 3ml YPAD (YPA supplemented with 2% glucose) overnight and left to sit on bench. In the evening, 3ml were transferred to 25ml YPAD overnight. In the morning, the cultures were added to 1L flasks of YPAD and grown to an $O.D_{600}$ between (0.8-1.5; ~6hrs). Cells were harvested by centrifugation, washed once with water and the resuspended cell pellet was then frozen by drops in liquid nitrogen. Lysis was performed by grinding the liquid nitrogen-frozen pellets with a coffee grinder (Hamilton Beach model 80374). The cell powder was melted in 0.2 volumes of 5X dynein lysis buffer (1X dynein lysis buffer: 30 mM HEPES (pH 7.2), 50 mM K-Acetate, 2 mM Mg-Acetate, 1 mM EGTA, 10% glycerol, 0.2% Triton X-100, 1 mM DTT, 0.5 mM Mg-ATP, 1 mM Pefabloc). Subsequent steps were at 4°C unless indicated. The lysates were centrifuged at 13,000rpm for 15 min. After centrifugation, 0.2% Triton-X-100 was added to dynactin supernatants. Supernatants were then incubated with IgG sepharose (Amersham Pharmacia) for 1 hour. The IgG beads containing bound protein were then washed 2 times with dynein lysis buffer with 0.1% Triton X-100, and washed twice with 'modified' TEV cleavage buffer (10 mM Tris (pH 8.0), 150 mM K-Acetate, 2mM Mg-Acetate, 0.005% TritonX-100, 0.5 mM ATP, 1 mM DTT, 1 mM Pefabloc). The beads were then incubated with either 1ul of 1mM SNAP-Alexa Fluor 647 ligand (New England Biolabs) or TMR HaloTag ligand (ProMega) or both for 10 minutes at room temperature in the dark. After washing 3-5 times with 'modified' TEV

cleavage buffer, beads were resuspended in 0.1ml and incubated with TEV protease for 1 hour at 16°C.

GST-2XTEV-Num1$_{CC}$ [1-325]-HALO or [95-303]-HALO purification. 3ml cultures of LB+Carbenicillin + Chloramphenicol with BL21 PlysS cells containing the Num1$_{CC}$ plasmid were grown overnight at 37ºC. Cells were diluted to O.D$_{600}$ of 0.05 in 1L of LB and grown at 25ºC until an O.D$_{600}$ 0.4-0.8. The temperature was decreased to 20ºC and induced with 0.5mM IPTG and grown overnight. Cells were harvested with centrifugation and washed with water before cell pellets were frozen at -80ºC. Cells were thawed in 2X bind buffer (300mM NaCl, 40mM Tris-Cl pH 7.5, 2mM EDTA) supplemented with protease inhibitor tablets (Pierce) and lysed via sonication or microfluidizer. All subsequent steps were performed on ice or at 4ºC. Cell lysate was clarified at 13,000K rpm for 15 min. 0.1% Triton-X-100 was added to supernatant before binding to glutathione beads (Pierce; Thermo Fisher Scientific) rotating for 1 hour. Beads were washed 3X with wash buffer (4.3mM Na_2POH_4, 1.47mM KH_2PO_4, 137mM NaCl, 2.7mM KCl) and 2X with TEV buffer (50mM Tris pH 8, 150mM K-acetate, 2mM Mg-acetate, 10% glycerol, 1mM EGTA, 1mM DTT, 0.5mM Pefabloc). To label with HaloTag Dye (ProMega), 1ul of 1mM HALO ligand was added to beads and incubated for 10 min at room temperature in the dark. Beads were washed 3X with 1ml of TEV buffer to remove excess dye. Beads were incubated with TEV protease for 3 hours at 16ºC or overnight at 4ºC. Eluate was dialyzed in dynein assay buffer to completely remove excess HALO dye. Approximate yield from 4L was ~0.6mg/ml (10µM).

Num1$_{CC}$ [94-303]-PCN-Stag-TEV-ZZ. Cells were grown and harvested as described for Num1$_{CC}$ [1-325] construct. Cells were thawed in 2X bind buffer (300mM NaCl, 40mM Tris-Cl pH 7.5, 2mM EDTA) supplemented with protease inhibitor tablets (Pierce) and lysed using sonication or a microfluidizer. All subsequent steps were performed on ice or at 4ºC. Cell lysate was clarified at 13,000K rpm for 15 min. 0.1% Triton-X-100 was added to supernatant before binding to IgG sepharose beads (Amersham Pharmacia) rotating for 1 hour. Beads were washed 3 times with 1X bind buffer and then 2X with TEV buffer. HaloTag labelling occurred the same as above. Beads

were incubated with TEV protease for 1 hour at 16ºC or overnight at 4ºC. Approximate yield from 4L was ~0.6mg/ml (10µM).

Pac1-1xFLAG-SNAPf was purified via 8X-HIS and ZZ tags. Cells were grown, harvested, and lysed as above. Lysed cells were resuspended in 0.2 volumes of 5X Buffer A (1X Buffer A: 50 mM K-Phosphate [pH 8.0], 150 mM K-Acetate, 150 mM NaCl, 2 mM Mg-Acetate, 5 mM β-mercaptoethanol, 10% glycerol, 0.2% Triton X-100, 0.5 mM Pefabloc, and 1 mM PMSF) supplemented with 10 mM imidazole (pH 8.0). Note: Mg-Acetate will crash out at the 5X concentration so this component was added after diluting buffer into cell lysate. Subsequent steps were at 4°C unless indicated. The lysate was clarified by centrifugation at 13,000rpm for 20 min. The supernatant was incubated with Ni-NTA agarose (QIAGEN) for 1 hour, washed three times with Buffer A + 20 mM imidazole, and eluted with 10ml Buffer A + 250 mM imidazole. Eluted protein was then incubated with IgG sepharose beads (Amersham Pharmacia) for 1 hour and washed twice with Buffer A + 20 mM imidazole and once with 'modified' TEV cleavage buffer. Beads containing bound Pac1 were incubated with 1µl of 1mM SNAP-Alexa Fluor 647 substrate (New England Biolabs) for 10 minutes at room temperature in the dark. After washing 3-5 times with 'modified' TEV cleavage buffer, beads were resuspended in 0.3-0.4ml and incubated with TEV protease overnight at 4°C. Approximate yield for 8L of Pac1-SNAPf was 0.36 mg/ml (4.5µM).

Size exclusion chromatography

$Num1_{CC}$[1-325]-HALO was purified as described. TEV digested protein was ran on Superose 6 Increase 10/300 column using a NGC Chromatography System (Bio-Rad) that had been equilibrated with dynein assay buffer (50 mM Tris–HCl [pH 8.0], 150 mM potassium acetate, 2 mM magnesium acetate, 1 mM EGTA, 5% glycerol, and 1 mM DTT). Fractions (0.5ml) were collected and combined. Fractions were concentrated to approximately 100-200µl using a Amicon ultra centrifugal filter 10K (MilliporeSigma). Protein concentration was determined using Bradford Reagent (Bio-Rad) and BSA standards. Approximate yield for 4L prep was 0.3mg/ml (5µM).

Single molecule motility assay and data analysis

The assay was performed as previously described with minor modifications (Ecklund et al., 2017). Flow chambers were constructed by adhering plasma cleaned and silanized coverslips to slides with double-sided adhesive tape. Anti-tubulin antibody solution was added to the chamber (8 µg/ml, YL1/2; Accurate Chemical & Scientific Corporation) then blocked with 1% Pluronic F-127 (Fisher Scientific). Next, taxol-stabilized microtubules assembled from unlabeled and fluorescently-labeled porcine tubulin (10:1 ratio; Cytoskeleton) were flowed into the chamber and incubated for 5-10 minutes. I washed the chamber with dynein assay buffer (DAB; 30 mM HEPES pH 7.2, 50mM potassium acetate, 2 mM magnesium acetate, 1 mM EGTA) supplemented with 20µM taxol and 1mM DTT. Purified dynein motors diluted in DAB were introduced into the chamber and incubated for 2 minutes. Potassium acetate concentration was adjusted in different experiments, see figure legend. Motility activation buffer was finally added (DAB plus 1 mM Mg-ATP, 0.05% Pluronic F-127, 20 µM taxol, and an oxygen-scavenging system consisting of 1.5% glucose, 1 U/ml glucose oxidase, 125 U/ml catalase) and motors were imaged. Experiments containing dynactin included ~6µl of dynactin incubated with ~1µl dynein (diluted 1:50 in assay buffer) and either assay buffer or 250nM $Num1_{CC}$. Because the concentration of dynein and dynactin were unknown, the complexes were diluted accordingly to achieve an optimal number of single molecules along microtubules in an imaging field. When including Pac1-FLAG-SNAPf, it was diluted to its working concentration in the motility activation buffer and flowed into the chamber in the last step. I ensured that comigrating $Num1_{CC}$ spots were not due to bleed-through from the Arp10-$HALO^{TMR}$ channel by performing two-color imaging with Arp10-$HALO^{TMR}$ alone (no spots were apparent in the far-red channel in these cases). In experiments to test Pac1 binding to microtubules, taxol-stabilized microtubules were digested with subtilisin according to Ecklund et al. 2017.

TIRFM images were collected using a 1.49 NA 100X TIRF objective on a Nikon Ti-E inverted microscope equipped with a Ti-S-E motorized stage, piezo Z-control (Physik Instrumente), and an iXon X3 DU897 cooled EM-CCD camera (Andor). 488 nm, 561 nm, and 640

nm lasers (Coherent) were used along with a multi-pass quad filter cube set (C-TIRF for 405/488/561/638 nm; Chroma) and emission filters mounted in a filter wheel (525/50 nm, 600/50 nm and 700/75 nm; Chroma). I acquired images at 2 second intervals for 8-10 min. Velocity and run length values were determined from kymographs generated using the MultipleKymograph plugin for ImageJ (http://www.embl.de/eamnet/html/body_kymograph.html). Those motors that moved for ≥ 3 time points were measured, unless noted otherwise. The runlength data was evaluated with a cumulative distribution function and fit with a one-phase exponential decay. The decay constant was used to represent the median run length. Average microtubule length was included in the fit as a parameter to control for short runs. For example, if microtubules were too short the CDF did not fit well, suggesting that the microtubules inhibited the motor runlength and motors from these microtubules were not analyzed.

Table 4.1. Strains used in this study.

Strain	*Genotype*	*Source*
SMY1172	*W303: ZZ-TEV-L-TEV-DYN1-HALO nip100Δ num1Δ*	*this study*
SMY1831	*W303: ZZ-TEV-GFP-3XHA-DYN1 PAC1-13myc nip100Δ*	*A. Gennerich*
SMY1194	*W303: ZZ-TEV-L-TEV-ARP10 NIP100-HALO dyn1Δ pac11Δ num1Δ*	*this study*
SMY1862	*W303: ZZ-TEV-L-TEV-ARP10-SNAPf NIP100-HALO pac11Δ*	*A. Gennerich*
SMY1918	*W303: ZZ-TEV-L-TEV-ARP10-SNAPf NIP100::HPH*	*this study*
SMY1	*YEF473A: Nip100-3GFP::TRP1 ura3-52 lys2-801 leu2-∆1 his3-∆200 trp1-∆63SMY288*	*W. Lee*
SMY288	*YEF473A: Dyn1-3YFP::TRP nip100∆::KANR ura3-52 lys2-801 leu2-∆1 his3-∆200 trp1-∆63*	*this study*
SMY696	*YEF473A: Gal1p:Num1CC[1-325] dyn1[∆MTBD] Jnm1-3mCherry mTurquoise2-Tub1*	*Lammers and Markus, 2015*
Plasmid	**Bacterial Expression Plasmids**	*Source*
B116	*pBSG02 (psY07:CC(Num1 94-303aa)-PCN-Stag-TEV-ZZ)*	*Tang et al., 2012*
B412	*pBSG02 (psY07:CC(Num1 94-303aa)-HALO-PCN-Stag-TEV-ZZ)*	*this study*
B534	*pGEX-KG:GST-2XTEV-Num1CC[1-325]-HALO*	*this study*
B414	*pBSG02 (HALO-psY07:CC(Num1 94-303aa)-PCN-Stag-TEV-ZZ)*	*this study*

CHAPTER 5

ALLOSTERIC CHANGES IN DYNEIN STRUCTURE AFFECT PAC1/LIS1 BINDING AND DISSOCIATION

5.1 INTRODUCTION

The mechanochemical cycle of dynein is unique in the fact that ATP is hydrolyzed a long distance from where stepping occurs compared to kinesin and myosin motor families (Vale and Milligan, 2000). Allosteric changes generated by ATP hydrolysis in the AAA+ ring must communicate to the microtubule binding domain (MTBD) that extends 15nm down from the ring to promote stepping along the microtubule (Imamula et al., 2007; Carter et al., 2008, 2011; Schmidt, 2015). Structural and biochemical studies have uncovered important and minute details about how each AAA+ module and domain coordinate to produce force and walk along microtubules. However, many questions remain regarding how the regulatory protein Pac1/Lis1, that interacts directly with the motor, affects and is affected by the different transitions of the mechanochemical cycle.

The AAA1 module is the major catalytic site, while AAA3 and AAA4 play minor roles in ATP hydrolysis (Kon et al., 2004; Cho et al., 2008; Silvanovich et al., 2003). ATP binding in AAA1 causes AAA2-AAA4 to move as a rigid body, which causes the ring to shift from an open to closed conformation (Figure 5.1A) (Schmidt et al., 2012; Kon et al., 2012; Bhabha et al., 2014; Schmidt et al., 2014). This movement also closes a gap between AAA2-4 and AAA5-6 such that AAA6 rotates inward toward the center of the ring. During this rotation the buttress domain that extends from AAA5, slides against the stalk and forces the anti-parallel, coiled-coil to slide along itself and change the MTBD from high affinity to low affinity (Figures 1.1 and 5.3B) (Gibbons et al., 2005; Carter et al., 2008; Kon et al., 2009, 2004; Redwine et al., 2012; Nishikawa et al., 2014). Taking a step forward and rebinding the microtubule, the MTBD shifts to a high affinity state and

communicates back to the AAA+ ring, which reopens by releasing ADP from AAA1 (Kon et al., 2012). AAA3 acts to internally regulate this movement by structurally inhibiting ring closure when bound to ATP, but not ADP, and acts as a 'gate' between AAA1 and the MTBD affinity state (DeWitt et al., 2015; Nicholas et al., 2015). The third moving part of the mechanochemical cycle is the linker domain that is N-terminal to AAA1 and connects the tail domain to the motor. When dynein is bound to microtubules (high affinity) and AAA1 is not bound to a nucleotide, the linker rests in a straight position at AAA5 (Figure 5.1A) (Schmidt et al., 2012). After ATP binds to AAA1, conformation changes in the ring force the linker to bend and recover its pre-powerstroke state at AAA2 (Figure 5.1A) (Burgess et al. 2003; Kon et al. 2005; Bhabha et al. 2014; Schmidt et al. 2014). The ring opens during release of hydrolysis products and coincides with the linker powerstroke swinging across the ring to its final position at AAA5 (Roberts et al., 2009, 2012; Lin et al., 2014). Altogether, ATP binding at AAA1 causes allosteric changes that communicate to the MTBD and release the motor from the microtubule. These structural changes further affect the linker to produce a powerstroke that releases ADP in conjunction with re-binding the microtubule to generate forward stepping along the microtubule track (Mogami et al., 2007; Imamula et al., 2007).

With so many moving parts throughout its mechanochemical cycle, it isn't surprising that dynein can be affected by Pac1/Lis1 binding directly to the AAA+ ring. Pac1/Lis1 interacts between AAA3 and AAA4 in a position that may interfere with the linker powerstroke (Figure 5.1B) (Huang et al., 2012; Toropova et al., 2014). An additional binding site at the junction between the stalk and AAA5 occurs only when the AAA+ ring is in the closed conformation and the two sites are in close proximity (Figure 5.1B) (DeSantis et al., 2017). Initially, binding at these positions led scientists to think Pac1/Lis1 affected the mechanochemical cycle by blocking the linker from swinging, therefore uncoupling ATP hydrolysis from microtubule binding to cause reduced motility and increased force generation (Huang et al., 2012; McKenney et al., 2010). This model fits well with in vivo studies that require Pac1/Lis1 for dynein-mediated transport of high load cargoes,

Figure 5.1

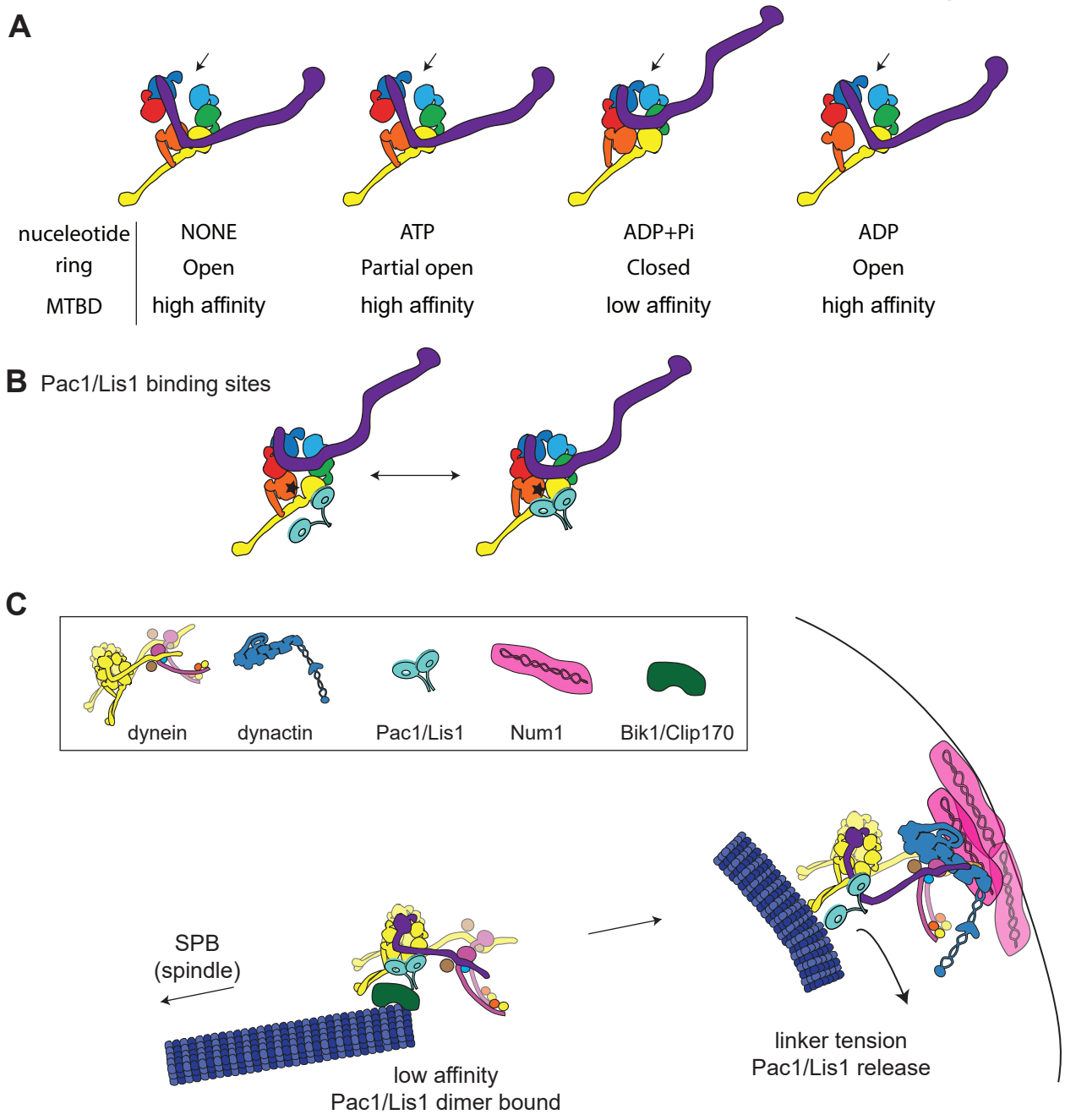

Figure 5.1. Cartoons of dynein structure, Pac1/Lis1 interaction, and model of Pac1/Lis1 release mechanism. (A) Drawing of dynein ring and linker conformations throughout the mechanochemical cycle. Arrows point to gap between AAA1 and AAA2 that closes throughout cycle. (B) Drawing of Pac1/Lis1 binding sites at either AAA4 or at AAA4 and the stalk. The black star shows the gap between AAA4 and AAA5. The linker is bent in the pre-powerstroke state due to steric hinderance. (C) Model of Pac1/Lis1 binding dynein in a low affinity state at plus ends. Upon interaction with Num1 at the cortex, tension is added to the linker and dynein shifts to the high affinity state. Pac1/Lis1 can only interact with one monomer and has a weaker association and dissociates.

particularly in axons (Yi et al., 2011; Pandey and Smith, 2011; Moughamian et al., 2013; Klinman and Holzbaur, 2015). However, recent data determined that Pac1/Lis1 binding acts to prevent dynein from forming its autoinhibitory conformation, the phi-particle, to promote interaction with dynactin and its cargo adapter (Marzo et al., 2019a; Elshenawy et al., 2019a; Qiu et al., 2019b; Htet et al., 2019). Thus, Pac1/Lis1 helps to activate motility rather than inhibit it (Gutierrez et al., 2017; Baumbach et al., 2017). In agreement, studies show that Pac1/Lis1 is rarely associated with moving dynein-dynactin-adapter (DDX) complexes suggesting that Pac1/Lis1 acts as an initiation factor and dissociates after complex formation is complete and active (Egan et al., 2012; Lenz et al., 2006; Moughamian et al., 2013; Jha et al., 2017; Elshenawy et al., 2019a; Qiu et al., 2019b). The two seemingly opposing models of Pac1/Lis1 regulation- activation and inhibition- may be important under different contexts; DDX complexes may require initial help in forming (activation), while dynein-Pac1/Lis1 may function with Ndl1/NudE to enhance load-bearing capabilities (inhibition) (Yamada et al., 2008; Torisawa et al., 2011; McKenney et al., 2010; Huang et al., 2012; Reddy et al., 2016).

In agreement with observations that Pac1/Lis1 dissociates from active DDX complexes, my work in Chapter 2 demonstrated that active dynein-dynactin complexes were not associated with Pac1/Lis1 molecules (Figure 2.4). Overexpression of the minimal dynein-interacting fragment of the cortical receptor Num1, $Num1_{CC}$, stimulated dynein-dynactin motility and caused dissociation of Pac1/Lis1. How association with Num1CC initiates Pac1/Lis1 release remains unresolved.

Cryo-EM structures of Pac1/Lis1 bound to dynein motors show binding at AAA3/4 and at the junction between the stalk and AAA5 (DeSantis et al., 2017; Htet et al., 2019). Conversely, dynactin and adapter proteins interact with the tail domain of dynein to orient the motor heads in a parallel orientation for optimal processivity (McKenney et al., 2014; Schlager et al., 2014; Urnavicius et al., 2015; Grotjahn et al., 2018). This difference in binding location would suggest that competition between dynactin, adapters, and Pac1/Lis1 is likely not the mechanism of

Pac1/Lis1 release. Although the Pac1/Lis1 interacting partner, Ndl1/NudE, does share an overlapping binding site with dynactin and may aid Pac1/Lis1 dissociation in cells (see Chapter 3), it is not required for Pac1/Lis1 release in these in vitro studies (Gutierrez et al., 2017; Elshenawy et al., 2019a; Htet et al., 2019; Qiu et al., 2019b; McKenney et al., 2011).

Evidence showing that Pac1/Lis1 dissociates from processive dynein and DDX complexes suggests that dissociation could simply be stochastic (Gutierrez et al., 2017; Marzo et al., 2019a; Elshenawy et al., 2019a; Htet et al., 2019). In support of this hypothesis, binding experiments using nucleotide analogs show that Pac1/Lis1 prefers to bind dynein in the presence of ADP+P_i (closed ring; low affinity) state and does not interact during other states of the mechanochemical cycle (McKenney et al., 2010). In contrast, Pac1/Lis1 occasionally is shown to comigrate with processive dynein and DDX complexes in vitro, which proves that Pac1/Lis1 can interact throughout the ATP hydrolysis cycle (Gutierrez et al., 2017; Marzo et al., 2019a; Elshenawy et al., 2019a).

These conflicting data demonstrate the gap in understanding of how Pac1/Lis1 affects dynein motility and the mechanism of its dissociation. In yeast, my results in Chapter 2 do not support the hypothesis that Pac1/Lis1 dissociation is stochastic. There is a strong correlation between $Num1_{CC}$ binding and Pac1/Lis1 release. Considering the location of Pac1/Lis1 binding near the stalk domain that controls microtubule affinity, it is possible that microtubule binding and the subsequent allosteric changes in the AAA+ ring may impact Pac1/Lis1 release in conjunction with Num1 binding. I predict that Pac1/Lis1 interaction with dynein at astral microtubule plus ends is stable, and switches to a transient interaction when offloading to Num1 sites for spindle positioning.

I constructed a dynein fragment with the microtubule binding domain deleted ($dyn1^{\Delta MTBD}$), and surprisingly, it was still recruited at high levels to track microtubule plus ends (Chapter 2, Figure 2.3). When $Num1_{CC}$ was overexpressed in these cells, the fragment was not depleted from plus ends, suggesting that dynein motility was required. Moreover, these results indicate that

Pac1/Lis1 remained associated with dynein because Pac1/Lis1 is required for dynein plus end localization (Lee et al., 2003b; Markus et al., 2009). If the MTBD is required for Pac1/Lis1 release initiated by Num1, microtubule binding and the associated structural changes may be involved in the mechanism. To test this hypothesis, I made mutations to restrict dynein's stalk domain from sliding, which controls the affinity state of the MTBD (Gibbons et al., 2005; Carter et al., 2008; Kon et al., 2009, 2004; Redwine et al., 2012; Nishikawa et al., 2014). I then observed whether these constrained structures affected $Num1_{CC}$-stimulated Pac1/Lis1 release.

5.2 RESULTS

As observed in Chapter 2 (Figure 2.3), the $dyn1^{\Delta MTBD}$ construct accumulates at plus ends and its localization is unaffected by overexpression of $Num1_{CC}$. When expressed in cells with wild type (WT) Num1, more $dyn1^{\Delta MTBD}$ cortical foci are seen than WT cells with full-length dynein (28.9 ± 4.2% vs. 79.6 ± 3.8%; Figure 5.2A-B), suggesting that higher levels of $dyn1^{\Delta MTBD}$ are initially recruited to plus ends to be delivered to the cortex. To be recruited at higher levels, $dyn1^{\Delta MTBD}$ may have a higher affinity for Pac1/Lis1 than WT dynein, possibly due to the structural conformation of the motor domain caused by deleting the MTBD. Additionally, I noticed an occasional microtubule "stuck" at these cortical sites- anchored and not being pulled. This was surprising because I expected $dyn1^{\Delta MTBD}$ to be delivered to the cortex but have no further interaction with microtubules without its MTBD. To better understand this phenomenon, I arrested cells in mitosis with hydroxyurea (HU) and imaged over the course of 20 minutes. This treatment allowed me to visualize microtubule dynamics more robustly. Normally, astral microtubules can be seen sliding along the cortex as dynein pulls on them to move the spindle through the mother-bud neck (For example: Chapter 3, Figure 3.2). However, in $dyn1^{\Delta MTBD}$ cells I observed stationary microtubules attached to the cortex without being pulled. The tips appeared to be anchored for long periods of time, up to 15 minutes without sliding or breaking (Figure 5.2C-E). This unusual microtubule-cortical attachment behavior suggests first, that delivery of dynein to the cortex by microtubules does not require direct interaction with the microtubule. Secondly, the microtubule

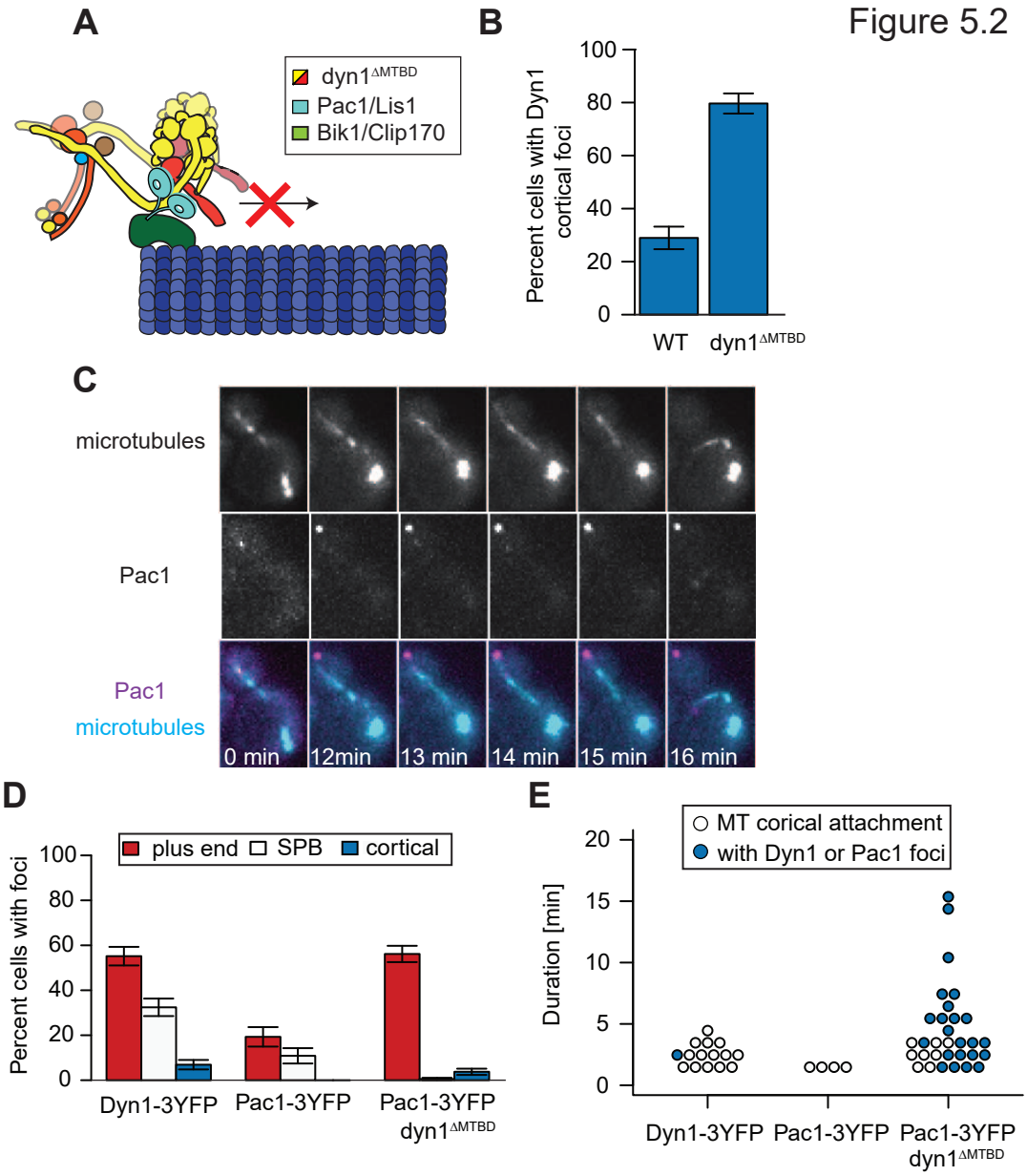

Figure 5.2

Figure 5.2. Deleting the MTBD prevents Pac1/Lis1 release and MT sliding. (A) Cartoon of dynein microtubule binding domain deletion construct. (B) The percentage of cells that exhibit cortical patches of Dyn1-3YFP or dyn1$^{\Delta MTBD}$-3YFP in cells grown to mid-log phase in SD plus glucose and imaged every 10 sec for 15 frames. Error bars represent the standard error of proportion (n ≥ 113 cells). (C) Representative images over time of dyn1$^{\Delta MTBD}$ cells expressing mTurquoise2-Tub1 (α-tubulin) and Pac1-3YFP used for quantification in B and C. Cells were grown to mid-log phase in SD media supplemented with glucose and arrested in SD media containing glucose and 200μM Hydroxyurea (HU). Cells were immobilized on agarose pads containing 200μM HU for the 20 minute duration of imaging. (D) The percentage of cells that exhibit plus end, SPB, or cortical Dyn1-3YFP or Pac1-3YFP in cells expressing wild-type or dyn1$^{\Delta MTBD}$ (n ≥ 83 cells). Error bars represent the standard error of proportion. (E) Scatter plot of duration of microtubule cortical attachments in cells expressing Dyn1 or dyn1$^{\Delta MTBD}$. Colored circles show Dyn1-3YFP or Pac1-3YFP colocalization with microtubule attachment (n ≥ 83 cells).

must be released, and dynein re-engage it through its MTBD to actively generate force and pull on the microtubule to move the spindle.

Because Pac1/Lis1 plays an essential role in dynein-microtubule association (Lee et al., 2003b), it may play a role in this second step of releasing the microtubule before dynein engages with its MTBD. I looked at Pac1-3YFP fluorescence in dyn1$^{\Delta MTBD}$ cells and in agreement with increased dyn1$^{\Delta MTBD}$ plus end accumulation (Chapter 2, Figure 2.3), plus end localization of Pac1-3YFP also increased compared to cells with WT dynein (WT: 19.3 ± 4.3% vs. dyn1$^{\Delta MTBD}$: 56.1 ± 3.6%; Figure 5.2D). Unexpectedly, Pac1/Lis1 also localized to the cortex in dyn1$^{\Delta MTBD}$ cells, which does not normally occur (Figure 5.2C-D). It is well established that although Pac1/Lis1 is required to recruit dynein to plus ends, Pac1/Lis1 no longer associates with dynein-dynactin once offloaded to cortical Num1 sites (Lee et al., 2003b). The unusual localization of Pac1/Lis1 at the cortex in dyn1$^{\Delta MTBD}$ cells was often associated with microtubule-cortical attachments (blue-filled circles; Figure 5.2C and E). These data support the hypothesis that Pac1/Lis1 remains associated with dynein until dynein engages the microtubule with its MTBD and becomes capable of force generation.

Restricting dynein to a high or low microtubule affinity conformation

When dynein offloads to a cortical Num1 site, it must reorient itself from tip-tracking to actively pulling on the microtubule. This might occur when the MTBD senses the microtubule lattice and shifts from low to high affinity. In addition to initiating force generation, the affinity shift may cause Pac1/Lis1 dissociation by forcing the AAA+ ring to change conformation. To test if the microtubule affinity state of dynein affects Pac1/Lis1 release during offloading events, I designed dynein mutants that replicate high or low microtubule affinity states. The stalk domain is responsible for shifting the MTBD from high to low affinity by sliding the alpha helices in the coiled-coil along each other (Gibbons et al., 2005; Carter et al., 2008; Kon et al., 2009, 2004; Redwine et al., 2012; Nishikawa et al., 2014). This sliding is induced by conformational changes in the AAA+ ring during ATP hydrolysis (Schmidt, 2015). I replaced the MTBD with a stable anti-parallel

coiled-coil from the *Thermus thermophilus* Seryl t-RNA Synthetase (SRS) to prevent sliding and lock the motor in high or low microtubule affinity states (Kon et al., 2009). The SRS coiled-coil was inserted into the dynein gene in three locations to form +beta, alpha, and -beta registries. In relation to coiled-coil 1 (CC1), coiled-coil 2 (CC2) is slid up (+beta) or down (-beta) one turn of a heptad repeat from its start (alpha) (Figure 5.3A-B) as originally created in *D. discoideum* (Kon et al. 2009). Because the SRS fusion mutants cannot bind microtubules, to confirm that they folded properly and have adopted the expected registries, I performed an ATPase assay (Figure 5.3C). As expected, the low affinity mutant, +beta, had a low ATP hydrolysis rate similar to unstimulated WT dynein and the high affinity mutants, alpha and -beta, had high ATPase rates that coincided with WT dynein stimulated by microtubules (Figure 5.3C) (Kon et al., 2009).

To make dyn1$^{\Delta MTBD}$, the MTBD sequence was deleted and the alpha helices on either side of the domain were ligated back together to continue the stalk (see Materials and Methods). Although the protein appears to fold correctly and localize appropriately in cells, the structure and flexibility of the new stalk domain is unknown. In the ATPase assay, dyn1$^{\Delta MTBD}$ hydrolyzes ATP near the levels of the high affinity mutants and WT dynein stimulated by microtubules (Figure 5.3C). This suggests that in cells the alpha and -beta mutants may have similar phenotypes to dyn1$^{\Delta MTBD}$.

Pac1/Lis1 preferentially binds the low affinity dynein mutant

To test the hypothesis that Pac1/Lis1 dissociation is triggered by both Num1 interaction and the dynein MTBD affinity state, I engineered the dynein mutants at the endogenous locus and C-terminally labeled them with YFP in cells containing Pac1-3mCherry and fluorescently labeled microtubules. Next to control Num1 interaction with dynein, the galactose inducible promoter GAL1 was incorporated upstream of the minimal interacting domain, Num1$_{CC}$. As shown in Chapter 2, dynein accumulates at plus ends in these cells because Num1$_{CC}$ is missing its Pleckstrin Homology domain that anchors it to the cortex and therefore prevents offloading from occurring. When Num1$_{CC}$ is overexpressed, dynein is activated and depleted from plus ends. By

Figure 5.3

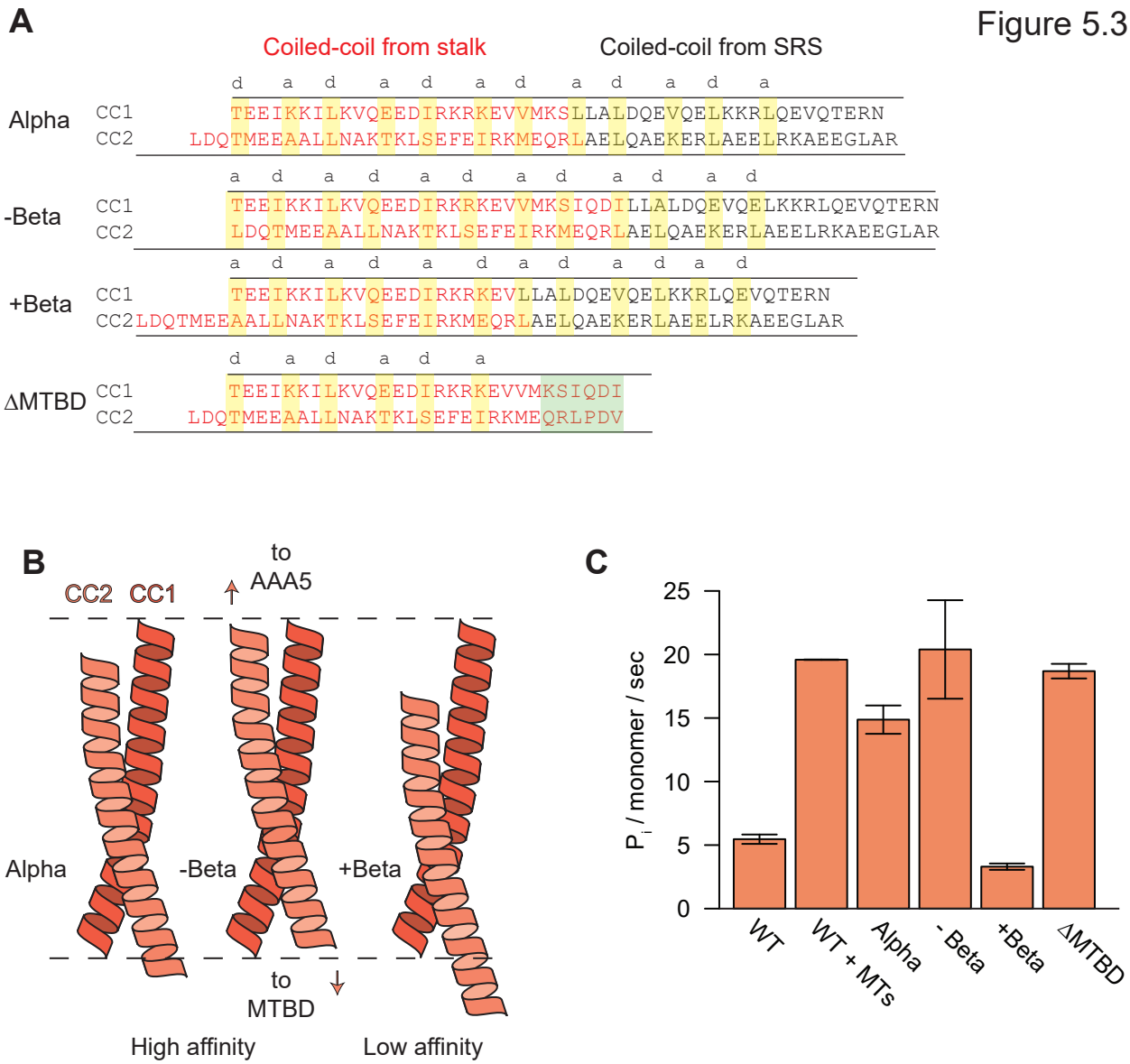

Figure 5.3. Dynein SRS fusion mutants lock motor domain in high and low ATP hydrolysis states. (A) Diagrams showing expected alignments between the two helices of the stalk coiled coil in the dyn1-SRS fusion mutants. The diagrams depict the junction between the stalk coiled coil and the coiled coil from SRS. SRS- derived residues are colored black; amino acids predicted to occupy the a and d positions of the heptad repeats are highlighted in yellow. Green box represents the loop portion of the ΔMTBD mutant. Alignment of ΔMTBD is based on a Phyre2 prediction not shown. (B) Cartoon representation of coiled coil mutants shifted one turn of a heptad repeat from each other. (C) ATPase activity of wild-type dynein, SRS mutants and dyn1$^{\Delta MTBD}$. Values are shown as the mean ± standard error of two experiments done on different days with the same protein preparations.

using this system, I could observe dynein and Pac1/Lis1 colocalization at plus ends and determine if the SRS fusion mutants were affected differently by $Num1_{CC}$ based on the level of depletion from plus ends.

I first looked at WT dynein (Dyn1-3YFP) localization in GAL1p:$Num1_{CC}$ cells containing Pac-3mCherry and saw that plus end localization was reduced 3-fold from 15.1 ± 3.4% of cells to 4.5 ± 1.9% upon $Num1_{CC}$ overexpression (Figure 5.4A-B). Whereas, SPB localization increased from 11.3 ± 3.1% to 16.1 ± 3.5% (Figure 5.4B). In congruence, the fluorescence intensity of plus end foci also decreased significantly (Figure 5.4C). Overall these trends are as expected from results in Chapter 2, although the magnitude of change is smaller than seen previously. Additionally, colocalization between dynein and Pac1/Lis1 was rare in this strain. Since Pac1/Lis1 is required to target dynein to plus ends, it can be assumed to be present even if its fluorescence is not observed (Lee et al., 2003b; Markus et al., 2009). Together, these results confirm that dynein with an intact MTBD is depleted from plus ends upon overexpression of $Num1_{CC}$.

I predicted that Pac1/Lis1 would not have difficulties recruiting the different SRS fusion mutants to plus ends. In vitro studies have shown that Pac1/Lis1 can interact with dynein throughout the mechanochemical cycle (Gutierrez et al., 2017; Marzo et al., 2019a; Elshenawy et al., 2019a). Further, Kon et al. (2009) made identical SRS fusion mutants with *D. discoideum* dynein and showed that the linker still swings at rates correlated with ATPase activity, demonstrating that the linker is not restricted to a position that would prevent Pac1/Lis1 binding. In striking contrast to my prediction, the high and low affinity mutants, alpha and +beta, respectively had opposite phenotypes. The alpha mutant was seen less frequently than WT dynein with only 10 plus end foci and a single Pac1/Lis1 foci observed in over 100 cells (Figure 5.4B).

Whereas, the +beta mutant was at plus ends in almost every cell and colocalized with Pac1/Lis1 in 87.4% of cells (Figure 5.4D-E). This suggests that the stalk conformation has a great

Figure 5.4

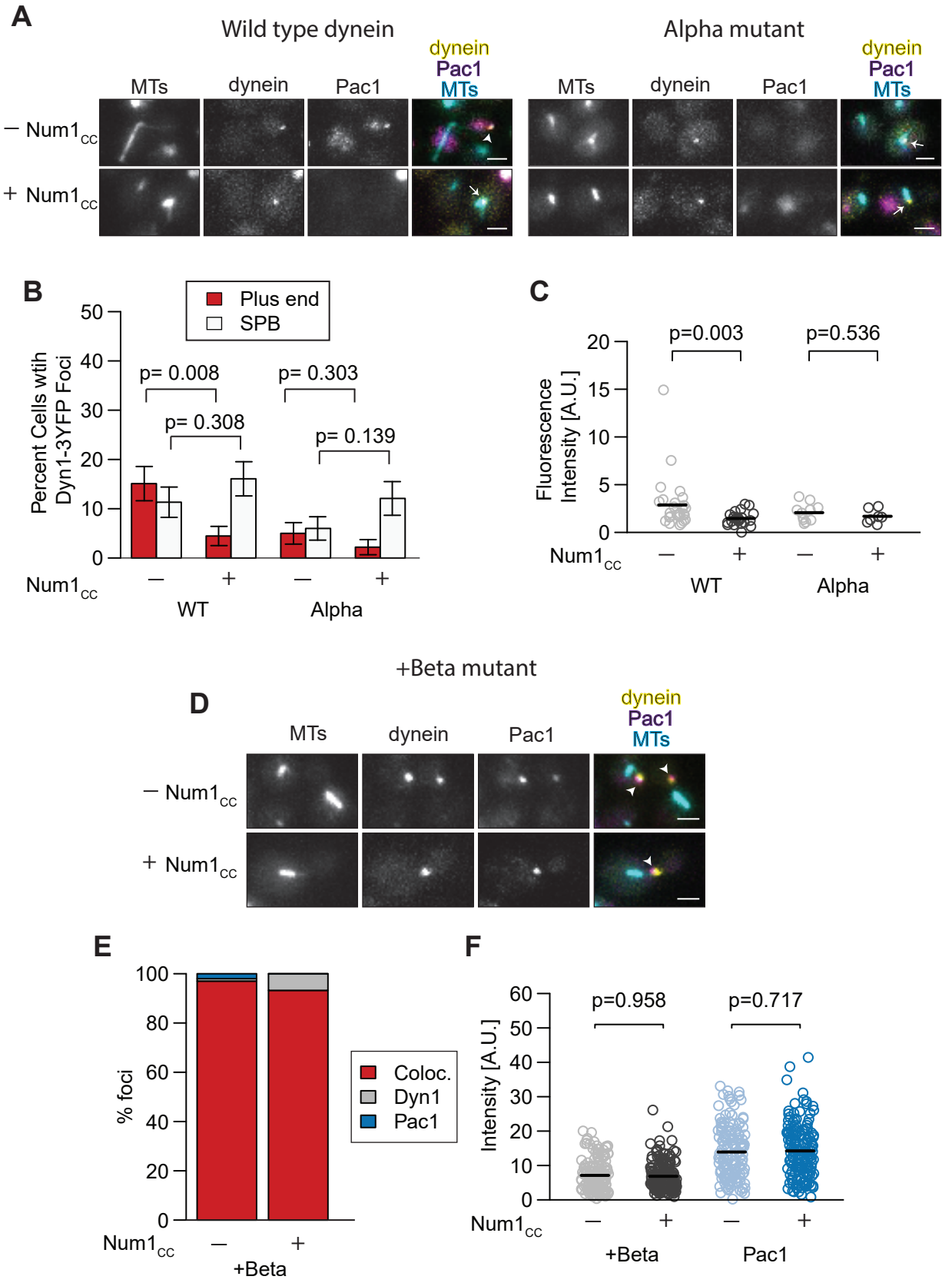
A
Wild type dynein
Alpha mutant
MTs
dynein
Pac1
dynein Pac1 MTs
− Num1cc
+ Num1cc
B
Plus end
SPB
Percent Cells wtih Dyn1-3YFP Foci
p= 0.008
p= 0.308
p= 0.303
p= 0.139
Num1cc
WT
Alpha
C
Fluorescence Intensity [A.U.]
p=0.003
p=0.536
Num1cc
WT
Alpha
+Beta mutant
D
MTs
dynein
Pac1
dynein Pac1 MTs
− Num1cc
+ Num1cc
E
% foci
Coloc.
Dyn1
Pac1
Num1cc
+Beta
F
Intensity [A.U.]
p=0.958
p=0.717
Num1cc
+Beta
Pac1

Figure 5.4. Pac1/Lis1 preferentially binds to the low affinity SRS fusion mutant. (A) Representative images of GAL1p:Num1$_{CC}$ cells expressing mTurquoise2-Tub1 (α-tubulin), dyn1-SRSα-3YFP or dyn1-SRS+β-3YFP mutants and Pac1-3mCherry used for quantification in B-E. Cells were grown overnight in SD media supplemented with raffinose and grown to mid-log phase in SD plus glucose (uninduced; - O/E Num1$_{CC}$) or galactose (induced; + O/E Num1$_{CC}$). Each image is a maximum-intensity projection of 2-µm Z-stack of wide-field images. Arrows indicate colocalized plus end foci and arrowheads indicate dynein only foci. Bars, 2 µm. (B) The percent of cells with either Dyn1-3YFP or dyn1-SRSα-3YFP foci at plus ends and SPB after overexpression of Num1$_{CC}$ ($n \geq 8$ fluorescent foci; $n \geq 91$ cells). Statistical significance ($p \leq .05$) was determined by a Z-test. (C) Scatter plots represent the fluorescence intensity distribution of either Dyn1-3YFP or dyn1-SRSα-3YFP plus end foci with or without Num1$_{CC}$ overexpression. (D) The extent of dyn1-SRS+β-3YFP and Pac1-3mCherry colocalization at plus ends ($n \geq 100$ fluorescent foci; $n \geq 111$ cells). (E) Scatter plots represent the intensity distribution of both dyn1-SRS+β-3YFP and Pac1-3mCherry fluorescent foci. The black line represents the mean intensity. Statistical significance ($p \leq .05$) was determined with a Mann-Whitney test because the data points do not fit a normal gaussian distribution (based on a Shapiro-Wilk analysis).

impact on Pac1/Lis1 association with the motor, even without Num1 involvement. Although linker movements are not restricted in these mutants (Kon et al., 2009), it has been shown that Pac1/Lis1 prefers to interact with dynein when AAA1 is bound to ADP+P_i, which coincides with the MTBD low affinity state (McKenney et al., 2010; Schmidt et al., 2014). Accordingly, the structural features of the +beta (low affinity) mutant appear to be more favorable for Pac1/Lis1 binding than the alpha mutant and support the hypothesis that Pac1/Lis1 interaction with dynein is transient and dependent on the mechanochemical cycle (McKenney et al. 2010). Finally, the -beta mutant had identical phenotypes to alpha (high affinity) and was shown to be a registry that rarely occurred, therefore the data from this mutant is not shown (Kon et al., 2009).

Interestingly the phenotype of the +beta mutant is similar to dyn1$^{\Delta MTBD}$, yet the ATP hydrolysis rate of +beta is low and dyn1$^{\Delta MTBD}$ is high (Figures 2.3 and 5.2C). This result is peculiar because the rate of ATP hydrolysis is strongly linked with AAA+ ring conformation. If the conformation of both +beta and dyn1$^{\Delta MTBD}$ are favorable for Pac1/Lis1 binding, I would expect the ATP hydrolysis rate to be similar.

Overexpression of Num1cc triggers Pac1/Lis1 release from the low affinity mutant

After I determined that the stalk conformation dramatically affects Pac1/Lis1 binding to dynein, I tested the effect of $Num1_{CC}$ overexpression on Pac1/Lis1-dynein interaction. Consider the two-step process of dynein delivery to Num1 sites first requiring Pac1/Lis1 for plus end association and then, dynein engages with the microtubule for force generation. In this scenario, I predict that dynein initially is in a low affinity microtubule binding state, and upon binding to Num1 and engaging the microtubule, switches to a high affinity state. During this switch, Pac1/Lis1 binding becomes unfavorable and it dissociates into the cytoplasm. Separating this hypothesis in to parts, the alpha mutant would be expected to induce Pac1/Lis1 release upon $Num1_{CC}$ overexpression. However, since so few Pac1/Lis1 molecules were visualized in the alpha mutant, the indication that Pac1/Lis1 binding was affected by $Num1_{CC}$ would be a decrease in alpha mutant frequency or intensity at plus ends. Neither the plus end frequency or intensity was significantly affected, but alpha mutant accumulation at the SPB increased 2-fold 6.0 ± 2.4% to 12.1 ± 3.4% upon $Num1_{CC}$ overexpression (Figure 5.4B-C). Because the alpha mutant does not have motile properties (lacking the MTBD), the increase in SPB localization cannot be mediated by $Num1_{CC}$. These data show that $Num1_{CC}$ does not affect the already low frequency of alpha mutant localization at microtubule plus ends.

Looking at the +beta (low affinity) mutant, I expected $Num1_{CC}$ overexpression to have no effect on Pac1/Lis1 association because I predicted that dissociation requires both $Num1_{CC}$ interaction and the high affinity state. In support of this hypothesis, no change in frequency or fluorescence intensity of the +beta mutant or Pac1/Lis1 foci was observed (Figure 5.4D-F). Altogether, mutating the stalk registry to a fixed position affects Pac1/Lis1 interaction with dynein significantly, and this restriction appears to prevent $Num1_{CC}$ from inducing Pac1/Lis1 release and dynein plus end depletion.

To better assess the effect of $Num1_{CC}$ on Pac1/Lis1 interaction with the dynein mutants, I anchored the mutants to a fixed location at the cortex, independently of Num1. Because dynein

and Pac1/Lis1 are codependent for plus end localization, it will be easier to monitor interaction if dynein is in a fixed location. I inserted a Pleckstrin Homology (PH) domain at the N-terminus of the dynein mutants to target them to the cortex and expressed them with a constitutively active promoter, TEF1. In the absence of $Num1_{CC}$, 36.0% of cells contained at least one alpha mutant cortical focus, and zero of those foci colocalized with Pac1/Lis1 (Figure 5.5A-B). This confirms what was seen in Figure 5.4, that Pac1/Lis1 interacts with the high affinity, alpha mutant infrequently, if at all. Since Pac1/Lis1 was not seen colocalizing with this mutant, overexpression of $Num1_{CC}$ had no visible effect. Looking at the low affinity, +beta mutant, Pac1/Lis1 colocalized with 47.3% of cortical patches in the absence of $Num1_{CC}$ (Figure 5.5A, lower panels). Percent colocalization is lower than seen at plus ends in Figure 5.4. This makes sense because dynein is not dependent on Pac1/Lis1 for localization to the cortex in these cells like it is for plus end localization. Notably, when cells were grown in galactose to overexpress $Num1_{CC}$, more cortical dynein patches accrued in both mutants. A similar phenomenon occurred previously when this technique was used (Chapter 2; Figure 2.4) and was considered to be a side-effect of $Num1_{CC}$ oligomerizing with the PH domains to increase patch density (Tang et al., 2012). Because of the increase in cortical patches in $Num1_{CC}$ overexpression, I compared the ratio of Pac1/Lis1 to +beta mutant fluorescence in -$Num1_{CC}$ (glucose) and +$Num1_{CC}$ (galactose), to determine that Pac1/Lis1 intensity significantly decreased when $Num1_{CC}$ was overexpressed (Figure 5.5C). Similarly, the frequency of Pac1/Lis1 colocalized with +beta mutant patches also decreased (Figure 5.5B). Although the frequency change is significant, it may be exaggerated by the increase in +beta mutant cortical foci and a limiting concentration of Pac1/Lis1. Taken together, $Num1_{CC}$ appears to influence Pac1/Lis1 binding to dynein even when the stalk is restricted to the +beta, low affinity state. This contrasts the hypothesis that the MTBD needs to be primed for microtubule binding, in the high affinity state, for Num1 to trigger Pac1/Lis1 release. Overall, these results show that the stalk registry dramatically affects Pac1/Lis1 interaction with dynein and secondarily, Num1 can still release Pac1/Lis1 binding despite the rigidity of the MTBD affinity state. To determine

Figure 5

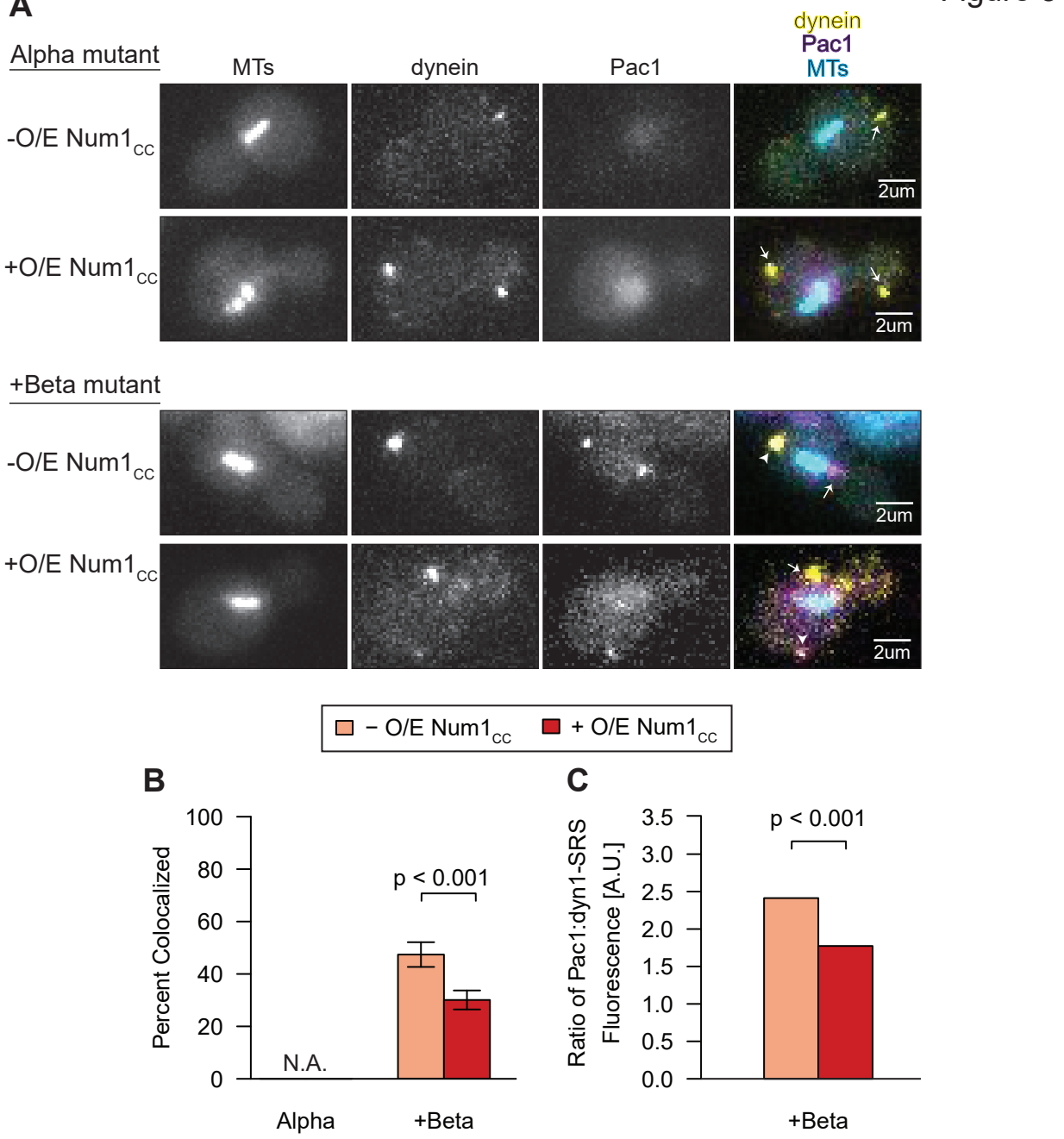

Figure 5. Overexpression of Num1$_{cc}$ triggers release of Pac1/Lis1 from the (low affinity) mutant. (A) Representative images of GAL1p:Num1$_{cc}$ cells expressing mTurquoise2-Tub1 (α-tubulin), TEF1p:PH-dyn1-SRSα-3YFP or TEF1p:PH-dyn1-SRS+β-3YFP mutants and Pac1-3mCherry used for quantification in B and C. Arrowheads indicate Pac1-3mCherry colocalized with cortical dynein foci and arrows indicate either dynein or Pac1 foci alone. (B) The extent of Pac1-3mCherry colocalization with cortical dynein patches for indicated mutant (n ≥ 112 foci). Z-test was used to determine the significance between the two percents. Error bars represent the standard error of proportion. (C) Ratio of Pac1-3mCherry to dyn1-SRS+β-3YFP patch fluorescence intensity. Z-test was used to determine the significance between the two proportions.

how important flexibility in dynein's structure is for Num1 triggered Pac1/Lis1 release further experimentation is needed.

5.3 DISCUSSION AND FUTURE DIRECTIONS

In summary, these data show that the MTBD is important for appropriate offloading of dynein to the cortex. In its absence, dynein remains attached to the astral microtubule that delivered it, likely through a continued interaction with Pac1/Lis1 and the +TIP protein Bik1 (Roberts et al., 2014b; Sheeman et al., 2003). The stalk mutants show that the registry impacts the interaction between dynein and Pac1/Lis1, suggesting that conformational changes in the MTBD may be involved in Pac1/Lis1 dissociation. Further, overexpression of the minimal dynein-interacting domain of the cortical anchor, Num1, can induce Pac1/Lis1 release from the low affinity stalk registry mutant, despite conformational restrictions. These interesting results open more questions of exactly how do these SRS fusion mutants affect Pac1/Lis1 binding sites and what is the mechanism of Num1-induced Pac1/Lis1 release from dynein motors?

Pac1/Lis1 weakly interacts with the high affinity dynein mutant

Based only on the registry of the coiled-coil stalk, the high affinity, alpha mutant conformation should coincide with the linker in a straight, post-powerstroke position resting at AAA5 and an open AAA+ ring conformation associated with no nucleotide and ADP hydrolysis states in AAA1 (Figure 5.1A) (Schmidt et al., 2012; Bhabha et al., 2014). However, the structure is not permanently in this state because ATP hydrolysis requires structural changes and the linker continues to swing at a high rate (Kon et al., 2009). The stalk mutations must add strain, though, that force the structure to prefer the linker in a particular position.

If the the linker frequently rests at AAA5 in the alpha mutant this would create a steric hinderance for Pac1/Lis1 binding. This is supported by my data that showed few alpha mutants were recruited to plus ends by Pac1/Lis1 and no colocalization between Pac1/Lis1 and the alpha mutant was seen anchored at the cortex with a PH domain (Figures 5.4 and 5.5) (Toropova et al., 2014). In further support of my results, McKenney et al. (2010) showed that Pac1/Lis1 did not

interact with dynein in a biochemical pulldown unless in the presence of ADP+vandate (representing ADP+Pi), which causes dynein to form the low affinity, closed conformation (Schmidt et al., 2015). However, because Kon et al. (2009) shows that the alpha mutant linker swings at a high rate in accordance with its high ATPase activity the Pac1/Lis1 binding site cannot be permanently blocked. In fact, Pac1/Lis1 can interact with dynein throughout the mechanochemical cycle as seen in motility assays (Gutierrez et al., 2017; Marzo et al., 2019a; Elshenawy et al., 2019a). These conflicting data indicate that Pac1/Lis1 interacts with dynein either transiently- only binding to a particular conformation- or stably, depending on the context.

In cells, Pac1/Lis1 targets dynein to plus ends and the interaction allows dynein to tip-track until reaching the cortex. Although the +TIP proteins EB1 and Clip170 treadmill at plus ends, binding and rebinding as the microtubule grows (Schuyler and Pellman, 2001), I photobleached dynein at plus ends and saw little to no turnover (not quantified). This supports a model of stable interaction between Pac1/Lis1 and dynein during this step of the dynein pathway (Figure 5.1C). My hypothesis suggests that upon offloading to Num1 at the cortex changes the interaction between Pac1/Lis1 and dynein from stable to transient. The transient interaction would occur when dynein entered the alpha conformation. If we compare the low levels of both the alpha mutant without overexpression of $Num1_{CC}$ and wild-type dynein in the presence of $Num1_{CC}$ at plus ends, this suggests that $Num1_{CC}$ may induce the alpha mutant conformation (Figure 5.4B).

A possible reason that Pac1/Lis1 interacts poorly with the alpha mutant is because it may form the autoinhibitory phi-particle. The structural restraints of the alpha mutant may cause it to form the phi-particle more tightly than WT dynein, which would prevent Pac1/Lis1 from associating. In the phi-particle the linker is bent in the pre-powerstroke position (associated with low affinity), yet its formation is nucleotide independent (Zhang et al., 2017). Therefore, it is possible that although the alpha mutant may prefer its linker to be straight, it could still form an autoinhibitory structure. However, dynein-2 motors that form the phi-particle upon dimerization have lower ATPase rates than the open monomer, suggesting that if the alpha mutant were

autoinhibited it would not have such a high rate of ATP hydrolysis (Toropova et al., 2017). Without more structural information, it is unclear what prevents Pac1/Lis1 from interacting with the alpha mutant at a higher frequency.

Pac1/Lis1 prefers to interact with the low affinity dynein mutant

Traditionally Pac1/Lis1 has been considered an inhibitor of dynein by inducing a high affinity state to remain bound to microtubules for an extended time (Huang et al., 2012; McKenney et al., 2010). More recent studies have challenged this function of Pac1/Lis1 demonstrating that the inhibitory effect was an artifact of assay conditions, and that Pac1/Lis1 can facilitate the formation of DDX complexes by preventing phi-particle formation (Marzo et al., 2019a; Elshenawy et al., 2019a; Htet et al., 2019; Qiu et al., 2019b). In agreement with this new paradigm, my data show that Pac1/Lis1 preferentially bound the +beta mutant that corresponds to dynein in the low affinity MTBD conformation. The linker should be predominately bent in this conformation leaving the Pac1/Lis1 binding sites open and the AAA+ ring closed (Schmidt et al., 2015). Because the second Pac1/Lis1 binding site is only available when the stalk and AAA5 are in close proximity during the closed ring conformation, it is logical that Pac1/Lis1 would have a higher affinity for the +beta mutant.

Despite the structural data available of Pac1/Lis1 bound to dynein, it is still difficult to understand how the structure of dynein influences Pac1/Lis1 binding and conversely, how Pac1/Lis1 influences dynein conformations. The second Pac1/Lis1 binding site was determined when the Walker B motif was mutated in AAA3, which allows ATP to bind, but not hydrolyzed (DeSantis et al., 2017). AAA3 hydrolyzes ATP a magnitude slower than the main AAA1 site and acts as a gate between fast and slow motility by blocking allosteric changes between AAA1 and the MTBD (Imamula et al., 2007; Bhabha et al., 2014; DeWitt et al., 2015; Nicholas et al., 2015). When AAA3 is bound to ATP, the linker cannot undock from the post-powerstroke position at AAA5 and prevents the stalk registry from shifting from high to low affinity when AAA1 binds ATP (Bhabha et al., 2014). The high affinity conformation of dynein is associated with an open ring

and straight linker which are both unfavorable positions for Pac1/Lis1 binding, yet somehow this condition provided two binding sites for Pac1/Lis1 (DeSantis et al., 2017). Although it is hard to understand why the AAA3 mutant would create two binding sites for Pac1/Lis1, binding of Pac1/Lis1 at either one or two sites causes the AAA+ ring to resemble the low affinity, ADP+P_i crystal structure (DeSantis et al., 2017; Schmidt et al., 2015). These EM structures provide important insight into the interaction between dynein and Pac1/Lis1 and reveal that the dynein structure may adopt more conformations than we understand. In cells, Pac1/Lis1 targets dynein to plus ends before delivery to the cortex. To conserve energy, Pac1/Lis1 may hold dynein in the low affinity, low ATPase activity state until arriving at the cortex where it is activated to pull the spindle. Further, the nucleotide state of AAA3 may regulate Pac1/Lis1 binding and might be an important regulatory step for dissociation during offloading.

To make the data more difficult to interpret the dyn1$^{\Delta MTBD}$ mutant has a high ATPase rate, and according to a Phyre2 analysis, its predicted coiled-coil alignment matches that of the alpha mutant (represented in Figure 5.3A). However, its phenotype is most similar to the +beta, low affinity mutant, which suggests that the rate of ATP hydrolysis is not a good indicator of whether Pac1/Lis1 will interact with dynein. The only difference between the alpha and dyn1$^{\Delta MTBD}$ mutants is the addition of the SRS stable coiled-coil. It is possible that dyn1 $^{\Delta MTBD}$ is more flexible, allowing the ring to accommodate Pac1/Lis1 binding more freely. This is unlikely though because the loop portion of the dyn1 $^{\Delta MTBD}$ predicted structure contains a conserved proline which should cause rigidity and prevent sliding. It is difficult to understand why the two mutants behave differently without a better analysis of their structural features.

Num1 may induce Pac1/Lis1 release regardless of MTBD conformation

Although the exact structural details of these mutants require additional study, I still tested my hypothesis that Num1$_{CC}$ would not be able induce Pac1/Lis1 dissociation from the +beta mutant because it could not change conformation into the high affinity state. Unexpectedly, Num1$_{CC}$ did release Pac1/Lis1 from binding the +beta mutant when anchored at the cortex (Figure

5.5). This suggests that the mechanism of release is not dependent on the stalk registry shifting the MTBD from low to high affinity. How can Num1 induce Pac1/Lis1 release? The linker is the connection between where Num1 interacts in the tail and where Pac1/Lis1 binds in the motor domain. A short peptide extension added between the linker and the motor causes spindle misorientation and Pac1/Lis1 mislocalization to the cortex (Markus and Lee, 2011). Deletion of Pac1/Lis1 partially rescues the spindle positioning defects caused by the mutant, suggesting that the extension prevents Pac1/Lis1 release from motor complexes. It is possible that Num1 and dynactin binding in the tail generates tension on the linker, which may affect Pac1/Lis1 binding. A recent paper showed that backward tension applied to the linker induces conformational changes between the buttress and stalk that force the MTBD to shift into the high affinity state (Rao et al., 2019). Although my data show that shifting from the low to high affinity state is not required for Num1-induced Pac1/Lis1 release, it is possible that other allosteric changes induced by tension in the linker are enough to cause Pac1/Lis1 dissociation. For example, tension applied to the linker bypasses the regulatory effect of AAA3 that holds dynein in a slow motility state (Nicholas et al., 2015). This AAA3 state (AAA3 bound to ATP) allows Pac1/Lis1 to bind at two sites. Therefore, tension added to the linker when Pac1/Lis1 is bound at two sites could force Pac1/Lis1 to release the stalk/AAA5 binding site and have a less stable interaction.

While this study was carried out, the role of Pac1/Lis1 was reestablished as a factor that prevents the autoinhibitory, phi-particle state of dynein to facilitate complex formation with dynactin and an adapter and become an active, processive motor complex to do work in the cell (Marzo et al., 2019a; Elshenawy et al., 2019a; Htet et al., 2019; Qiu et al., 2019b). Pac1/Lis1 achieves this by first engaging dynein at the AAA3/4 and stalk binding sites (Figure 5.1B). As an open complex, human dynein can interact with microtubules, but is still not processive (Zhang et al., 2017). Its tail domain needs to be oriented in a parallel fashion by dynactin and an adapter to finally form a processive complex (Chowdhury et al., 2015; Urnavicius et al., 2015). In yeast, Pac1/Lis1, dynein, and dynactin likely arrive at the cortex unassembled and upon interaction with

Num1, dynein-dynactin become active (Chapter 2; Figure 5.1C). My findings here suggest that Pac1/Lis1 does not dissociate randomly, but it is likely due to conformational changes in the motor domain that occur when Num1 and dynactin bind, possibly triggered by tension in the linker. The dissociation of Pac1/Lis1 allows for dynein to switch from tip-tracking to lateral binding for its role in positioning the mitotic spindle by pulling on astral microtubules. The exact details of this fascinating mechanism of Pac1/Lis1 release from dynein motors will require more exploration.

5.4 FUTURE DIRECTIONS

First, it will be important to better characterize the interaction between Pac1/Lis1 and the SRS fusion mutants. Pulldowns using purified proteins should be performed to confirm that the alpha mutant has low binding affinity for Pac1/Lis1 and the +beta and dyn1$^{\Delta MTBD}$ mutants have a high affinity for Pac1/Lis1. Included in this pulldown, WT dynein should be used as a control to determine the baseline level of Pac1/Lis1 interaction when the MTBD is intact. Because the alpha and dyn1$^{\Delta MTBD}$ have similar ATPase activities, but opposite phenotypes this discrepancy needs to be addressed. If the pulldowns are congruent with the in vivo data, the next step could include negative stain EM to visualize how the structures may differ. The structural information will be valuable for understanding how Pac1/Lis1 may or may not be interacting. If the pulldown results suggest that alpha and dyn1 $^{\Delta MTBD}$ interact similarly with Pac1/Lis1, the in vivo data will need to be repeated after the mutants have been sequenced.

Next, the experiments in Figure 5.5 with dynein anchored to the cortex by a N-terminally fused PH domain should be expanded to include WT dynein and the minimal motor construct that lacks the tail domain (GST-dyn1^{331kDa}) as controls. WT dynein should be used a baseline for Pac1/Lis1 depletion when Num1$_{CC}$ is overexpressed to determine if the depletion seen in +beta cells is normal, or less than WT. If the depletion is less than WT, this would suggest that the restriction in the stalk hinders Pac1/Lis1 release and would indicate that sliding of the stalk registry is involved in the mechanism. GST-dyn1^{331kDa} would be a negative control because neither Num1$_{CC}$ or dynactin should interact with dynein and affect Pac1/Lis1 interaction. Deleting a

component of the dynactin complex would be another negative control to prevent $Num1_{CC}$ interaction. The PH domain experiments should include dyn1 $^{\Delta MTBD}$ for comparison to determine if $Num1_{CC}$ affects Pac1/Lis1 release from this mutant. Because +beta and dyn1 $^{\Delta MTBD}$ have opposite ATPase activities, it is possible that $Num1_{CC}$ will have a different effect.

To test whether +beta or dyn1 $^{\Delta MTBD}$ have defective phi-particle formation, their cortical localization can be tested in cells with Pac1/Lis1 deleted. If the mutants have any cortical foci in cells lacking Pac1/Lis1, this will indicate that they can bypass the plus end and be recruited directly from the cytoplasm as is observed in mutants that cannot form the phi-particle (Marzo et al., 2019a).

Because structural data shows that the nucleotide state of AAA3 affects Pac1/Lis1 binding, it is important to examine how this may regulate dynein localization in cells. The Walker B mutation in AAA3 that favors two Pac1/Lis1 binding sites has not been observed in cells (DeSantis et al., 2017). It is possible that cells expressing the AAA3 Walker B mutation would have increased targeting of dynein to plus ends and the cortex because of increased Pac1/Lis1 recruitment. Additionally, if the nucleotide state of AAA3 is important for Pac1/Lis1 release then Pac1/Lis1 foci may be seen at the cortex, as shown in Figure 5.2 with the dyn1 $^{\Delta MTBD}$ mutant. Coupling the AAA3 Walker B mutation with the stalk mutants, I would not expect much difference in Pac1/Lis1 binding to the +beta mutant because the structure already favors Pac1/Lis1 binding at both sites. It could however, improve Pac1/Lis1 binding to the alpha mutant if it changes the conformation in a favorable way.

If the presence or absence of the second Pac1/Lis1 binding site is important for dissociation, three point mutations on the stalk that abolition binding can be made (DeSantis et al., 2017). In cells, DeSantis et al. (2017) observed that dynein localization decreased at plus ends and the cortex with these mutations, suggesting that Pac1/Lis1 interacts less frequently or stably. To determine if this site is important for $Num1_{CC}$ induced release, the PH-fusion cells can be used to measure Pac1/Lis1 colocalization. I predict that Pac1/Lis1 binding would be unaffected

by $Num1_{CC}$ if the release mechanism relies on removing the stalk binding site. This is because Pac1/Lis1 would already have a weakened interaction.

5.5 MATERIALS AND METHODS

Media and strain construction

All strains are derived from either YEF473A (Bi and Pringle, 1996)for imaging or W303 (constructed by Rodney J. Rothstein) (Ralser et al., 2012) for protein purification and are listed in Table 5.1. We transformed yeast strains using the lithium acetate method (Knop et al., 1999a). Strains carrying the upstream TEF1 promoter were constructed by PCR product-mediated transformation (Longtine et al., 1998b). Transformants were clonally purified by streaking to individual colonies on selective media. Proper tagging was confirmed by PCR. Strains carrying fluorescently-labeled proteins were constructed by mating followed by tetrad dissection. Strains were confirmed via microscopy. Yeast synthetic defined (SD) media were obtained from Sunrise Science Products.

To generate yeast strains with the dynein MTBD replaced by Seryl-tRNA-synthetase coiled-coil at three locations for the +β, α and -β mutants, we used the site-specific genomic mutagenesis approach (Gray et al., 2004b). In brief, after integration of the URA3 cassette into the DYN1 locus (replacing nucleotides 9304-9675, corresponding to amino acids 3102-3225), a PCR product containing a stable coiled-coil (Kon et al., 2009) was amplified from a plasmid containing the seryl-tRNA synthetase (SRS) gene from *Thermo thermophilus* (see Plasmid construction) was transformed into the URA3-integrated strain. To replace the microtubule binding domain and position the coiled-coil stalk in different registries, the homologous recombination region of the forward primers aligned with amino acids 3094, 3098, and 3102 to create the +β, α and -β mutants, respectively. The reverse primer inserted the PCR product at amino acid 3228 in the DYN1 gene. Subsequently, colonies were grown on 5-fluoroorotic acid–containing plates.

Resistant colonies were selected and confirmed by colony PCR and sequencing of the genomic DNA region.

To generate a yeast strain with the dynein MTBD deleted, URA3 was integrated at the same location as above, but was replaced with a PCR product amplified from the DYN1 gene downstream of the MTBD. This technique deletes a section of a gene and recombines the gene with the rest of the downstream open reading frame to form an intact protein. Yeast cells were transformed and colonies selected as described above.

Plasmid construction

Using genomic DNA from Thermus thermophilus obtained from AddGene, the entire Seryl-tRNA synthetase gene was amplified using PCR and inserted into the pRS305 vector (Sikorski and Hieter, 1989) using BamHI and NotI restriction sites.

Protein purification and ATPase assay

To purify wild-type 6xHis-GFP-3XHA-GST-DYN1^{331kD}-HALO or stalk mutations ΔMTBD, +β, α, or -β, yeast cells were grown in 3ml YPAD (YPA supplemented with 2% glucose) overnight, transferred to 25ml YPAD for the day, poured into 200ml YPA supplemented with 2% raffinose overnight and finally overexpressed in 1L YPA supplemented with 2% galactose for 24hrs to overexpress the protein via a galactose inducible promoter (GAL1). Cells were harvested by centrifugation, washed once with water and the resuspended cell pellet was then frozen by drops in liquid nitrogen. Lysis was performed by grinding the liquid nitrogen-frozen pellets with a coffee grinder (Hamilton Beach model 80374). The cell powder was melted in 0.2 volumes of 5X dynein lysis buffer (1X dynein lysis buffer: 30 mM HEPES (pH 7.2), 50 mM K-Acetate, 2 mM Mg-Acetate, 1 mM EGTA, 10% glycerol, 0.2% Triton X-100, 1 mM DTT, 0.5 mM Mg-ATP, 1 mM Pefabloc). Subsequent steps were at 4°C unless indicated. After lysis, the initial supernatant was centrifuged at 13,000rpm for 15 min. The resulting supernatant was then incubated with IgG sepharose (Amersham Pharmacia) for 1 hour. The IgG beads containing bound protein were then washed 2 times with dynein lysis buffer with 0.1% Triton X-100 and washed twice with ‘modified’ TEV

cleavage buffer (10 mM Tris (pH 8.0), 150 mM K-Acetate, 2mM Mg-Acetate, 0.005% TritonX-100, 0.5 mM ATP, 1 mM DTT, 1 mM Pefabloc). The beads were then incubated with 1ul of 1mM SNAP-Alexa Fluor 647 substrate (New England Biolabs) for 10 minutes at room temperature in the dark. After washing 3-5 times with 'modified' TEV cleavage buffer, beads were resuspended in 0.1ml and incubated with TEV protease for 1 hour at 16°C. Ndl1 protein was similarly purified via its ZZ tag, with the exception that all buffers lacked Mg-ATP and TEV cleavage was left overnight at 4ºC in 0.3-0.4ml of 'modified' TEV cleavage buffer to increase efficiency. Approximate yield for 1L of $Dyn1_{331kD}$ was 0.20µM (0.13 mg/ml).

Basal and microtubule-stimulated ATPase activities were determined using the EnzChek phosphate assay kit (Life Technologies). Assays were performed in dynein assay buffer (30 mM HEPES pH 7.2, 50mM potassium acetate, 2 mM magnesium acetate, 1 mM EGTA) supplemented with 2 mM Mg ATP, with 0–2 µM taxol-stabilized microtubules, and 5 nM of either wild-type 6His–GST–dynein331 or ΔMTBD, +β, α, or -β mutants. Reactions were initiated with the addition of dynein, and the absorbance at 360 nm was monitored by a spectrophotometer for 10–20 min. Background phosphate release levels (presumably from microtubules) for each reaction were measured for 5 min before addition of dynein to account for any variation as a consequence of differing microtubule concentrations, and were subtracted out from each data point. $K_{m(MT)}$, k_{basal}, and k_{cat} were determined from fitting the data to equation below, as previously described (Kon et al., 2004), where k_{obs} and k_{basal} are the observed and basal ATPase rates, and x is the concentration of tubulin used to generate microtubules for a given data point:

$$k_{obs} = \left(\frac{x(k_{cat} - k_{basal})}{(K_{m(MT)} + x) + k_{basal}} \right)^2$$

Wide-field image acquisition and data analysis

Yeast cultures were grown overnight in SD media supplemented with 2% glucose (SD glucose) or 2% raffinose (SD raffinose; strains containing a GAL1 promoter) and diluted in the morning to mid-log phase to maximize cells in mitosis. Cells grew in either SD glucose or for overexpression

phenotypes, SD galactose. Cells were mounted on 1.7% agarose pads containing non-fluorescent SD media. Wide-field fluorescence images were collected using a 1.49 NA 100× objective on a Ti-E inverted microscope equipped with a Ti-S-E motorized stage (Nikon), piezo Z-control (Physik Instrumente), a SOLA SM II LE LED light engine (Lumencor), a motorized filter cube turret, and an iXon X3 DU897 cooled EM-CCD camera (Andor). The microscope system was controlled by NIS-Elements software (Nikon). A step size of 0.5 µm was used to acquire 2-µm-thick Z-stack images. Sputtered/ET filter cube sets (Chroma Technology) were used for imaging mTurquoise2 (49001), YFP (49003), and mCherry (49008) fluorescence. Images were analyzed as single Z-stack maximum projections in Fiji software (ImageJ, National Institutes of Health). Plus end, SPB or cortical foci were identified in three color movies and scored accordingly. Specifically, plus end molecules were recognized as those foci that localized to the distal tips of dynamic microtubules (identified via mTurquoise2-Tub1 imaging), whereas SPB molecules were recognized as those foci that localized to one of the spindle poles. Cortical molecules were identified as those foci not associated with an astral microtubule plus end that remained stationary near the cell cortex for at least four frames. Colocalization between dynein and Pac1 molecules were determined by overlapping fluorescence in the corresponding channel for at least two frames. Intensity measurements were determined by the integrated pixel density (ImageJ) of a 3 x 3 pixel box defining the focus. Two data sets were considered statistically significant if a Student's *t* test (assuming unequal variance) returned a p-value < 0.05. When comparing ratios of fluorescence between dynein and Pac1, the prop.test function in R used the the standard z-test equation, where p_A and p_B are the two ratios with sample size n_A and n_B, and p is the overall proportion to determine the z-score and subsequent p-value.

$$z = \frac{p_A - p_B}{\sqrt{p(1-p)(\frac{1}{n_A} + \frac{1}{n_B})}}$$

Table 5.1 Strains used in this study.

Strain	Genotype	Source
SMY1008	W303: pGAL-ZZ-TEV-6xHis-GFP-3XHA-GST-D6-DYN1-gsDHA	S. Reck-Peterson
SMY1045	W303: pGAL-ZZ-TEV-6xHis-GFP-3XHA-GST-D6-DYN1(+BSRS ΔMTBD)-gsDHA	this study
SMY1046	W303: pGAL-ZZ-TEV-6xHis-GFP-3XHA-GST-D6-DYN1(alpha-SRS ΔMTBD)-gsDHA	this study
SMY1047	W303: pGAL-ZZ-TEV-6xHis-GFP-3XHA-GST-D6-DYN1(-BSRS ΔMTBD)-gsDHA	this study
SMY1295	W303: pGAL-ZZ-TEV-6xHis-GFP-3XHA-GST-D6-DYN1-ΔMTBD-gsDHA	this study
SMY398	YEF473A: Gal1p:Num1CC[1-325]-stop Pac1-3mCherry Dyn1-3YFP mTurquoise2-Tub1	Lammers and Markus, 2015
SMY1715	YEF473A: GAL1p:Num1CC[1-325]-13myc dyn1(ΔMTBD)-SRSalpha-3YFP Pac1-3mCherry CFP-Tub1	this study
SMY1881	YEF473A: GAL1p:Num1CC[1-325]-13myc dyn1(ΔMTBD)-SRS+beta-3YFP Pac1-3mCherry CFP-Tub1	this study
SMY2025	YEF473A: Gal1p:Num1CC[1-325]-13myc TEF1-PH-dyn1(ΔMTBD)-SRSalpha-3YFP Pac1-3mCherry CFP-Tub1	this study
SMY2036	YEF473A: GAL1p:Num1CC[1-325]-13myc TEF1-PH-dyn1(ΔMTBD)-SRS+beta-3YFP Pac1-3mCherry CFP-Tub1	this study
SMY396	YEF473A: Dyn1-3YFP mTurquoise2-Tub1	this study
SMY769	YEF473A: dyn1[ΔMTBD]-3YFP mTurquoise2-Tub1	this study
SMY691	YEF473A: dyn1[ΔMTBD] mTurquoise2-Tub1 Pac1-3YFP	this study
SMY854	YEF473A: Pac1-3YFP mTurquoise-Tub1	this study

CHAPTER 6

FINAL DISCUSSION AND REMARKS

Dynein has a complex regulatory network to ensure it is spatially and temporally controlled for its important functions in mitosis. My dissertation explored the regulatory pathway that recruits and delivers dynein to the cell cortex where it is activated to generate forces on astral microtubules and position the mitotic spindle in budding yeast. In each chapter, I took a closer look at one aspect of the dynein pathway to understand how dynein switches from being inactive to active once it reaches its site of activity, the cortex.

Dynein is first targeted to the plus ends of astral microtubules emanating from the spindle poles by Ndl1/NudE and Pac1/Lis1 (Lee et al., 2003a; Li et al., 2005). Although Ndl1/NudE had been identified in this step, its role has not been well characterized. Chapter 3 determined that Ndl1/NudE may have two important roles: 1. To aid Pac1/Lis1 in dynein targeting to plus ends and 2. To compete for Pac1/Lis1 binding to dynein (Figure 6.1). Depending on the context, Ndl1/NudE may switch from being a 'helper' to a 'competitor' of Pac1/Lis1. In its first role, Ndl1/NudE enhances the efficacy of Pac1/Lis1-mediated targeting of dynein to plus ends. Loss of Ndl1/NudE reduces the amount of dynein recruited to plus ends, and subsequently the cortex, which causes spindle positioning defects (Chapter 3, Figure 3.1-3.2) (Li et al., 2005). This is important because in the cytoplasm, dynein samples an autoinhibitory state that precludes Pac1/Lis1 from binding (Marzo et al., 2019a; Zhang et al., 2017; Torisawa et al., 2014). Ndl1/NudE may function to recruit a high, local concentration of Pac1/Lis1 to be available when dynein opens its autoinhibitory state randomly (Figure 6.1). The second role may occur during dynein offloading to the cortex. In this step, dynein associates with dynactin that shares an overlapping binding site with Ndl1/NudE in the dynein tail domain (Stehman et al., 2007; McKenney et al., 2011). When Ndl1/NudE cannot interact with dynein (i.e. when dynactin is bound), it competes with dynein for

Pac1/Lis1 (Chapter 3, Figure 3.4-3.5), which suggests that it could participate in the mechanism of Pac1/Lis1 release during offloading.

The next steps in the pathway include dynein associating with its activating partner, dynactin, and being delivered to cortical receptor sites where the motor is active for spindle pulling (Sheeman et al., 2003; Lee et al., 2003a). Although dynactin is named for being an activating factor of dynein (DYNein ACTivator), yeast dynein does not move processively to minus ends of astral microtubules (Gill et al., 1991; Sheeman et al., 2003; Lee et al., 2003a). Similarly, human dynein can interact with plus end associated dynactin, but only moves toward the minus end in the presence of an adapter protein (Jha et al., 2017; McKenney et al., 2014; Schlager et al., 2014). With no known adapter-like proteins in yeast, we hypothesized that the cortical receptor Num1 may function to activate dynein motility with a similar mechanism. Chapter 2, which resulted in publication, discovered that Num1 is indeed sufficient to activate dynein-dynactin motility through two possible mechanisms (Lammers and Markus, 2015). The first being an adapter-like mechanism to create a stable dynein-dynactin complex. Interestingly, more evidence pointed to a second mechanism of activation resulting from the release of Pac1/Lis1 binding. These results were an exciting step in understanding how dynein switches from inactive to active.

To assess these mechanisms further in vitro, I purified intact dynactin complexes from yeast in Chapter 4. I determined that dynactin only interacts with dynein weakly on its own and has no effect on motility. This result supports the hypothesis that Num1 acts as an adapter, but contrasts published work by Kardon et al., 2009 that misidentified dynein-dynactin complexes due to errors in how the proteins were fluorescently labeled and imaged. After correcting these errors, I attempted to include the minimal dynein-interacting domain of Num1 ($Num1_{CC}$) in the motility assay to test its adapter-like qualities, but different experimental approaches will be required to fully answer this question.

Finally, I investigated the mechanism of Pac1/Lis1 release initiated by Num1 binding. I wondered if Num1 binding, in conjunction with dynein-dynactin engaging the microtubule could

cause Pac1/Lis1 dissociation. In Chapter 5, I determined that the conformational changes associated with microtubule binding affinity in the dynein motor domain dramatically affect Pac1/Lis1 interaction. Interestingly, restricting these structural changes did not completely prevent Num1 from releasing Pac1/Lis1 from dynein. I speculate that tension on the linker domain caused by Num1 binding may play a role in Pac1/Lis1 release and will require more investigation.

Overall, the work in this dissertation improves our comprehension of the dynein activation pathway. Based on the conclusions from my work combined with recently published data, the dynein activation model begins with Pac1/Lis1 and Ndl1/NudE association with autoinhibited dynein in the cytoplasm (Figure 6.1) (Marzo et al., 2019a; Qiu et al., 2019b; Elshenawy et al., 2019a; Htet et al., 2019). Once bound to Pac1/Lis1, open dynein is targeted to plus ends and associates unstably with dynactin (Lee et al., 2003a). From the plus end, dynein-dynactin is delivered to cortical Num1 sites that activate the complex. This activation occurs by Num1 forming a stable dynein-dynactin interaction and initiating the release of Pac1/Lis1 through three non-mutually exclusive mechanisms: Ndl1/NudE competition, the affinity state of the MTBD affect dynein structure in an unfavorable way to Pac1/Lis1 binding, or through Num1-mediated linker tension that also forces the structure to become unfavorable to Pac1/Lis1 (Figure 6.1).

Although my work elucidated important details of how dynein switches from inactive to active, many exciting questions remain. Looking at the first step in the pathway again, my results suggest that Pac1/Lis1 has a shared binding site for both Ndl1/NudE and dynein, but more in vivo experiments are needed to address the importance of this site. Does Ndl1/NudE recruit a high population of Pac1/Lis1 to autoinhibited dynein by interacting with dynein first? Can Ndl1/NudE interact with an autoinhibited dynein? What does the structure of the tri-partite complex look like? Is Ndl1/NudE truly involved in the mechanism of Pac1/Lis1 release? Next, it is still unknown exactly how dynactin affects dynein motility. Because yeast dynein is active in vitro, it is unclear what role dynactin plays in the cell. Does it allow dynein to generate more force? Is it only important to attach it to the cortex through Num1? In complex with Num1 can dynactin bind

multiple dyneins, allowing for higher velocity like in humans (Grotjahn et al., 2018; Urnavicius et al., 2018; Htet et al., 2019)? Does this allow more dyneins to bind at the cortex to generate enough force to move the spindle? Finally, the mechanism of Pac1/Lis1 release is also fascinating. Because of the distance between where Num1 and Pac1/Lis1 bind, the mechanism of release may be complex and unique. It is likely that structural changes are involved, but how Num1 facilitates this will be exciting and challenging to discover. To answer these questions, better purification strategies of dynactin and dynein will be key. In vivo studies are important to determine the relevance of in vitro findings, such as the role of Ndl1/NudE in Pac1/Lis1 competition, but in vitro and structural studies are powerful tools to discover the intricate details of these complex regulatory mechanisms.

Figure 6.1

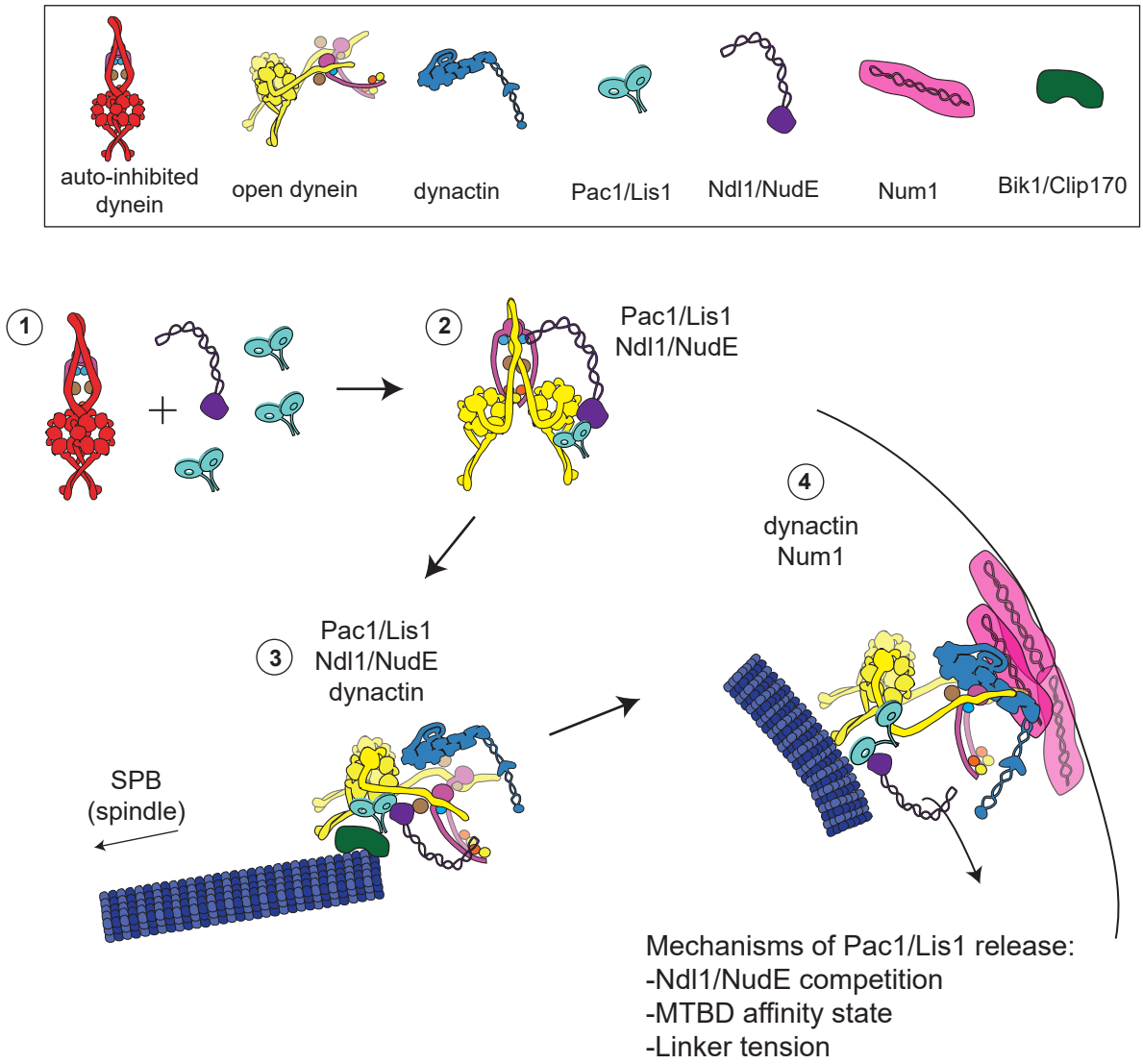

Figure 6.1. Final model of dynein activation for spindle positioning in budding yeast. (1) In the cytoplasm dynein exists in an autoinhibitory state. (2) Upon interaction with Ndl1/NudE, a high concentration of Pac1/Lis1 is recruited to dynein. Pac1/Lis1 binds the open conformation of the motor and prevents autoinhibition. (3) Pac1/Lis1 binding targets open dynein to astral microtubule plus ends where its activating partner, dynactin, interacts. (4) An active dynein-dynactin complex is not formed until interaction with cortical Num1 sites. At the time of dynein-dynactin binding to Num1, Pac1/Lis1 dissociates by three potential mechanisms: Ndl1/NudE competition, MTBD affinity state, and linker tension.

REFERENCES

Adames, N.R., and J.A. Cooper. 2000. Microtubule interactions with the cell cortex causing nuclear movements in Saccharomyces cerevisiae. *J Cell Biol*. 149:863–874.

Ananthanarayanan, V., M. Schattat, S.K. Vogel, A. Krull, N. Pavin, and I.M. Tolić-Nørrelykke. 2013. Dynein Motion Switches from Diffusive to Directed upon Cortical Anchoring. 153. Elsevier.

Baumbach, J., A. Murthy, M.A. Mcclintock, C.I. Dix, R. Zalyte, H.T. Hoang, and S.L. Bullock. 2017. Lissencephaly-1 is a context-dependent regulator of the human dynein complex. 1–31. doi:10.7554/eLife.21768.

Bhabha, G., H.C. Cheng, N. Zhang, A. Moeller, M. Liao, J.A. Speir, Y. Cheng, and R.D. Vale. 2014. Allosteric communication in the Dynein motor domain. *Cell*. 159:857–868. doi:10.1016/j.cell.2014.10.018.

Bhabha, G., G.T. Johnson, C.M. Schroeder, and R.D. Vale. 2015. How Dynein Moves Along Microtubules. *Trends Biochem. Sci.* 41:94–105. doi:10.1016/j.tibs.2015.11.004.

Bi, E., and J.R. Pringle. 1996. ZDS1 and ZDS2, genes whose products may regulate Cdc42p in Saccharomyces cerevisiae. *Mol Cell Biol*. 16:5264–5275.

Bradshaw, N.J., W. Hennah, and D.C. Soares. 2013. NDE1 and NDEL1: twin neurodevelopmental proteins with similar “nature” but different “nurture”. *Biomol. Concepts*. 4:447–464. doi:10.1515/bmc-2013-0023.

Carter, A.P., C. Cho, L. Jin, and R.D. Vale. 2011. Crystal structure of the dynein motor domain. *Science (80-.).* 331:1159–1165. doi:10.1126/science.1202393.

Carter, A.P., J.E. Garbarino, E.M. Wilson-Kubalek, W.E. Shipley, C. Cho, R.A. Milligan, R.D. Vale, and I.R. Gibbons. 2008. Structure and functional role of dynein’s microtubule-binding domain. *Science (80-.).* 322:1691–1695. doi:10.1126/science.1164424.

Carvalho, P., M.L. Gupta Jr., M.A. Hoyt, and D. Pellman. 2004. Cell cycle control of kinesin-mediated transport of Bik1 (CLIP-170) regulates microtubule stability and dynein activation. *Dev Cell*. 6:815–829. doi:10.1016/j.devcel.2004.05.001S1534580704001625.

Cho, C., S.L. Reck-Peterson, and R.D. Vale. 2008. Regulatory ATPase sites of cytoplasmic dynein affect processivity and force generation. *J Biol Chem*. 283:25839–25845. doi:M802951200.

Chowdhury, S., S.A. Ketcham, T.A. Schroer, and G.C. Lander. 2015. Structural organization of the dynein-dynactin complex bound to microtubules. *Nat. Struct. Mol. Biol.* 22:345–347. doi:10.1038/nsmb.2996.

Cicalese, A., G. Bonizzi, C.E. Pasi, M. Faretta, S. Ronzoni, B. Giulini, C. Brisken, S. Minucci, P.P. Di Fiore, and P.G. Pelicci. 2009. The tumor suppressor p53 regulates polarity of self-renewing divisions in mammary stem cells. *Cell*. 138:1083–1095. doi:10.1016/j.cell.2009.06.048.

Clark, S.W., and M.D. Rose. 2006. Arp10p is a pointed-end-associated component of yeast dynactin. *Mol Biol Cell*. 17:738–748. doi:E05-05-0449.

Derr, N.D., B.S. Goodman, R. Jungmann, A.E. Leschziner, W.M. Shih, and S.L. Reck-Peterson. 2012. Tug-of-war in motor protein ensembles revealed with a programmable DNA origami scaffold. *Science*. 338:662–665. doi:10.1126/science.1226734.

DeSantis, M.E., M.A. Cianfrocco, Z.M. Htet, P.T. Tran, S.L. Reck-Peterson, and A.E. Leschziner. 2017. Lis1 Has Two Opposing Modes of Regulating Cytoplasmic Dynein. *Cell*. 170:1197-1208.e12. doi:10.1016/j.cell.2017.08.037.

DeWitt, M.A., C.A. Cypranowska, F.B. Cleary, V. Belyy, and A. Yildiz. 2015. The AAA3 domain of cytoplasmic dynein acts as a switch to facilitate microtubule release. *Nat Struct Mol Biol*. 22:73–79. doi:10.1038/nsmb.2930.

Dilsaver, M. 2019. The regulation of cytoplasmic dynein. Colorado State University.
Dix, C.I., H.C. Soundararajan, N.S. Dzhindzhev, F. Begum, B. Suter, H. Ohkura, E. Stephens, and S.L. Bullock. 2013. Lissencephaly-1 promotes the recruitment of dynein and dynactin to transported mRNAs. *J. Cell Biol.* 202:479–494. doi:10.1083/jcb.201211052.
Duellberg, C., M. Trokter, R. Jha, I. Sen, M.O. Steinmetz, and T. Surrey. 2014. Reconstitution of a hierarchical +TIP interaction network controlling microtubule end tracking of dynein.
Ecklund, K.H., T. Morisaki, L.G. Lammers, M.G. Marzo, T.J. Stasevich, and S.M. Markus. 2017. She1 affects dynein through direct interactions with the microtubule and the dynein microtubule-binding domain. *Nat. Commun.* 8. doi:10.1038/s41467-017-02004-2.
Efimov, V.P. 2003. Roles of NUDE and NUDF proteins of Aspergillus nidulans: insights from intracellular localization and overexpression effects. *Mol Biol Cell*. 14:871–888. doi:10.1091/mbc.E02-06-0359.
Efimov, V.P., and N.R. Morris. 2000. The LIS1-related NUDF protein of Aspergillus nidulans interacts with the coiled-coil domain of the NUDE/RO11 protein. *J. Cell Biol.* 150:681–688. doi:10.1083/jcb.150.3.681.
Egan, M.J., K. Tan, and S.L. Reck-Peterson. 2012. Lis1 is an initiation factor for dynein-driven organelle transport. *J. Cell Biol.* 197:971–982. doi:10.1083/jcb.201112101.
Elshenawy, M.M., J.T. Canty, L. Oster, L.S. Ferro, Z. Zhou, S.C. Blanchard, and A. Yildiz. 2019a. Cargo adaptors regulate stepping and force generation of mammalian dynein–dynactin. *Nat. Chem. Biol.* 15:1093–1101. doi:10.1038/s41589-019-0352-0.
Elshenawy, M.M., E. Kusakci, S. Volz, J. Baumbach, and S.L. Bullock. 2019b. Lis1 activates dynein motility by pairing it with dynactin. 1–23.
Feng, Y., E.C. Olson, P.T. Stukenberg, L.A. Flanagan, M.W. Kirschner, and C.A. Walsh. 2000. LIS1 regulates CNS lamination by interacting with mNudE, a central component of the centrosome. *Neuron*. 28:665–679. doi:10.1016/s0896-6273(00)00145-8.
Gama, J.B., C. Pereira, P.A. Simões, R. Celestino, R.M. Reis, D.J. Barbosa, H.R. Pires, C. Carvalho, J. Amorim, A.X. Carvalho, and D.K. Cheerambathur. 2017. Molecular mechanism of dynein recruitment to kinetochores by the Rod – Zw10 – Zwilch complex and Spindly. 216.
Gibbons, I.R., J.E. Garbarino, C.E. Tan, S.L. Reck-Peterson, R.D. Vale, and A.P. Carter. 2005. The affinity of the dynein microtubule-binding domain is modulated by the conformation of its coiled-coil stalk. *J Biol Chem*. 280:23960–23965. doi:10.1074/jbc.M501636200.
Gibbons, I.R., and A.J. Rowe. 1965. Dynein : A Protein with Adenosine Triphosphatase Activity from Cilia. 149:424–426.
Gibson, D.G., L. Young, R.Y. Chuang, J.C. Venter, C.A. Hutchison 3rd, and H.O. Smith. 2009. Enzymatic assembly of DNA molecules up to several hundred kilobases. *Nat Methods*. 6:343–345. doi:10.1038/nmeth.1318.
Gill, S.R., T.A. Schroer, I. Szilak, E.R. Steuer, M.P. Sheetz, and D.W. Cleveland. 1991. Dynactin, a conserved, ubiquitously expressed component of an activator of vesicle motility mediated by cytoplasmic dynein. *J. Cell Biol.* 115:1639–1650. doi:10.1083/jcb.115.6.1639.
Gray, M., M. Kupiec, and S.M. Honigberg. 2004a. Site-specific genomic (SSG) and random domain-localized (RDL) mutagenesis in yeast.
Gray, M., M. Kupiec, and S.M. Honigberg. 2004b. Site-specific genomic (SSG) and random domain-localized (RDL) mutagenesis in yeast. *BMC Biotechnol*. 4:7. doi:10.1186/1472-6750-4-71472-6750-4-7.
Grotjahn, D.A., S. Chowdhury, Y. Xu, R.J. Mckenney, T.A. Schroer, and G.C. Lander. 2018. Cryo-electron tomography reveals that dynactin recruits a team of dyneins for processive motility. *Nat. Struct. Mol. Biol.* 25:203–207.
Guan, K.L., and J.E. Dixon. 1991. Eukaryotic proteins expressed in Escherichia coli: an improved thrombin cleavage and purification procedure of fusion proteins with glutathione S-transferase. *Anal. Biochem.* 192:262–267. doi:10.1016/0003-2697(91)90534-z.

Guntas, G., R.A. Hallett, S.P. Zimmerman, T. Williams, H. Yumerefendi, J.E. Bear, and B. Kuhlman. 2015. Engineering an improved light-induced dimer (iLID) for controlling the localization and activity of signaling proteins. *Proc. Natl. Acad. Sci.* 112:112 LP – 117. doi:10.1073/pnas.1417910112.

Gutierrez, P.A., B.E. Ackermann, M. Vershinin, and R.J. McKenney. 2017. Differential effects of the dynein-regulatory factor Lissencephaly-1 on processive dynein-dynactin motility. *J. Biol. Chem.* 292:12245–12255. doi:10.1074/jbc.M117.790048.

Htet, Z.M., J.P. Gillies, R.W. Baker, and A.E. Leschziner. 2019. Lis1 promotes the formation of maximally activated cytoplasmic dynein-1 complexes. 1–30.

Huang, J., A.J. Roberts, A.E. Leschziner, and S.L. Reck-Peterson. 2012. Lis1 acts as a “clutch” between the ATPase and microtubule-binding domains of the dynein motor. *Cell*. 150:975–986. doi:10.1016/j.cell.2012.07.022.

Imamula, K., T. Kon, R. Ohkura, and K. Sutoh. 2007. The coordination of cyclic microtubule association/dissociation and tail swing of cytoplasmic dynein. *Proc. Natl. Acad. Sci. U. S. A.* 104:16134–16139. doi:10.1073/pnas.0702370104.

Jha, R., J. Roostalu, M. Trokter, and T. Surrey. 2017. Combinatorial regulation of the balance between dynein microtubule end accumulation and initiation of directed motility.

Kardon, J.R., S.L. Reck-Peterson, and R.D. Vale. 2009. Regulation of the processivity and intracellular localization of Saccharomyces cerevisiae dynein by dynactin. *Proc Natl Acad Sci U S A*. 106:5669–5674. doi:0900976106.

King, S.J., C.L. Brown, K.C. Maier, N.J. Quintyne, and T.A. Schroer. 2003. Analysis of the dynein-dynactin interaction in vitro and in vivo. *Mol Biol Cell*. 14:5089–5097. doi:10.1091/mbc.E03-01-0025E03-01-0025.

Klinman, E., and E.L.F. Holzbaur. 2015. Stress-Induced CDK5 Activation Disrupts Axonal Transport via Lis1/Ndel1/Dynein. *Cell Rep*. 12:462–473. doi:10.1016/j.celrep.2015.06.032.

Knop, M., K. Siegers, G. Pereira, W. Zachariae, B. Winsor, K. Nasmyth, and E. Schiebel. 1999a. Epitope tagging of yeast genes using a PCR-based strategy: more tags and improved practical routines. *Yeast*. 15:963–972. doi:10.1002/(SICI)1097-0061(199907)15:10B<963::AID-YEA399>3.0.CO;2-W.

Knop, M., K. Siegers, G. Pereira, W. Zachariae, B. Winsor, K. Nasmyth, and E. Schiebel. 1999b. Epitope tagging of yeast genes using a PCR-based strategy: more tags and improved practical routines.

Kon, T., K. Imamula, A.J. Roberts, R. Ohkura, P.J. Knight, I.R. Gibbons, S.A. Burgess, and K. Sutoh. 2009. Helix sliding in the stalk coiled coil of dynein couples ATPase and microtubule binding. *Nat Struct Mol Biol*. 16:325–333. doi:nsmb.1555.

Kon, T., M. Nishiura, R. Ohkura, Y.Y. Toyoshima, and K. Sutoh. 2004. Distinct Functions of Nucleotide-Binding / Hydrolysis Sites in the Four AAA Modules of Cytoplasmic Dynein †. *Construction*. 4:11266–11274.

Kon, T., T. Oyama, R. Shimo-Kon, K. Imamula, T. Shima, K. Sutoh, and G. Kurisu. 2012. The 2.8 Å crystal structure of the dynein motor domain. Nature Publishing Group.

Kushnirov, V. V. 2000. Rapid and reliable protein extraction from yeast. *Yeast*. 16:857–860. doi:10.1002/1097-0061(20000630)16:9<857::AID-YEA561>3.0.CO;2-B.

Lammers, L.G., and S.M. Markus. 2015. The dynein cortical anchor Num1 activates dynein motility by relieving Pac1/LIS1-mediated inhibition. *J. Cell Biol.* 1–14. doi:10.1083/jcb.201506119.

Lee, W.L., M.A. Kaiser, and J.A. Cooper. 2005. The offloading model for dynein function: differential function of motor subunits. *J Cell Biol*. 168:201–207. doi:jcb.200407036.

Lee, W.L., J.R. Oberle, and J. a. Cooper. 2003a. The role of the lissencephaly protein Pac1 during nuclear migration in budding yeast. *J. Cell Biol.* 160:355–364. doi:10.1083/jcb.200209022.

Lee, W.L., J.R. Oberle, and J.A. Cooper. 2003b. The role of the lissencephaly protein Pac1

during nuclear migration in budding yeast. *J Cell Biol*. 160:355–364. doi:10.1083/jcb.200209022jcb.200209022.
Lenz, J.H., I. Schuchardt, A. Straube, and G. Steinberg. 2006. A dynein loading zone for retrograde endosome motility at microtubule plus-ends.
Li, J., W.L. Lee, and J.A. Cooper. 2005. NudEL targets dynein to microtubule ends through LIS1. *Nat Cell Biol*. 7:686–690. doi:ncb1273.
Liang, Y., W. Yu, Y. Li, Z. Yang, X. Yan, Q. Huang, and X. Zhu. 2004. Nudel functions in membrane traffic mainly through association with Lis1 and cytoplasmic dynein. *J. Cell Biol.* 164:557–566. doi:10.1083/jcb.200308058.
Lin, J., K. Okada, M. Raytchev, M.C. Smith, and D. Nicastro. 2014. Structural mechanism of the dynein power stroke. *Nat. Cell Biol.* 16:479–485. doi:10.1038/ncb2939.
Longtine, M.S., A. McKenzie 3rd, D.J. Demarini, N.G. Shah, A. Wach, A. Brachat, P. Philippsen, and J.R. Pringle. 1998a. Additional modules for versatile and economical PCR-based gene deletion and modification in Saccharomyces cerevisiae. *Yeast*. 14:953–961. doi:10.1002/(SICI)1097-0061(199807)14:10<953::AID-YEA293>3.0.CO;2-U.
Longtine, M.S., A. McKenzie, D.J. Demarini, N.G. Shah, A. Wach, A. Brachat, P. Philippsen, and J.R. Pringle. 1998b. Additional modules for versatile and economical PCR-based gene deletion and modification in Saccharomyces cerevisiae.
Markus, S.M., K.A. Kalutkiewicz, and W.L. Lee. 2012. She1-mediated inhibition of dynein motility along astral microtubules promotes polarized spindle movements. *Curr Biol*. 22:2221–2230. doi:10.1016/j.cub.2012.10.017.
Markus, S.M., and W.L. Lee. 2011. Regulated offloading of cytoplasmic dynein from microtubule plus ends to the cortex. *Dev Cell*. 20:639–651. doi:10.1016/j.devcel.2011.04.011.
Markus, S.M., S. Omer, K. Baranowski, and W.-L. Lee. 2015. Improved Plasmids for Fluorescent Protein Tagging of Microtubules in Saccharomyces cerevisiae. *Traffic*. 16:773–786. doi:10.1111/tra.12276.
Markus, S.M., K.M. Plevock, B.J. St Germain, J.J. Punch, C.W. Meaden, and W.L. Lee. 2011. Quantitative analysis of Pac1/LIS1-mediated dynein targeting: Implications for regulation of dynein activity in budding yeast. *Cytoskelet.* 68:157–174. doi:10.1002/cm.20502.
Markus, S.M., J.J. Punch, and W.L. Lee. 2009. Motor- and tail-dependent targeting of dynein to microtubule plus ends and the cell cortex. *Curr Biol*. 19:196–205. doi:S0960-9822(09)00540-5 [pii]10.1016/j.cub.2008.12.047.
Marzo, M.G., J.M. Griswold, and S.M. Markus. 2019a. Pac1 / LIS1 promotes an uninhibited conformation of dynein that coordinates its localization and activity. 1–55.
Marzo, M.G., J.M. Griswold, K.M. Ruff, R.E. Buchmeier, C.P. Fees, S.M. Markus, and S.M. Markus. 2019b. Molecular basis for dyneinopathies reveals insight into dynein regulation and dysfunction.
Matanis, T., A. Akhmanova, P. Wulf, E. Del Nery, T. Weide, T. Stepanova, N. Galjart, F. Grosveld, B. Goud, C.I. De Zeeuw, A. Barnekow, and C.C. Hoogenraad. 2002. Bicaudal-D regulates COPI-independent Golgi-ER transport by recruiting the dynein-dynactin motor complex. *Nat Cell Biol*. 4:986–992. doi:10.1038/ncb891.
McKenney, R.J., W. Huynh, M.E. Tanenbaum, G. Bhabha, and R.D. Vale. 2014. Activation of cytoplasmic dynein motility by dynactin-cargo adapter complexes. *Science (80-.).* 345:337–341. doi:10.1126/science.1254198.
McKenney, R.J., M. Vershinin, A. Kunwar, R.B. Vallee, and S.P. Gross. 2010. LIS1 and NudE induce a persistent dynein force-producing state. *Cell*. 141:304–314. doi:S0092-8674(10)00188-1.
McKenney, R.J., S.J. Weil, J. Scherer, and R.B. Vallee. 2011. Mutually exclusive cytoplasmic dynein regulation by NudE-Lis1 and dynactin. *J. Biol. Chem.* 286:39615–39622. doi:10.1074/jbc.M111.289017.
Miura, M., A. Matsubara, T. Kobayashi, M. Edamatsu, and Y.Y. Toyoshima. 2010. Nucleotide-

dependent behavior of single molecules of cytoplasmic dynein on microtubules in vitro. *FEBS Lett.* 584:2351–2355. doi:10.1016/j.febslet.2010.04.016.
Mogami, T., T. Kon, K. Ito, and K. Sutoh. 2007. Kinetic characterization of tail swing steps in the ATPase cycle of Dictyostelium cytoplasmic dynein. *J. Biol. Chem.* 282:21639–21644. doi:10.1074/jbc.M701914200.
Moore, J.K., J. Li, and J.A. Cooper. 2008. Dynactin function in mitotic spindle positioning. *Traffic*. 9:510–527. doi:TRA710.
Moore, J.K., D. Sept, and J.A. Cooper. 2009. Neurodegeneration mutations in dynactin impair dynein-dependent nuclear migration. *Proc Natl Acad Sci U S A*. 106:5147–5152. doi:0810828106.
Moughamian, A.J., G.E. Osborn, J.E. Lazarus, S. Maday, and E.L.F. Holzbaur. 2013. Ordered Recruitment of Dynactin to the Microtubule Plus-End is Required for Efficient Initiation of Retrograde Axonal Transport.
Nicholas, M.P., F. Berger, L. Rao, S. Brenner, C. Cho, and A. Gennerich. 2015. Cytoplasmic dynein regulates its attachment to microtubules via nucleotide state-switched mechanosensing at multiple AAA domains. *Proc. Natl. Acad. Sci. U. S. A.* 112:6371–6376. doi:10.1073/pnas.1417422112.
Niethammer, M., D.S. Smith, R. Ayala, J. Peng, J. Ko, M.S. Lee, M. Morabito, and L.H. Tsai. 2000. NUDEL is a novel Cdk5 substrate that associates with LIS1 and cytoplasmic dynein. *Neuron*. 28:697–711. doi:10.1016/s0896-6273(00)00147-1.
Nishikawa, Y., T. Oyama, N. Kamiya, T. Kon, Y.Y. Toyoshima, H. Nakamura, and G. Kurisu. 2014. Structure of the entire stalk region of the Dynein motor domain. *J. Mol. Biol.* 426:3232–3245. doi:10.1016/j.jmb.2014.06.023.
Noatynska, A., M. Gotta, and P. Meraldi. 2012. Mitotic spindle (DIS)orientation and DISease: Cause or consequence? 199.
Okumura, M., T. Natsume, and M.T. Kanemaki. 2018. Dynein – Dynactin – NuMA clusters generate cortical spindle-pulling forces as a multi- arm ensemble. 1–24.
Olenick, M.A., and E.L.F. Holzbaur. 2019. Dynein activators and adaptors at a glance. 1–7. doi:10.1242/jcs.227132.
Pandey, J.P., and D.S. Smith. 2011. A Cdk5-Dependent Switch Regulates Lis1 / Ndel1 / Dynein-Driven Organelle Transport in Adult Axons. 31:17207–17219. doi:10.1523/JNEUROSCI.4108-11.2011.
Paschal, B.M., H.S. Shpetner, and R.B. Vallee. 1987. MAP 1C is a microtubule-activated ATPase which translocates microtubules in vitro and has dynein-like properties. *J Cell Biol*. 105:1273–1282.
Qiu, R., J. Zhang, and X. Xiang. 2019a. Insights into LIS1 function in cargo-adapter-mediated dynein activation. *preprint*. 1:1–41.
Qiu, R., J. Zhang, and X. Xiang. 2019b. LIS1 regulates cargo-adapter–mediated activation of dynein by overcoming its autoinhibition in vivo. *J. Cell Biol.* 218:3630 LP – 3646. doi:10.1083/jcb.201905178.
Raaijmakers, J.A., and R.H. Medema. 2014. Function and regulation of dynein in mitotic chromosome segregation. *Chromosoma*. 123:407–422. doi:10.1007/s00412-014-0468-7.
Raaijmakers, J.A., M.E. Tanenbaum, and R.H. Medema. 2013. Systematic dissection of dynein regulators in mitosis.
Ralser, M., H. Kuhl, M. Ralser, M. Werber, H. Lehrach, M. Breitenbach, and B. Timmermann. 2012. The Saccharomyces cerevisiae W303-K6001 cross-platform genome sequence: insights into ancestry and physiology of a laboratory mutt. *Open Biol.* 2:120093. doi:10.1098/rsob.120093.
Rao, L., F. Berger, M.P. Nicholas, and A. Gennerich. 2019. Molecular mechanism of cytoplasmic dynein tension sensing. *Nat. Commun.* 10. doi:10.1038/s41467-019-11231-8.
Reck-Peterson, S.L., A. Yildiz, A.P. Carter, A. Gennerich, N. Zhang, and R.D. Vale. 2006.

Single-molecule analysis of dynein processivity and stepping behavior. *Cell*. 126:335–348. doi:S0092-8674(06)00862-2.
Reddy, B.J.N., M. Mattson, C.L. Wynne, O. Vadpey, A. Durra, D. Chapman, R.B. Vallee, and S.P. Gross. 2016. Load-induced enhancement of Dynein force production by LIS1–NudE in vivo and in vitro. *Nat. Commun.* 7:12259. doi:10.1038/ncomms12259.
Redwine, W.B., R. Hernandez-Lopez, S. Zou, J. Huang, S.L. Reck-Peterson, and A.E. Leschziner. 2012. Structural basis for microtubule binding and release by dynein. *Science (80-.).* 337:1532–1536. doi:10.1126/science.1224151.
Reiner, O., R. Carrozzo, Y. Shen, M. Wehnert, F. Faustinella, W.B. Dobyns, C.T. Caskey, and D.H. Ledbetter. 1993. Isolation of a Miller-Dieker lissencephaly gene containing G protein beta-subunit-like repeats. *Nature*. 364:717–721. doi:10.1038/364717a0.
Roberts, A.J., B.S. Goodman, and S.L. Reck-Peterson. 2014a. Reconstitution of dynein transport to the microtubule plus end by kinesin. *Elife*. 3:e02641. doi:10.7554/eLife.02641.
Roberts, A.J., B.S. Goodman, and S.L. Reck-Peterson. 2014b. Reconstitution of dynein transport to the microtubule plus end by kinesin. *Elife*. 3:e02641. doi:10.7554/eLife.02641.
Roberts, A.J., B. Malkova, M.L. Walker, H. Sakakibara, N. Numata, T. Kon, R. Ohkura, T.A. Edwards, P.J. Knight, K. Sutoh, K. Oiwa, and S.A. Burgess. 2012. ATP-Driven Remodeling of the Linker Domain in the Dynein Motor.
Roberts, A.J., N. Numata, M.L. Walker, Y.S. Kato, B. Malkova, T. Kon, R. Ohkura, F. Arisaka, P.J. Knight, K. Sutoh, and S.A. Burgess. 2009. AAA+ Ring and linker swing mechanism in the dynein motor. *Cell*. 136:485–495. doi:S0092-8674(08)01600-0.
Samora, C.P., B. Mogessie, L. Conway, J.L. Ross, A. Straube, and A.D. McAinsh. 2011. MAP4 and CLASP1 operate as a safety mechanism to maintain a stable spindle position in mitosis.
Sasaki, S., D. Mori, K. Toyo-oka, A. Chen, L. Garrett-Beal, M. Muramatsu, S. Miyagawa, N. Hiraiwa, A. Yoshiki, A. Wynshaw-Boris, and S. Hirotsune. 2005. Complete loss of Ndel1 results in neuronal migration defects and early embryonic lethality. *Mol. Cell. Biol.* 25:7812–7827. doi:10.1128/MCB.25.17.7812-7827.2005.
Sasaki, S., A. Shionoya, M. Ishida, M.J. Gambello, J. Yingling, A. Wynshaw-Boris, and S. Hirotsune. 2000. A LIS1/NUDEL/Cytoplasmic Dynein Heavy Chain Complex in the Developing and Adult Nervous System.
Schlager, M.A., H.T. Hoang, L. Urnavicius, S.L. Bullock, and A.P. Carter. 2014. In vitro reconstitution of a highly processive recombinant human dynein complex.
Schmidt, H. 2015. Dynein motors: How AAA+ ring opening and closing coordinates microtubule binding and linker movement. *Bioessays*. 37:532–543. doi:10.1002/bies.201400215.
Schmidt, H., and A.P. Carter. 2016. Review Structure and Mechanism of the Dynein Motor ATPase. 105:557–567. doi:10.1002/bip.22856.
Schmidt, H., E.S. Gleave, and A.P. Carter. 2012. Insights into dynein motor domain function from a 3.3-Å crystal structure.
Schmidt, H., R. Zalyte, L. Urnavicius, and A.P. Carter. 2014. Structure of human cytoplasmic dynein-2 primed for its power stroke. *Nature*. doi:10.1038/nature14023.
Schmidt, H., R. Zalyte, L. Urnavicius, and A.P. Carter. 2015. Structure of human cytoplasmic dynein-2 primed for its power stroke. *Nature*. 518:435–438. doi:10.1038/nature14023.
Schroeder, C.M., and R.D. Vale. 2016. Assembly and activation of dynein–dynactin by the cargo adaptor protein Hook3. *J. Cell Biol.* 214:309 LP – 318. doi:10.1083/jcb.201604002.
Schroer, T.A. 2004. Dynactin. doi:10.1146/annurev.cellbio.20.012103.094623.
Schroer, T.A., and M.P. Sheetz. 1991. Two activators of microtubule-based vesicle transport. *J. Cell Biol.* 115:1309–1318. doi:10.1083/jcb.115.5.1309.
Schuyler, S.C., and D. Pellman. 2001. Search, capture and signal: games microtubules and centrosomes play. *J Cell Sci*. 114:247–255.
Sheeman, B., P. Carvalho, I. Sagot, J. Geiser, D. Kho, M.A. Hoyt, and D. Pellman. 2003.

Determinants of S. cerevisiae dynein localization and activation: implications for the mechanism of spindle positioning. *Curr Biol*. 13:364–372. doi:S0960982203000137 [pii].
Siglin, A.E., S. Sun, J.K. Moore, S. Tan, M. Poenie, J.D. Lear, T. Polenova, J.A. Cooper, and J.C. Williams. 2013. Dynein and Dynactin Leverage Their Bivalent Character to Form a High-Affinity Interaction.
Sikorski, R.S., and P. Hieter. 1989. A system of shuttle vectors and yeast host strains designed for efficient manipulation of DNA in Saccharomyces cerevisiae. *Genetics*. 122:19–27.
Silvanovich, A., M. Li, M. Serr, S. Mische, and T.S. Hays. 2003. The Third P-loop Domain in Cytoplasmic Dynein Heavy Chain Is Essential for Dynein Motor Function and ATP-sensitive Microtubule Binding.
Splinter, D., D.S. Razafsky, M.A. Schlager, A. Serra-Marques, I. Grigoriev, J. Demmers, N. Keijzer, K. Jiang, I. Poser, A.A. Hyman, C.C. Hoogenraad, S.J. King, and A. Akhmanova. 2012. BICD2, dynactin, and LIS1 cooperate in regulating dynein recruitment to cellular structures.
Stehman, S.A., Y. Chen, R.J. Mckenney, and R.B. Vallee. 2007. NudE and NudEL are required for mitotic progression and are involved in dynein recruitment to kinetochores. 178:583–594. doi:10.1083/jcb.200610112.
Tang, X., B.S. Germain, and W.L. Lee. 2012. A novel patch assembly domain in Num1 mediates dynein anchoring at the cortex during spindle positioning. *J Cell Biol*. 196:743–756. doi:10.1083/jcb.201112017.
Torisawa, T., M. Ichikawa, A. Furuta, K. Saito, K. Oiwa, H. Kojima, Y.Y. Toyoshima, and K. Furuta. 2014. Autoinhibition and cooperative activation mechanisms of cytoplasmic dynein.
Torisawa, T., A. Nakayama, K. Furuta, M. Yamada, S. Hirotsune, and Y.Y. Toyoshima. 2011. Functional dissection of LIS1 and NDEL1 towards understanding the molecular mechanism of cytoplasmic dynein regulation. *J Biol Chem*. 286:1959–1965. doi:M110.169847.
Toropova, K., M. Mladenov, and A.J. Roberts. 2017. Intraflagellar transport dynein is autoinhibited by trapping of its mechanical and track-binding elements. *Nat. Publ. Gr.* 24:461–468. doi:10.1038/nsmb.3391.
Toropova, K., S. Zou, A.J. Roberts, W.B. Redwine, B.S. Goodman, S.L. Reck-Peterson, and A.E. Leschziner. 2014. Lis1 regulates dynein by sterically blocking its mechanochemical cycle. *Elife*. 3. doi:10.7554/eLife.03372.
Urnavicius, L., C.K. Lau, M.M. Elshenawy, E. Morales-Rios, C. Motz, A. Yildiz, and A.P. Carter. 2018. Cryo-EM shows how dynactin recruits two dyneins for faster movement. *Nature*. 554:202–206. doi:10.1038/nature25462.
Urnavicius, L., K. Zhang, A.G. Diamant, C. Motz, M.A. Schlager, M. Yu, N.A. Patel, C. V Robinson, and A.P. Carter. 2015. The structure of the dynactin complex and its interaction with dynein. *Science (80-.).* 347:1441–1446. doi:10.1126/science.aaa4080.
Vale, R.D., and R.A. Milligan. 2000. The way things move: looking under the hood of molecular motor proteins. *Science*. 288:88–95. doi:10.1126/science.288.5463.88.
Vaughan, K.T., and R.B. Vallee. 1995. Cytoplasmic dynein binds dynactin through a direct interaction between the intermediate chains and p150Glued. *J Cell Biol*. 131:1507–1516.
Vicente, J.J., and L. Wordeman. 2015. Mitosis, microtubule dynamics and the evolution of kinesins. *Exp. Cell Res.* 334:61–69. doi:10.1016/J.YEXCR.2015.02.010.
Wang, S., S. a Ketcham, A. Schön, B. Goodman, Y. Wang, W. Bement, J. Yates, E. Freire, T. a Schroer, and Y. Zheng. 2013. Nudel/NudE and Lis1 promote dynein and dynactin interaction in the context of spindle morphogenesis. *Mol. Biol. Cell*. 24:3522–33. doi:10.1091/mbc.E13-05-0283.
Wang, S., and Y. Zheng. 2011. Identification of a novel dynein binding domain in nudel essential for spindle pole organization in Xenopus egg extract. *J. Biol. Chem.* 286:587–593. doi:10.1074/jbc.M110.181578.
Waterman-Storer, C.M., S. Karki, and E.L. Holzbaur. 1995. The p150Glued component of the

dynactin complex binds to both microtubules and the actin-related protein centractin (Arp-1). *Proc. Natl. Acad. Sci.* 92:1634 LP – 1638. doi:10.1073/pnas.92.5.1634.
Williams, S.E., S. Beronja, H.A. Pasolli, and E. Fuchs. 2011. Asymmetric cell divisions promote Notch-dependent epidermal differentiation. *Nature*. doi:10.1038/nature09793.
Woodruff, J.B., D.G. Drubin, and G. Barnes. 2009. Dynein-driven mitotic spindle positioning restricted to anaphase by She1p inhibition of dynactin recruitment. *Mol Biol Cell*. 20:3003–3011. doi:E09-03-0186.
Wynshaw-Boris, A., T. Pramparo, Y.H. Youn, and S. Hirotsune. 2010. Lissencephaly: mechanistic insights from animal models and potential therapeutic strategies. *Semin. Cell Dev. Biol.* 21:823–830. doi:10.1016/j.semcdb.2010.07.008.
Yamada, M., S. Toba, Y. Yoshida, K. Haratani, D. Mori, Y. Yano, Y. Mimori-Kiyosue, T. Nakamura, K. Itoh, S. Fushiki, M. Setou, A. Wynshaw-Boris, T. Torisawa, Y.Y. Toyoshima, and S. Hirotsune. 2008. LIS1 and NDEL1 coordinate the plus-end-directed transport of cytoplasmic dynein. *EMBO J.* 27:2471–2483. doi:emboj2008182.
Yan, S., H. Zhang, G. Hou, S. Ahmed, J.C. Williams, and T. Polenova. 2015. Internal Dynamics of Dynactin CAP-Gly Is Regulated by Microtubules and Plus End Tracking Protein EB1 *. 290:1607–1622. doi:10.1074/jbc.M114.603118.
Yi, J.Y., K.M. Ori-Mckenney, R.J. Mckenney, M. Vershinin, S.P. Gross, and R.B. Vallee. 2011. High-resolution imaging reveals indirect coordination of opposite motors and a role for LIS1 in high-load axonal transport.
Yingling, J., Y. Youn, D. Darling, K. Toyooka, T. Pramparo, S. Hirotsune, and A. Wynshawboris. 2008. Neuroepithelial Stem Cell Proliferation Requires LIS1 for Precise Spindle Orientation and Symmetric Division.
Zhai, Y., D. Zhang, L. Yu, F. Sun, and F. Sun. 2019. SmartBac, a new baculovirus system for large protein complex production. *J. Struct. Biol. X*. 1:100003. doi:https://doi.org/10.1016/j.yjsbx.2019.100003.
Zhang, K., H.E. Foster, A. Rondelet, S.E. Lacey, N. Bahi-Buisson, A.W. Bird, and A.P. Carter. 2017. Cryo-EM Reveals How Human Cytoplasmic Dynein Is Auto-inhibited and Activated. *Cell*. 169:1303-1314.e18. doi:10.1016/j.cell.2017.05.025.

APPENDIX 1

SUPPLEMENTARY FIGURES FOR CHAPTER 2

Figure S1.1

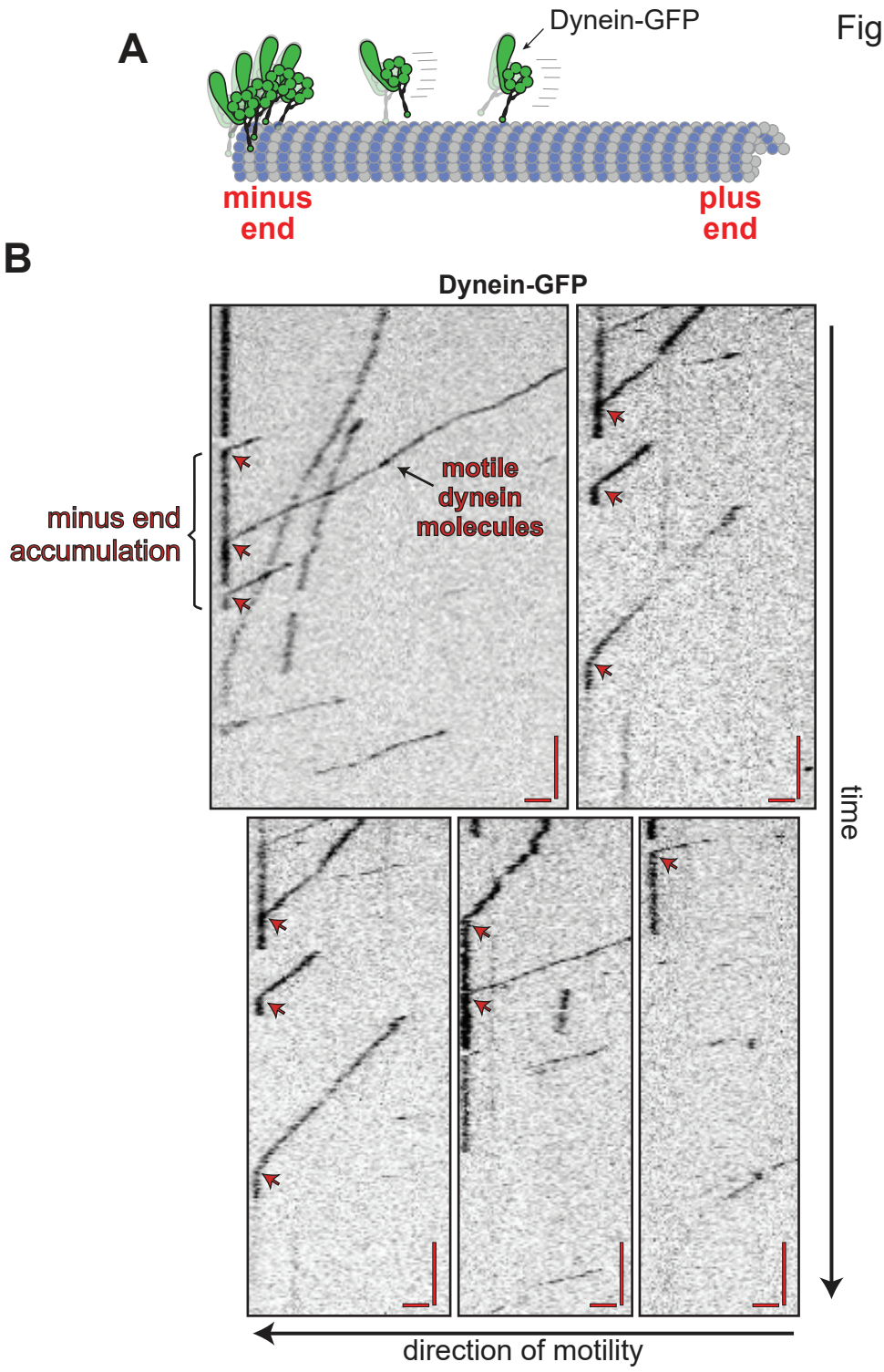

Figure S1.1. Purified dynein motors pause at microtubule minus ends before detaching. Schematic (A) and example kymographs (B) depicting single molecules of purified dynein motors walking toward and then pausing at the minus end of a taxol-stabilized microtubule before detaching. The dwell time of 0.1 s per step was approximated based on a mean velocity of 85 nm/s and a mean center-of-mass step size of 8 nm (Reck-Peterson et al., 2006). Bars: (vertical) 1 min; (horizontal) 2 µm. Also see Video 2.1 (uploaded to CSU server or see published paper online at doi.org/10.1083/jcb.201506119.) Related to Fig. 2.1.

Figure S1.2

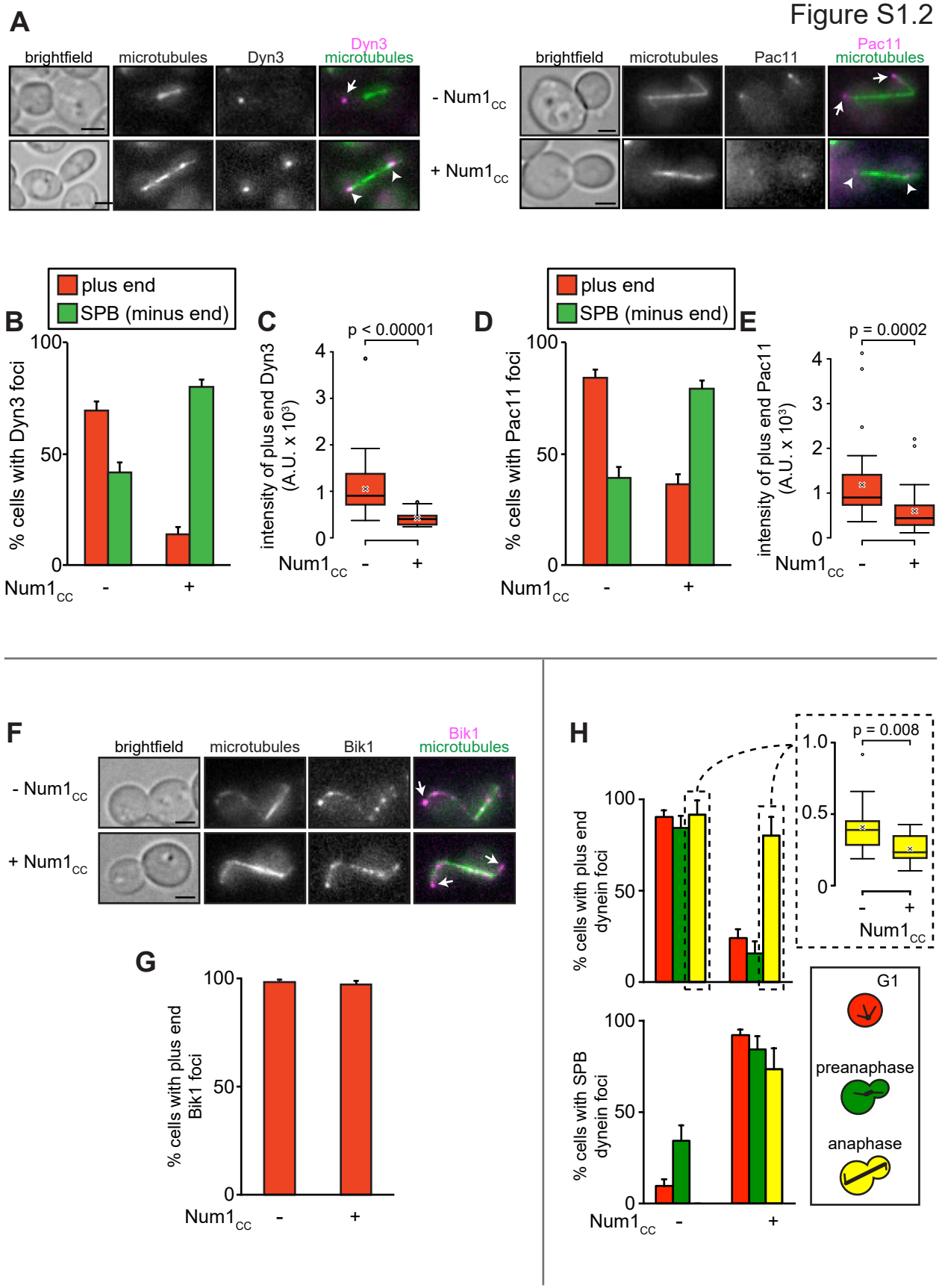
A
brightfield
microtubules
Dyn3
Dyn3 microtubules
- Num1cc
+ Num1cc
brightfield
microtubules
Pac11
Pac11 microtubules
B
plus end
SPB (minus end)
% cells with Dyn3 foci
Num1cc
C
p < 0.00001
intensity of plus end Dyn3 (A.U. x 10³)
D
% cells with Pac11 foci
E
p = 0.0002
intensity of plus end Pac11 (A.U. x 10³)
F
brightfield
microtubules
Bik1
Bik1 microtubules
G
% cells with plus end Bik1 foci
H
p = 0.008
% cells with plus end dynein foci
% cells with SPB dynein foci
G1
preanaphase
anaphase

Figure S1.3

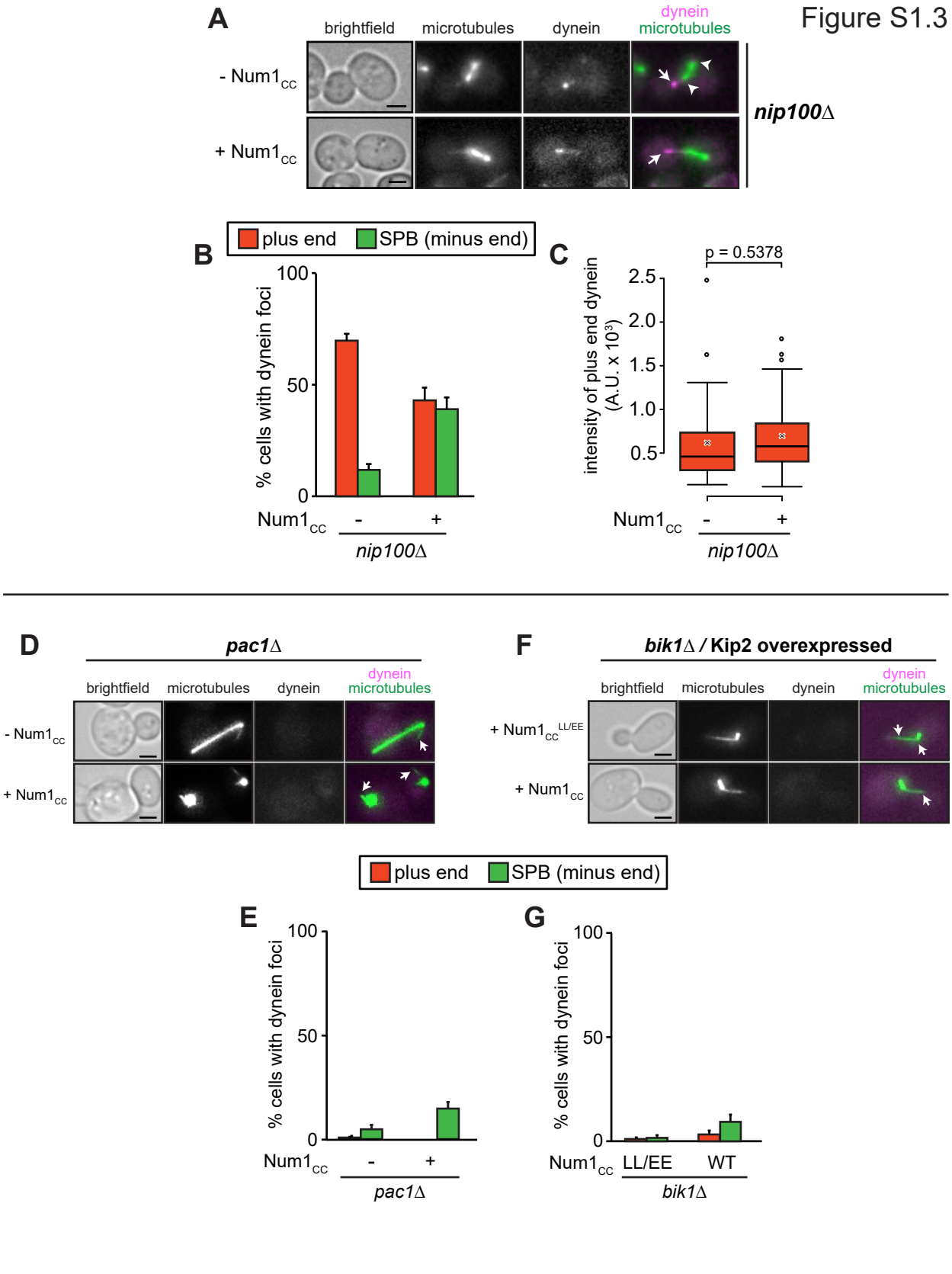
A
brightfield
microtubules
dynein
dynein microtubules
- Num1CC
+ Num1CC
nip100Δ
B
plus end
SPB (minus end)
% cells with dynein foci
100
50
0
Num1CC - +
nip100Δ
C
p = 0.5378
intensity of plus end dynein (A.U. x 10³)
2.5
2.0
1.5
1.0
0.5
Num1CC - +
nip100Δ
D
pac1Δ
brightfield
microtubules
dynein
dynein microtubules
- Num1CC
+ Num1CC
F
bik1Δ / Kip2 overexpressed
brightfield
microtubules
dynein
dynein microtubules
+ Num1CC LL/EE
+ Num1CC
plus end
SPB (minus end)
E
% cells with dynein foci
100
50
0
Num1CC - +
pac1Δ
G
% cells with dynein foci
100
50
0
Num1CC LL/EE WT
bik1Δ

Figure S1.4

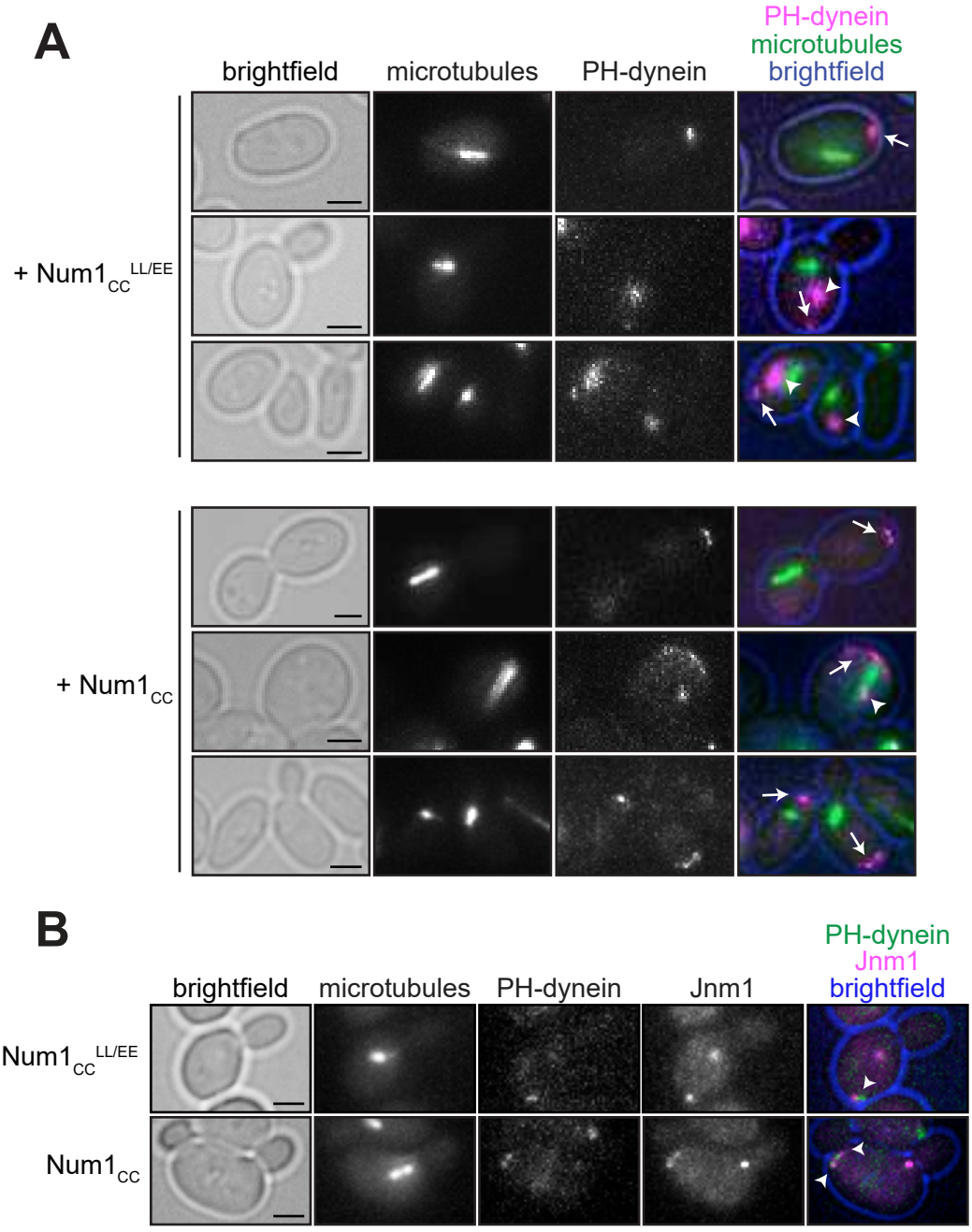

Figure S2.4. Num1$_{CC}$ overexpression affects the size of PH-Dyn1-3mCherry cortical patches, and cortical PH-Dyn1 foci colocalize with dynactin. (A) Representative images of cells induced to express PH-Dyn1-3mCherry and either Num1$_{CC}^{LL/EE}$ (top) or Num1$_{CC}$ (bottom). Cells were grown as described in Fig. 1. Arrows indicate cortical dynein patches; arrowheads indicate motile cytoplasmic foci not associated with microtubule-based structures (presumably aggregates). (B) Representative images of GAL1p:PH-DYN1-3mCherry cells expressing Jnm1-3YFP and either Num1$_{CC}$ or Num1$_{CC}^{LL/EE}$ (as indicated). Arrowheads indicate colocalized cortical PH-Dyn1-Jnm1 foci. All images are maximum-intensity projections of a 2-µm Z-stack of wide-field images. Bars, 2 µm. Related to Fig. 2.4.

Figure S1.5

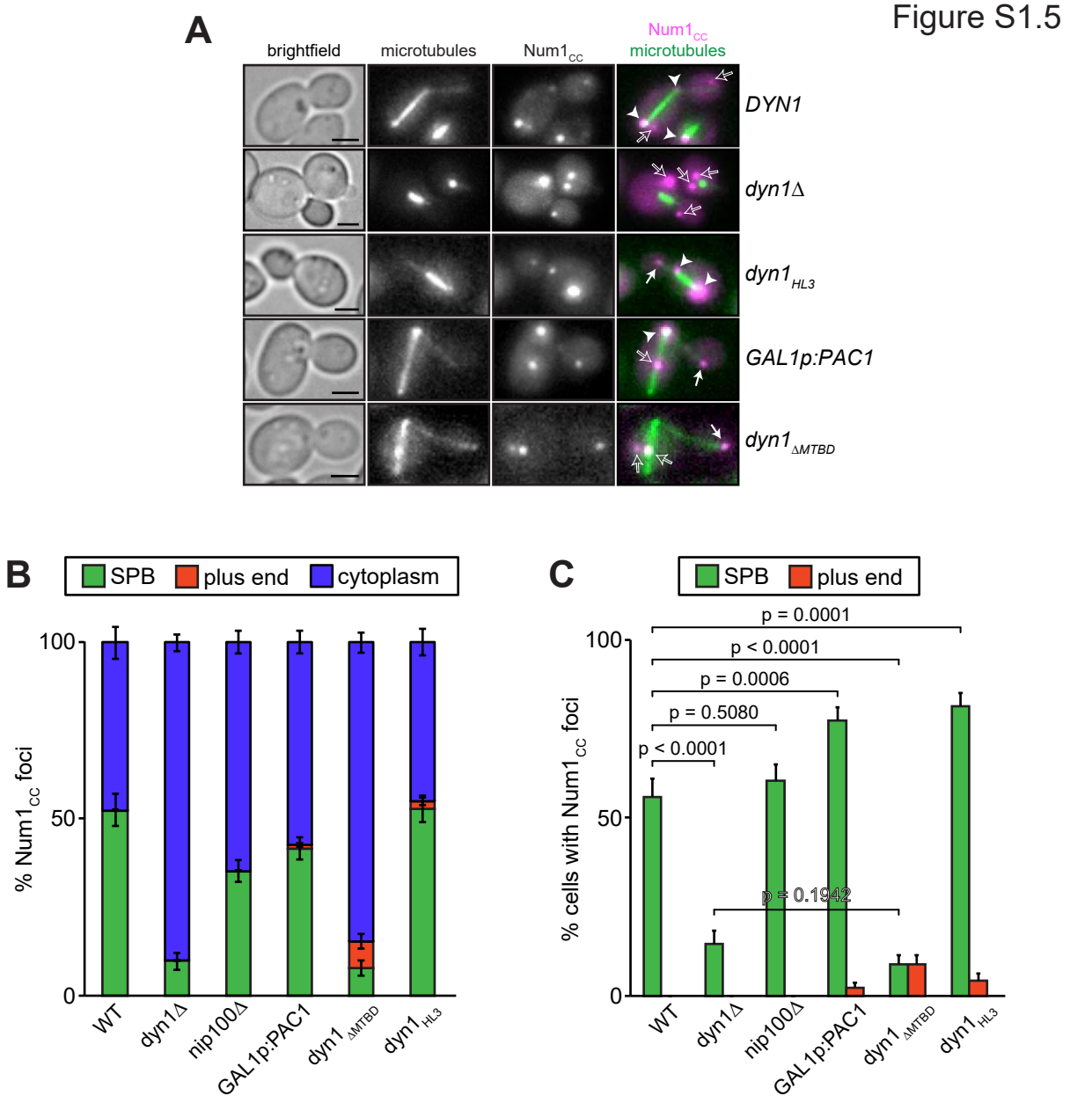
A
brightfield
microtubules
Num1CC
Num1CC microtubules
DYN1
dyn1Δ
dyn1HL3
GAL1p:PAC1
dyn1ΔMTBD
B
SPB
plus end
cytoplasm
% Num1CC foci
100
50
0
WT
dyn1Δ
nip100Δ
GAL1p:PAC1
dyn1 ΔMTBD
dyn1HL3
C
SPB
plus end
p = 0.0001
p < 0.0001
p = 0.0006
p = 0.5080
p < 0.0001
p = 0.1942
% cells with Num1CC foci
100
50
0
WT
dyn1Δ
nip100Δ
GAL1p:PAC1
dyn1 ΔMTBD
dyn1HL3
D
+ Num1CC GAL1p:KIP2
i.
dynein
dynein microtubules
ii.
iii.
iv.
time
+ microtubule –
+
–
+
–
+
–

Figure S1.2. Overexpression of $Num1_{CC}$ depletes dynein light-intermediate and intermediate chains, but not Bik1 from microtubule plus ends, and assessment of $Num1_{CC}$-affected dynein localization throughout the cell cycle. (A) Representative images of GAL1p:$num1_{CC}$ cells expressing mTurquoise2-Tub1 and either Dyn3- (left) or Pac11-3mCherry (right) used for quantitation in B–E. Cells were cultured as described in Fig. 2.1. (B–E) Frequency (B and D) and plus end intensity (C and E) of Dyn3- (left) and Pac11-3mCherry (right) in uninduced cells or cells induced to overexpress $Num1_{CC}$. Plus end or SPB foci were identified in two-color movies and scored accordingly. In B and D, error bars represent the standard error of proportion (n ≥ 102 cells). For box plots in C and E (n ≥ 19 foci), whiskers define the range of data, boxes encompass the 25th to 75th quartiles, the line depicts the median value, and the "x" depicts the mean value. (F) Representative images of GAL1p:$num1_{CC}$ cells expressing mTurquoise2-Tub1 and Bik1-3mCherry used for quantitation in G. (G) The percentage of cells that exhibit plus end Bik1-3mCherry foci is plotted. Error bars represent the standard error of proportion (n ≥ 115 cells). (H) The percentage of cells in the indicated phase of the cell cycle that exhibit plus end (left) or SPB (right) localized Dyn1-3mCherry foci in uninduced cells or cells induced to express $Num1_{CC}$ (n ≥ 63, 32, or 12 cells for G1, preanaphase, or anaphase, respectively). The inset shows fluorescence intensity measurements for Dyn1-3mCherry at the plus ends of anaphase spindle microtubules (n ≥ 16 foci). All images are maximum-intensity projections of a 2-µm Z-stack of wide-field images. Arrows indicate plus end foci, and arrowheads indicate SPB foci. Bars, 2 µm. Related to Fig. 2.1.

Figure S1.3. Complete $Num1_{CC}$-mediated depletion of dynein from plus ends requires dynactin, and plus end targeting is a requisite for robust SPB localization of dynein in $Num1_{CC}$-overexpressing cells. (A) Representative images of GAL1p:$num1_{CC}$ nip100Δ cells expressing mTurquoise2-Tub1 and Dyn1-3mCherry used for quantitation in B. (B) The percentage of cells that exhibit plus end (red) or SPB (green) Dyn1-3mCherry foci is plotted for the cells shown in A. Error bars represent the standard error of proportion (n ≥ 169 cells). (C) Box plot of fluorescence intensity values of plus end–associatedDyn1-3mCherry (n ≥ 30 foci). Whiskers define the range of data, boxes encompass the 25th to 75th quartiles, the line depicts the median value, and the "x" depicts the mean value. Related to Fig. 2.1. (D) Representative images of GAL1p:$num1_{CC}$ pac1Δ cells cultured in either SD plus glucose or SD plus galactose/raffinose used for quantitation in E. (E) The percentage of cells that exhibit plus end (red) or SPB (green) Dyn1-3mCherry foci is plotted for the cells shown in D. Error bars represent the standard error of proportion (n ≥ 111 cells). (F) Representative images illustrating Dyn1-3mCherry targeting in bik1Δ cells overexpressing $Num1_{CC}$ or $Num1_{CC}^{LL/EE}$. To compensate for the short astral microtubule phenotype in bik1Δ cells (Berlin et al., 1990), we overexpressed Kip2 using the GAL1p:KIP2 allele, which, when induced, restores microtubule lengths to near wild-type (WT) levels. For this reason, we compared GAL1p:-$num1_{CC}$ GAL1p:KIP2 bik1Δ (bottom) with GAL1p:$num1_{CC}^{LL/EE}$ GAL1p:KIP2 bik1Δ cells (top), both of which were cultured in SD plus galactose/raffinose (to induce overexpression of Kip2 and either $Num1_{CC}$ or $Num1_{CC}^{LL/EE}$). (G) The percentage of cells that exhibit plus end (red) or SPB (green) Dyn1-3mCherry foci is plotted for the cells shown in F. Error bars represent the standard error of proportion (n ≥ 64 cells). All images are maximum-intensity projections of a 2-µm Z-stack of wide-field images. For A, arrows indicate plus end foci, and arrowheads indicate SPB foci. For D and F, arrows indicate plus ends without foci. Bars, 2 µm. Related to Fig. 2.1.

Figure S1.5. Localization of $Num1_{CC}$ mirrors that of dynein, and additional examples of $Num1_{CC}$-induced minus end–directed dynein motility. (A) Representative images of cells induced to express $Num1_{CC}$-EGFP with the indicated genotype used for quantitation in B and C. Cells were grown as described in Fig. 2.1. Each image is a maximum-intensity projection of a 2-µm Z-stack of wide-field images. Open arrows indicate cytoplas-mic foci, closed arrows indicate plus end foci, and arrowheads indicate SPB foci. Bars, 2 µm. Plus end, SPB, or cytoplasmic foci were identified in two-color movies and scored accordingly. (B) The percentage of $Num1_{CC}$- EGFP foci that localize to the SPB (green), plus end (red), or cytoplasm (blue) is plotted (n ≥ 116 foci). (C) The percentage of cells that exhibit plus end (red) or SPB (green) $Num1_{CC}$-EGFP foci is plotted for the cells shown in A. Error bars in B and C represent the standard error of proportion (n ≥ 89 cells). Given the lack of colocaliza-tion between $Num1_{CC}$ and microtubules, these data also suggest that $Num1_{CC}$ is not sufficient to bind microtu-bules. (D) Additional example kymographs depicting minus end–directed motility of dynein along astral microtu-bules in cells overexpressing $Num1_{CC}$ and Kip2. Kymographs were generated from time-lapse images acquired using highly inclined and laminated optical sheet microscopy (see Materials and Methods). Bars: (vertical) 1 min; (horizontal) 1 µm. Related to Figs. 2.3, 2.5, 2.6, and 2.7. WT, wild type.